The Pennsylvania State University

The Graduate School

Department of Chemical Engineering

PURIFICATION OF PLASMID DNA USING MEMBRANE-BASED PROCESSES

A Dissertation in

Chemical Engineering

by

Ehsan Allah Espah Borujeni

Submitted in Partial Fulfillment
of the Requirements
for the Degree of

Doctor of Philosophy

December 2014

The thesis of Ehsan Allah Espah Borujeni was reviewed and approved* by the following:

Andrew Zydney
Professor of Chemical Engineering
Dissertation Advisor
Chair of Committee

Themis Matsoukas
Professor of Chemical Engineering

Michael Janik
Associate Professor of Chemical Engineering&
John J. and Jean M. Brennan Clean Energy
Early Career Professor in the College of Engineering

William Hancock
Professor of Biomedical Engineering

Phillip Savage
Professor of Chemical Engineering
Head of the Department of Chemical Engineering
Walter L. Robb Family Endowed Chair

*Signatures are on file in the Graduate School

ABSTRACT

There is significant interest in therapeutic applications of plasmid DNA, requiring new separations technologies for the purification of plasmids. Recent studies have demonstrated the potential of using ultrafiltration for separating plasmid topological isoforms; however these data were obtained over short times with very dilute solutions. The overall objective of this dissertation was to address these issues thereby providing a more extensive evaluation of the potential of ultrafiltration in the large-scale production of plasmid DNA.

Data obtained at higher plasmid concentrations showed a significant reduction in plasmid transmission during ultrafiltration even under conditions where the filtrate flux remained relatively constant. These results were explained using a simple model in which the membrane pores become partially blocked by plasmids that are trapped at the pore entrance. These "blocked" pores remain permeable to fluid due to the very open structure of the plasmid. The extent of plasmid fouling increased with increasing plasmid size, consistent with the greater probability of having a "knot" in the long DNA molecule. Model calculations were in excellent agreement with the experimental data over a wide range of conditions in both constant pressure and constant flux ultrafiltration.

The effects of plasmid fouling could be dramatically reduced by backpulsing. Experiments were performed over a range of pulse duration, frequency, and amplitude to identify the optimal set of operating parameters. High performance could be achieved using a pulse with zero back-pressure, i.e. by simply clamping the permeate exit line while maintaining crossflow, suggesting that the trapped plasmids were removed from

the pore primarily by the crossflow. A diafiltration process with pulsing provided more than 98% recovery of the plasmid in the permeate compared to only a 35% yield without pulsing.

The performance of the ultrafiltration process could be further improved by altering the membrane pore structure / morphology. Data obtained with asymmetric ultrafiltration membranes in the reverse orientation showed much greater plasmid transmission at the same filtrate flux. This increase in transmission was due to the pre-extension of the plasmid which facilitates elongation and transmission of the plasmid through the small pores in the membrane skin. Membrane fouling was significantly reduced in this reverse filtration, possibly due to the "un-knotting" of the plasmid in the large pores within the membrane support.

A laboratory-scale centrifugal ultrafiltration process was developed as a high-throughput method for quickly screening ultrafiltration for plasmid purification. A simple model was developed to evaluate the filtrate flux as a function of centrifugal conditions. Plasmid transmission in the centrifugal device was similar to that seen in pressure-driven ultrafiltration under comparable conditions.

The results obtained in this thesis provide important insights into plasmid ultrafiltration, while furthering the development of ultrafiltration processes for the purification of plasmid DNA isoforms.

TABLE OF CONTENTS

List of Figures vii

List of Tables xi

Acknowledgements xii

Chapter 1 Introduction 1

1.1. Key characteristics of plasmid DNA 1
1.2. Applications of plasmid DNA 4
1.2.1. Cloning 4
1.2.2. DNA vaccination 4
1.2.3. Gene therapy 5
1.3. Downstream processes of plasmid DNA production 6
1.4. Overall objectives 10
1.5. Thesis outline 11

Chapter 2 Theoretical background of plasmid DNA structure and elongation 14

2.2. Double stranded DNA structure 14
2.2. DNA elongation 18
2.2.1. Relaxation time 19
2.2.2. Characteristic flow time 20
2.2.3. Critical flux 22

Chapter 3 Membrane fouling during ultrafiltration of plasmid DNA through semipermeable membranes 24

3.1. Introduction 24
3.2. Material and Methods 26
3.2.1. Materials 26
3.2.2. Methods 30
3.3. Results and Analysis 34
3.3.1. Permeability evaluation 34
3.3.2. Fouling phenomena 34
3.3.3. Fouling model 40
3.3.4. Hydrodynamic effects 48
3.3.5. Plasmid topology effects 55
3.4. Discussion 56

Chapter 4 Application of periodic backpulsing to reduce membrane fouling during ultrafiltration of plasmid DNA 58

4.1. Introduction 58
4.2. Material and methods 60

4.2.1.Materials....60
4.2.2.Methods....63
4.3. Results and analysis....65
4.3.1.Backpulsing....65
4.3.2.Model development....68
4.3.3.Optimization of backpulse conditions....69
4.3.4.Diafiltration....75
4.4. Conclusion....78

Chapter 5 Effect of membrane pore structure on transmission of plasmid DNA....80

5.1 Introduction....80
5.2. Materials and method....82
5.2.1.Materials....82
5.2.2.Methods....84
5.3. Results and analysis....85
5.3.1.Hydraulic membrane permeability....85
5.3.2.Ultrafiltration experiments....85
5.3.3.Fouling....92
5.4. Conclusions....94

Chapter 6 Purification of plasmid DNA isoforms using centrifugal ultrafiltration....97

6.1. Introduction....97
6.2. Materials and Methods....99
6.2.1.Materials....99
6.2.2.Methods....100
6.3. Results and analysis....104
6.4. Discussion....114

Chapter 7 Conclusions and recommendations for future works....116

7.1 Conclusions....116
7.2. Recommendations for future work....119
7.2.1.Fundamental studies....120
7.2.2.Practical studies....121

References....125

Appendix Plasmid DNA vectors maps and sequences....136
A.1. 2.96 kbp plasmid (p-EMP)....136
A.2. 9.8 kbp plasmid (p-MDY)....139
A.3. 16.9 kbp plasmid (p-FDY)....139

LIST OF FIGURES

Figure 1-1: The map of pUC19 gene sequence showing various regions of replication (ori), ampicillin resistance (amp), and restriction sites (LacZα). 2

Figure 1-2:Structural images of linear (L), supercoiled (S), and relaxed (R) conformations of a 2.7 kbp pUC18 obtained using atomic force microscopy (AFM) (Jiang et al., 2010). 3

Figure 2-1: Schematic figure of four different nucleotides connected together through the phosphodiester bonds (Sinden, 1994). 15

Figure 2-2: Schematic of the helical structure of B-form double-stranded DNA (Sinden, 1994) 16

Figure 3-1:Schematic structures of (A) Tris.HCl and (B) EDTA. 27

Figure 3-2:Schematic of experimental set-up used for ultrafiltration, adopted from (Latulippe, 2010). 30

Figure 3-3:The schematic structure of PicoGreen dye showing binding sites of intercalation and electrostatic interactions with DNA, adopted from (Dragan et al., 2010). 32

Figure 3-4:Effect of plasmid concentration on the filtrate flux and observed sieving coefficient of the 16.9 kbp supercoiled plasmid during constant pressure ultrafiltration at 16.5 kPa through a 100 kDa Omega membrane. The dashed curves are model calculations using parameters values in Table 3-1. 36

Figure 3-5: Effect of plasmid concentration on the observed sieving coefficient of a 16.9 kbp supercoiled plasmid through a 100 kDa Omega membrane at a constant filtrate flux of 55 x 10^{-6} m/s. Dashed curves are model calculations using parameter values in Table 3-1. 38

Figure 3-6: Effect of plasmid size on transmission of the supercoiled plasmid through a 100 kDa Omega membrane. Data obtained with a 7.2 x 10^{-3} kg/m3 solution of the16.9 kbp plasmid and a 6.8 x 10^{-3} kg/m^3 solution of the 2.9 kbp plasmid at constant transmembrane pressure (initial filtrate flux of approximately 50 x 10^{-6} m/s for both experiments). Dashed curves are model calculations using parameter values in Table 3-1. 40

Figure 3-7: Scaled values of the observed sieving coefficient for the 1.2 x 10^{-3} kg/m3 solution of the 16.9 kbp plasmid (data from Figure 3-4) plotted in the form given by Equation (3-9). 43

Figure 3-8: Observed sieving coefficient of the 16.9 kbp plasmid in TE buffer containing 150 mM NaCl as a function of filtrate flux during ultrafiltration through the 100 kDa Omega membranes. The dashed line is the linear regression fit to the data. 47

Figure 3-9: Comparison of experimental and predicted values of the plasmid sieving coefficients for the 16.9 kbp plasmid over a range of concentrations at both constant pressure and constant filtrate flux. 48

Figure 3-10: Effect of filtrate flux value on the observed sieving coefficient of a 6.2 x 10^{-3} kg/m3 solution of the 16.9 kbp plasmid in TE buffer with 150 mM NaCl during constant flux filtration through two separate 100 kDa Omega membranes. Dashed curves are model calculations with $\beta = 0.46$ and $k = 1.1 \times 10^4$ m^2/kg and 1.6×10^4 m^2/kg at $J_v = 55$ and 30×10^{-6} m/s, respectively. 49

Figure 3-11: Effect of stirring on the ultrafiltration of a 7.4 x 10^{-3} kg/m3 solution of the 16.9 kbp supercoiled plasmid through a 100 kDa Omega membrane at a constant filtrate flux of 55 x 10^{-6} m/s. Dashed curves are model calculations using $\beta = 0.46$ and $k = 1.6 \times 10^4$ m^2/kg. 51

Figure 3-12: Ultrafiltration of a 1.0 x 10^{-3} kg/m3 solution of the 16.9 kbp supercoiled plasmid through a 100 kDa Omega membrane at a constant transmembrane pressure of 11 kPa first without and then with stirring. Stirring was initiated after filtration of 18 L/m^2 as shown by the dashed vertical line. 53

Figure 3-13: Effect of membrane pore size on the observed sieving coefficient of a 16.9 kbp supercoiled plasmid. Data were obtained at constant transmembrane pressure using a 7.2 x 10^{-3} kg/m^3 solution with an initial filtrate flux of 55 x 10^{-6} m/s. Dashed curves are model calculations with $\beta = 0.46$ and $k = 1.5 \times 10^4$ m^2/kg for the 100 kDa membrane and $k = 0.2 \times 10^4$ m^2/kg for the 300 kDa membrane. 54

Figure 3-14: Effect of plasmid concentration on the observed sieving coefficient of the linear isoform of a 16.9 kbp plasmid. Data were obtained at constant filtrate flux using 1.1 and 7.1 x 10^{-3} kg/m^3 solutions with an initial filtrate flux of 55 x 10^{-6} m/s. 56

Figure 4-1: Cross-sectional image of a PS ultrafiltration hollow fiber membrane provided by GE Healthcare. 61

Figure 4-2: Schematic of the set-up used in the ultrafiltration experiments with periodic backpulsing 63

Figure 4-3: Effect of backpulsing on the observed sieving coefficient (top panel) and filtrate flux (bottom panel) during ultrafiltration of 3.2 ± 0.2 µg/mL solutions of a 9.8 kbp plasmid through a 500 kDa GE hollow fiber membrane at a feed flow rate of 100 mL/min and a positive transmembrane pressure of 55 kPa. Backpulsing was performed every 180 s for 20 s at a backpressure of 55 kPa. Solid and dashed curves are model calculations described subsequently. 67

Figure 4-4: The effects of backpulse amplitude on the observed sieving coefficient during ultrafiltration of 3.2 ± 0.2 µg/mL solutions of a 9.8 kbp plasmid through a 500 kDa GE hollow fiber membrane at a feed flow rate of 100 mL/min and a positive transmembrane pressure of 55 kPa (giving an initial filtrate flux of 43 ± 1 µm/s). Backpulses were applied every 180 s for a fixed duration of 20 s. 70

Figure 4-5: The effects of pulse duration (at 0 kPa backpulse) on the observed sieving coefficient during ultrafiltration of 3.2 ± 0.2 μg/mL solutions of a 9.8 kbp plasmid through a 500 kDa GE hollow fiber membrane at a feed flow rate of 100 mL/min with an initial filtrate flux of 43 ± 1 μm/s. Pulses were applied every 180 s. Dashed curves are model calculations using α = 0.66, 0.79, and 0.85 for the experiments with 5, 10, and 20 s pulses, respectively. 72

Figure 4-6: The effects of volumetric feed (cross) flow rate on the best fit value of α during ultrafiltration of 3.2 ± 0.2 μg/mL solutions of a 9.8 kbp plasmid using a 500 kDa GE hollow fiber membrane with an initial filtrate flux of 43±1 μm/s. 10 s pulses (with no filtration) were applied every 180 s. 73

Figure 4-7: The effects of pulse frequency (at 0 kPa backpulse) on the observed sieving coefficient during ultrafiltration of 3.2 ± 0.2 μg/mL solutions of a 9.8 kbp plasmid through a 500 kDa hollow fiber membrane at a feed flow rate of 100 mL/min with an initial filtrate flux of 43±1 μm/s. Pulses were applied for a duration of 10 s. Dashed curves are the model calculations using α = 0.79 and 0.96 for the experiments with 180 and 90 s pulse periods, respectively. 75

Figure 4-8: Diafiltration of 3.2 ± 0.2 μg/mL solutions of a 9.8 kbp plasmid through a 500 kDa hollow fiber membrane but with (●) and without (▲) pulsing. Data obtained at a feed flow rate of 100 mL/min and a transmembrane pressure of 55 kPa. Pulses with 10 s duration (with no filtration) were applied every 90 s. The solid and dashed lines are model calculations for the runs with and without pulsing, respectively, using various θ values. 78

Figure 5-1: The effect of membrane orientation on the observed sieving coefficient of a 16.9 kbp supercoiled plasmid transmitted through a 500 kDa PS hollow fiber membrane**.** 86

Figure 5-2: The observed sieving coefficient of a 16.9 kbp plasmid filtered through a 50 kDa and 500 kDa PS hollow fiber membrane in the reverse orientation. 89

Figure 5-3: Ultrafiltration of the linear and supercoiled isoforms of a 2.9 kbp plasmid through a 50 kDa PS hollow fiber membrane using both the forward and reverse orientations. 90

Figure 5-4: Observed sieving coefficient of the 2.9 and 16.9 kbp supercoiled plasmids through a 50 kDa PS hollow fiber membrane in the reverse orientation. 91

Figure 5-5: AGE image of a mixture of the linear and supercoiled isoforms of the 2.9 kbp plasmid using a 50 kDa PS hollow fiber membrane. Lane 1 is a calibration standard constructed using a DNA ladder with different size of linear DNA. Lane 2 is the feed solution containing equal amounts of the two isoforms. Lane 3 is the permeate sample obtained at a filtrate flux of 10 μm/s, while Lane 4 is the filtrate sample at 20 μm/s 92

Figure 5-6: Effect of membrane orientation on fouling of a 3.0 μg/mL solution of the 16.9 kbp plasmid using a 500 kDa PS hollow fiber membrane at an initial flux of 46 ± 1 um/s. 94

Figure 6-1: Schematic diagram of the centrifugal ultrafiltration (UF) system 101

Figure 6-2: Cumulative filtrate volume as a function of time during centrifugal ultrafiltration. The symbols (♦), (●), and (■) represent experimental data obtained at angular velocities of 3000, 4500, and 6500 rpm, using TE buffer with 10 mM NaCl using the 100 kDa Omega membrane. Solid and dashed curves are numerical and analytical solutions as described in text using $L_p = 1.9 \times 10^{-6}$ m/(s.kPa). 105

Figure 6-3: Concentration of linear (♦), supercoiled (●), and open circular (▲) isoforms of a 9.8 kbp plasmid collected during centrifugal ultrafiltration through a 100 kDa Omega membrane as a function of the angular velocity. 106

Figure 6-4: Scaled filtrate concentration as a function of the average filtration velocity for centrifugal (▲) and pressure-driven (●) ultrafiltration of the supercoiled 9.8 kbp plasmid through a 100 kDa membrane. 108

Figure 6-5: AGE image of feed, retentate, and filtrate samples obtained during centrifugal ultrafiltration after collection of A) 160 ± 10 μL and (B) 370 ± 10 μL filtrate. Feed solutions are binary mixtures containing 0.7 μg/ml of the supercoiled (SC) 9.8 kbp plasmid and 0.3 μg/ml of the linear isoform in TE buffer containing 10 mM NaCl. Images were taken after running the gels for 2 hours at 75 V. 109

Figure 6-6: AGE image of feed, retentate, and filtrate samples obtained during three-step discontinuous diafiltrations which were performed to separate binary mixtures of the different isoforms of a 9.8 kbp plasmid in TE buffer containing 10 mM NaCl. 100 kDa Omega centrifugal UF membranes were used and images were taken after running the gels for 130 min at 75 V. (A) Separation of a feed containing 0.7 μg/mL of the supercoiled and 0.3 μg/mL of the linear isoform at 3000 rpm. (B) Separation of a mixture of 0.2 μg/mL of the open circular and 0.8 μg/mL of the linear isoform at 3300 rpm. 112

Figure A-1: Vector map of 2.96 kbp plasmid (p-EMP), adopted from (Latulippe, 2010). 138

Figure A-2: Vector map of 9.8 kbp plasmid (p-MDY), adopted from (Latulippe, 2010). 139

Figure A-3: Vector map of 16.9 kbp plasmid (p-FDY), adopted from (Latulippe, 2010). 140

LIST OF TABLES

Table 1-1: The purity requirements of the produced plasmid regulated by FDA (Prather et al., 2003) 7

Table 3-1: Best fit values of β and k for plasmid ultrafiltration experiments in Figures 3-4 to 3-6. 45

Table 5-1: Plasmid sieving coefficients through the 100 kDa Ultracel membrane in three configurations: skin-side up, skin-side down, and in a double layer with a 0.22 μm PVDF membrane..... 87

ACKNOWLEDGEMENTS

First and foremost, I would like to express my deepest gratitude to my advisor, Dr. Andrew Zydney for his fantastic advices, encouragements, and guidance throughout my PhD study. It was a great honor to work with him over the past six years. In addition to all the invaluable technical and scientific knowledge that I learnt from him, he had a strong influence on my problem-solving, mentorship, and team-working skills, which surely will help me in my future careers. I eagerly look forward to having an opportunity to collaborate with him in the future.

I would like to acknowledge my committee members Dr. Themis Matsoukas, Dr. Michael Janik, and Dr. William Hancock for their encouraging comments and feedback on my research and reviewing this dissertation. I also would like to sincerely thank Dr. Ali Borhan for all of his advice and supports in my both academic and personal life.

I acknowledge all of the past and current members of Dr. Zydney research group: David Latulippe, Meisam Bakhshayeshi, Mahsa Rohani, Dharmesh kanani, Kris Ruanjaikaen, Elaheh Binabaji, Mahsa Hadidi, Melissa Woods, Achyuta Teella, Ying Li, and Shudipto Dishari for their supports and friendship. A special thanks to David Latulippe whose theoretical and technical mentorship at the beginning of my PhD significantly helped me in starting my research. Mahsa Rohani and Meisam Bakhshayeshi also patiently taught me the basic lab works when I joined the group. I also had the chance to work with Steven Benner, Aaron Dranko, and David Currie as undergraduate students who helped me in conducting some of the experiments. I found all of them smart and talented and wish them all the bests throughout their future career.

I would like to thank the members of Dr. Howard Salis and Dr. Wayne Curtis research groups for giving me a full access to the instruments of their laboratories. I greatly appreciate Loida Escote-Carlson and Beth Schlagnhaufer in Department of Biochemistry and Molecular biology for teaching me the majority of the molecular biology techniques that I applied in my research. I also acknowledge Dr. Paula Clemens from the University of Pittsburg and Dr. Jeff Chamberlain from the University of Washington for their generous donation of plasmid DNAs used in this study.

Finally, I dedicate this dissertation to my lovely, caring and wonderful parents, Nasrin and Houshang, my siblings, Arash, Amin and Nasim, and also my dearest uncle, Abbas, who encouraged me to come to the United States for pursing my graduate studies. Although I was not able to return home and visit them over the past years, their unconditional love and support kept me hopeful and determined to successfully finish this chapter of my life. A special thanks to my younger brother and closest friend, Amin Espah Borujeni, whose priceless assistance and cares, certainly eased tolerating this being-far-away-from-family time. I am truly blessed to have all of them in my life.

Chapter 1

Introduction

1.1. Key characteristics of plasmid DNA

Plasmid DNA is a circular double-stranded DNA existing mostly in prokaryotic organisms like bacteria and also in some eukaryotic cells. It is composed of a sequence of hundreds to hundreds of thousands of paired nucleotides connected to each other through a set of intra-strand phosphodiester and inter-strand hydrogen bonds; the plasmid size is typically measured in units of base pairs (bp) or kilo base pairs (kbp). Bacterial plasmids are significantly smaller than the chromosomal genomic DNA, typically providing adaptability of the host cell to the surrounding environment. Plasmid DNA is self-replicating because of the presence of a gene sequence in its structure known as origin of replication or oriV site. Self-replication is initiated by a protein, encoded by a gene sequence next to the oriV site, and is continued through either the theta or rolling circle mechanisms involving the host cell primase, ligase, and / or DNA polymerase III (Schleef, 2001). The number of identical plasmids present in a cell, the copy number, depends on the type of oriV region. High-copy number plasmids like pUC-derived vectors produce hundreds of copies per cell (Camps, 2010) while F plasmids have relatively few copies (Wada and Yura, 1984).

Bacterial plasmids are typically designed to contain one or more genes that provide resistance to antibiotics like kanamycin (Gray and Fitch, 1983) or ampicillin

(Sutcliffe, 1978) or to toxic heavy metals ions like Ag^{+}, Cu^{2+} (Nies, 2003). This enables positive selection of cells containing the desired plasmid. Bacterial plasmids can also be designed with restriction sites that facilitate insertion of specific DNA fragments that code for exogenous (e.g., human) proteins. Figure 1-1 shows the schematic diagram of the pUC19 plasmid used in this work, including the distinct regions of self-replication (ori), selection marker (amp), and restriction sites (lacZα).

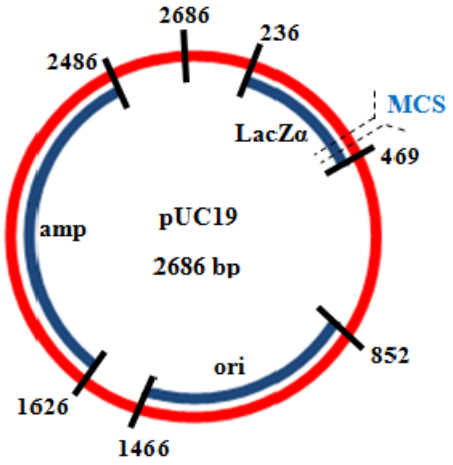

Figure 1-1: The map of pUC19 gene sequence showing various regions of replication (ori), ampicillin resistance (amp), and restriction sites (LacZα).

Plasmid DNA naturally has a twisted circular shape (with no free ends) which is typically referred to as covalently closed circular (CCC) or supercoiled (SC). The supercoiled isoform is internally twisted when the ends are connected; this twist is relaxed when the DNA is partially unwound during replication. Enzymatic or mechanical breakage of a phosphodiester bond in one of the strands allows the DNA to untwist while maintaining the circular shape; this conformation is typically referred to as open circular (OC). A linear DNA is produced by cutting phosphodiester bonds in both

strands (Latulippe and Zydney, 2010). Although these conformations have different structural properties, they have identical gene sequence and number of base pairs. In addition, oligomeric and interwound topologies can also be formed during replication or plasmid production.

Several techniques are used to characterize or quantify the concentration of the different plasmid isoforms including atomic force microscopy (Vologodskii and Cozzarelli, 1994; Jiang et al., 2010), static slight scattering (Latulippe and Zydney, 2010), UV absorbance, capillary and agarose gel electrophoresis (GE) (Schmidt et al., 1999; Holovics et al., 2010), and analytical anion exchange (Molloy et al., 2004; Sun et al., 2013) and hydrophobic chromatography (Iuliano et al., 2002). Figure 1-2 shows an image of the three isoforms of a 2.7 kbp pUC18 plasmid using atomic force microscopy (AFM) (Jiang et al., 2010). The topological properties of plasmid DNA will be described in more detail in Chapter 2.

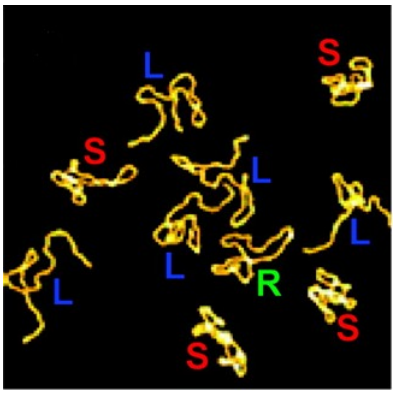

Figure 1-2: Structural images of linear (L), supercoiled (S), and relaxed (R) conformations of a 2.7 kbp pUC18 obtained using atomic force microscopy (AFM) (Jiang et al., 2010).

1.2. Applications of plasmid DNA

The dominant biopharmaceutical applications of plasmid DNA, explained as follows, is based on its critical attributes as self-replicability, antibiotic resistance and the capability of hosting the external DNA fragment without alteration of other properties.

1.2.1. Cloning

Plasmid DNA is ideal for use in cloning and the rapid production of a desired protein coded in the plasmid DNA sequence. Most plasmids used as cloning vectors are modified forms of natural plasmids, including pBR322, pBluescript SK (+/-), and pUC19 (Schleef, 2001). The desired gene is inserted into the vector using restriction endonucleases, with the resulting recombinant plasmid transformed into the host cells using appropriate molecular techniques like heat-shock (Froger and Hall, 2007) or electroporation (Lessard, 2013). The recombinant cells are screened, isolated, and used to produce the protein of interest (Norrander et al., 1983; Errampalli et al., 1999).

1.2.2. DNA vaccination

More recently, there has been interest in using plasmid DNA as a vaccine, in this case by designing the plasmid to express a specific antigen using the patient's natural translation machinery. The expressed antigen stimulates the host immune system and generates the desired immunological response. DNA vaccination has been examined in a variety of clinical and preclinical studies for prevention of cancer (Teja Colluru et al.,

2013), HIV (Jaoko et al., 2008), influenza (Donnelly et al., 1995), and tuberculosis (Tascon et al., 1996), among others. The main advantages over traditional vaccination include the stability of the vaccine (relative to live or attenuated organisms), easier scale-up, and the absence of infectious agents (K.H., 2013). There is also some evidence that the ongoing production of the antigen leads to an enhanced immune response. The plasmid vectors used in DNA vaccination are typically 1 to > 20 kbp in size and include the origin of replication and selective marker for initial production (typically in bacteria) and an appropriate promoter and gene sequence for production of the desired antigen in the human or animal host.

Plasmid vectors can be delivered into tissue as non-packaged DNA (naked) (Liu et al., 2001), packaged into liposomes or polymers (Zhdanov et al., 2002), or coated onto gold particles (Ding et al., 2014). Naked plasmids can be used as a high-dose DNA carrier with intramuscular injection. Plasmid-coated gold particles are typically delivered through the skin using gunshot bombardment. In all cases, the supercoiled circular isoform is the preferred topology since it provides a more efficient transient transfection of cells (Weintraub et al., 1986).

1.2.3. Gene therapy

Gene therapy involves the use of specific DNA sequences to directly treat disease, typically in which the patient has a missing or malfunctioning gene. An external gene segment can be used to directly express the desired protein (e.g., clotting agent, enzyme, or receptor), or it can replace the mutated gene sequence in the genomic DNA. Both viral

and non-viral vectors can be used for delivery. Although viral vectors give higher cell transformation efficiency, higher gene expression, and specific targeting of the desired cells, the virus itself can generate an adverse immune response (Ginn et al., 2013). In contrast, plasmid DNA doesn't cause an adverse immune response and can deliver gene segments of any size. However, plasmids show a lower level of transformation into the cells and poorer cell-targeting than viral vectors. The number of clinical trials using naked plasmid DNA has increased from 14% in 2004 to 17.7% in 2014 according to Gene Therapy Clinical Trials Worldwide (2014). A novel combination of naked plasmid and other types of viral vectors (like adenovirus) have been used in 0.6% of total clinical trials (2014).

1.3. Downstream processes of plasmid DNA production

As mentioned previously, plasmids are typically produced in E. Coli using either batch or fed-batch fermentation. A number of studies have reviewed the processes used for production of plasmid DNA for both DNA vaccination and gene therapy (Ferreira et al., 2000; Voß, 2007; Cai et al., 2009; Ghanem et al., 2013). The plasmid concentration depends on the plasmid copy number and cell density; typical values range up to 3 % of wet weight of the E. coli. The desired specifications of the final plasmid product are regulated by FDA, with key parameters given in Table 1-1.

Table 1-1: The purity requirements of the produced plasmid regulated by FDA (Prather et al., 2003)

Components	**level**
Genomic DNA (qPCR)	< 1%
Protein (BCA assay)	<1%
RNA (HPLC ribose assay)	< 0.1%
Endotoxins (LAL assay)	<0.5 EU (Endotoxin/mg plasmid DNA)
Supercoiled plasmid DNA (AGE)	>90%

The key impurities that must be removed in the plasmid purification process include: i) cellular impurities like genomic DNA, RNA, host cell proteins (HCPs) and endotoxins, ii) undesired plasmid conformations like open circular, linear, dimers, and oligomers, which can be formed during both the upstream and purification process, and iii) salts and chemicals added throughout the cell lysis and downstream unit operations. The scale of plasmid DNA required to be purified varies from milligram (laboratory scale) to gram (pilot plant scale) to kilogram (large scale) depending on the clinical demand. The large differences in scale lead to a range of downstream unit operations, operating conditions, safety-related concerns, and economic issues. For example, phenol extraction and EtBr/CsCl density gradient ultracentrifugation have been extensively used for laboratory scale purification of plasmid DNA, however safety-concerns associated with phenol and EtBr/CsCl are major obstacles for using these techniques in large scale plasmid DNA production.

The downstream processes for plasmid production are usually divided into harvest and lysis, primary isolation, intermediate recovery, and final polishing. The produced cells are harvested using centrifugation (Kong et al., 2008; Sun et al., 2013) or tangential flow filtration (TFF) technique (Quaak et al., 2008) followed by cell lysis to release the plasmid DNA. High pressure mechanical cell disruption like microfluidization is typically not suitable because of the possibility of DNA damage (Levy et al., 1999). Alkaline lysis, originally presented by Birnboim and Doly (1979), is the most common method for cell disruption (Feliciello and Chinali, 1993; Clemson and Kelly, 2003).

The primary isolation stage includes removal of large impurities like genomic DNA, RNA, endotoxins, host cell proteins (HCP), and other cell debris, the majority of which precipitate after alkaline lysis/neutralization steps. The volume of the clarified solution is typically reduced using either plasmid precipitation or ultrafiltration (Urthaler et al., 2005; Sun et al., 2013). Plasmids can be precipitated using polyethylenglycol (PEG) (Schmitz and Riesner, 2006) or alcohols like isopropanol and ethanol. Urthaler et al. (2007) proposed an automated process in which they combined the lysis and primary isolation steps by connecting alkaline lysis, neutralization, clarification, and concentration steps.

Intermediate recovery is focused on removal of the remaining impurities including proteins, RNA, undesired plasmid isoforms, and other small contaminants like DNA fragments. Chromatography-based methods are the most commonly used, with the separations based on differences in electrostatic charge, surface charge density, size, and hydrophobicity. Examples include anion exchange (AEX) (Urthaler et al., 2005; Przybylowski et al., 2007), hydrophobic interaction (HIC) (Li et al., 2005; Berg et al.,

2009), different types of affinity (AC) (Sousa et al., 2006; Sousa et al., 2011; Bai et al., 2014), and multimodal chromatography (Matos et al., 2014). Size exclusion chromatography (SEC) is commonly used in the polishing step to remove salt and chemical impurities and trace amounts of small proteins and RNA (Urthaler et al., 2005). For example, Sun et al. (Sun et al., 2013) developed a large scale process for plasmid purification including AEX, HIC, and SEC chromatography. Several authors have reviewed the application of chromatography in the downstream purification of plasmid DNA (Diogo et al., 2005; Ghanem et al., 2013).

The major drawback of traditional packed-bead column chromatography is the low dynamic binding capacity of plasmid DNA (typically on the order of 1 g plasmid per L resin (Ghanem et al., 2013)) due to the large size of the plasmids leading to poor accessibility and slow diffusion into the internal structure of beads. Monolithic stationary phases with macro- and mesopores connected through large pathways, have emerged as an attractive alternative with increased binding capacity and process throughput (Shin et al., 2011). Smrekar et al. (2010) examined a plasmid purification process using AEX and HIC chromatography systems with monolithic stationary supports having a binding capacity of 4 g plasmid per L resin at a flow rate of 380 cm/h.

Another unique challenge in plasmid purification is the isolation of the supercoiled isoform from the open circular plasmid. These two isoforms have very similar structural characteristics; the open circular has a slightly more relaxed and larger structure than the supercoiled, which does lead to small differences in accessibility of hydrophobic and negatively charged groups. However, existing stationary phases for preparative-scale chromatography are unable to effectively separate these isoforms.

In addition to chromatography, there has also been interest in using membrane-based processes for the recovery and purification of plasmid DNA. Several studies (Latulippe et al., 2007; Arkhangelsky et al., 2008; Latulippe and Zydney, 2008; Ager et al., 2009; Arkhangelsky et al., 2011) have shown that plasmid DNA elongates in the converging flow field into the individual pores in ultrafiltration membranes, allowing the plasmids to pass through pores that are smaller than the radius of gyration of the plasmid when the filtrate flux is larger than a critical value. Since the different plasmid isoforms have different elongational flexibility, they have different critical filtrate flux (Latulippe and Zydney, 2011) thereby providing an opportunity for purification of the supercoiled plasmid. Latulippe and Zydney (2011) described a scenario in which the supercoiled plasmid could be purified using a two-stage ultrafiltration process in which the linear plasmid is removed in the filtrate during the first step (with the supercoiled retained), while the open circular plasmid is removed in the second ultrafiltration unit with the supercoiled collected in the permeate. The key advantages of this membrane-based process are high throughput, no safety issues due to the use of harmful chemical agents, and the ease of scale-up/down. On the other hand, membrane fouling can lead to significant reductions in fluid flow and solute transmission during plasmid ultrafiltration (Zydney and Zeman, 1996).

1.4. Overall objectives

Although recent results have shown that ultrafiltration has significant potential for purification of supercoiled plasmid DNA from the undesired topological impurities, there

are a number of the operational challenges that still need to be overcome. In particular, previous studies have been performed over short times (typically less than 15 min) and with very dilute plasmid solutions (concentrations < 1 μg/mL), which are well below the practical concentrations (ten to several hundred μg of plasmid per mL solution) required for large-scale plasmid production (Prather et al., 2003). These conditions provide no insights into the possible effects of membrane fouling during long-term ultrafiltration processes. Furthermore, the resolution obtained using ultrafiltration (Latulippe and Zydney, 2011) is below the requirements set by regulatory agencies, particularly for the removal of the open circular isoform.

The overall objective of this work is to address these key issues in the use of ultrafiltration for the separation of supercoiled plasmid DNA from the unwanted open circular and linear isoforms. This includes a detailed analysis of membrane fouling phenomena during plasmid ultrafiltration as well as the examination of different techniques for the control and minimization of fouling. Experiments were also performed to investigate the effect of pore shape on the resolution of the ultrafiltration process and on the use of very small-scale centrifugal ultrafiltration systems for screening studies and the identification of the optimal operational conditions for plasmid ultrafiltration.

1.5. Thesis outline

Chapter 2 includes a brief review of the physicochemical characteristics of double stranded DNA and its various topological conformations followed by a short description

of the theoretical background and mathematical framework used for the analysis of flow-induced plasmid DNA elongation during ultrafiltration.

Chapter 3 examines membrane fouling phenomena during ultrafiltration of supercoiled plasmid DNA including the dependence of DNA and solvent transmission on the plasmid concentration, process time, plasmid size, and membrane pore size. A new theoretical model based on partial pore blockage is developed to describe the fouling behavior.

In chapter 4, a periodic pulsing method is developed to reduce the effects of membrane fouling by removal of trapped plasmids from the membrane pores. Data were obtained over a wide range of conditions to identify the optimal pulsing operation. The partial blockage model from chapter 3 was extended to describe the effects of pulsing on fouling reduction during ultrafiltration. A diafiltration process with periodic pulsing was used for ultrafiltration of the supercoiled plasmid, with the results demonstrating the large benefits of pulsed operation.

Chapter 5 presents experimental and theoretical studies of the effects of using converging pores on the transmission of the different plasmid isoforms. This includes the use of commercially available ultrafiltration membranes but with the flow directed in the reverse orientation, i.e., through the membrane substructure and then the selective skin. These studies provide additional fundamental insights on the effects of pore morphology on plasmid ultrafiltration as well as opportunities to improve the overall quality of the plasmid isoforms separation by ultrafiltration.

Chapter 6 examines the performance of a laboratory-scale centrifugal ultrafiltration system for plasmid separation. A simple theoretical framework was

developed for predicting the filtrate volume and the separation performance as a function of operational parameters (i.e. centrifugal speed and time) and device geometry. This centrifugal system provided similar separation performance as that obtained in pressure driven ultrafiltration studies, providing an opportunity to perform very small scale (i.e. < 500 μL working solutions) high throughput screening studies to identify the optimal conditions for plasmid isoforms separation.

Chapter 7 presents the key conclusions from this work along with recommendations for future studies to continue the development of ultrafiltration systems for plasmid DNA purification.

Chapter 2

Theoretical background of plasmid DNA structure and elongation

As discussed in the Introduction, DNA translocation through nanopores under the influence of external hydrodynamic or electrophoretic forces occurs by a flow-induced elongation. There are several works reviewing the structural and elongation properties of DNA (Fyta et al., 2011; Dorfman et al., 2013). This chapter provides a short summary of the key properties of the double-stranded DNA structure followed by a review of the fundamental mathematical models that have been developed to describe the elongational characteristics of plasmid DNA.

2.2. Double stranded DNA structure

ds-DNA is a biopolymer molecule containing two linear strands of nucleotides each composed of a deoxyribose sugar, a phosphate group, and a nitrogen "base". There are four different bases present in native DNA: Thymine (T), Cytosine (C), Guanine (G), and Adenine (A). Nucleotides in each strand are sequentially connected through a set of phosphodiester covalent bonds as shown in Figure 2-1.

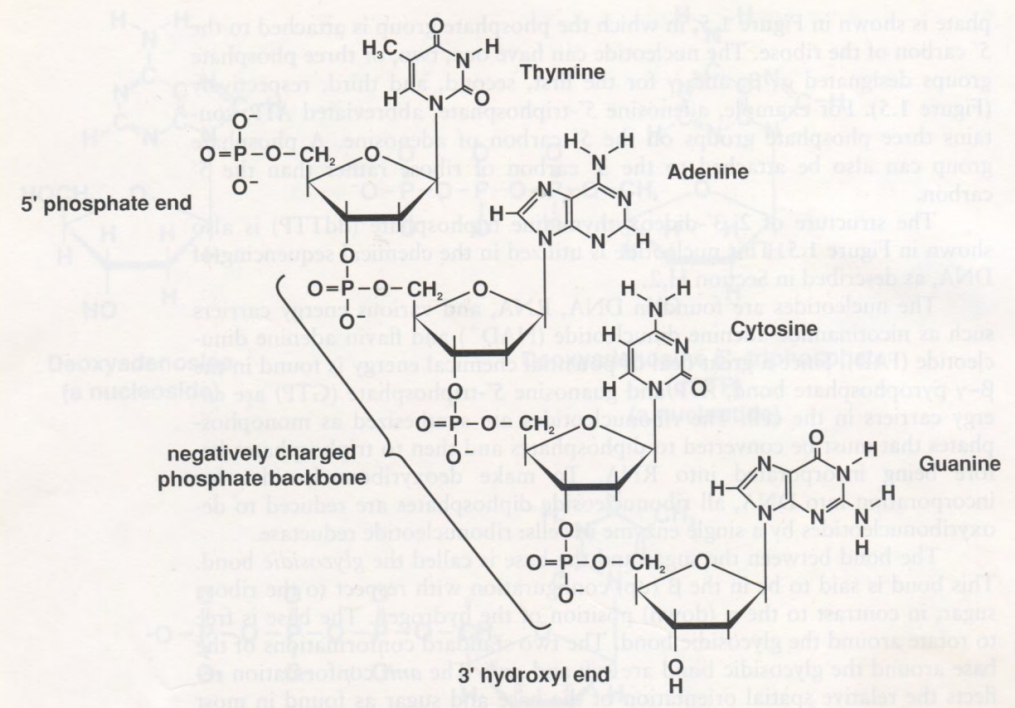

Figure 2-1: Schematic figure of four different nucleotides connected together through the phosphodiester bonds (Sinden, 1994).

The two DNA strands are "base-paired" through hydrogen bonding interactions between A-T and C-G. The connected strands naturally form a double helix as first described by Watson and Crick (1953). The native structure of ds-DNA is a right-handed double helix, called negative B-form, as shown in Figure 2-2 (Sinden, 1994). The paired bases are stacked on top of each other at the center of the helix with π-π interactions between the nitrogen rings of adjacent bases helping to stabilize the helical structure. The overall stability is a function of the DNA sequence, with the most stable π-stacking between two sequential pairs of G-C bases (Ornstein et al., 1978). The phosphate and sugar groups of nucleotides are located at the outer surface of DNA with the phosphate groups giving DNA a strong negative charge. Each complete turn of the B-form helix

roughly consists of 10.5 pairs of bases with a 0.34 nm rise in helix axis per base pair. This results in a 3.57 nm rise for one complete turn of helix (the helix pitch). The distance between the complementary stands in this helical structure is approximately 2 nm with a 34º twist of each base pair relative to the nearest neighbor. The minor and major grooves present in the DNA structure make the functional groups in the base pairs accessible to proteins and small molecules in the surrounding solution.

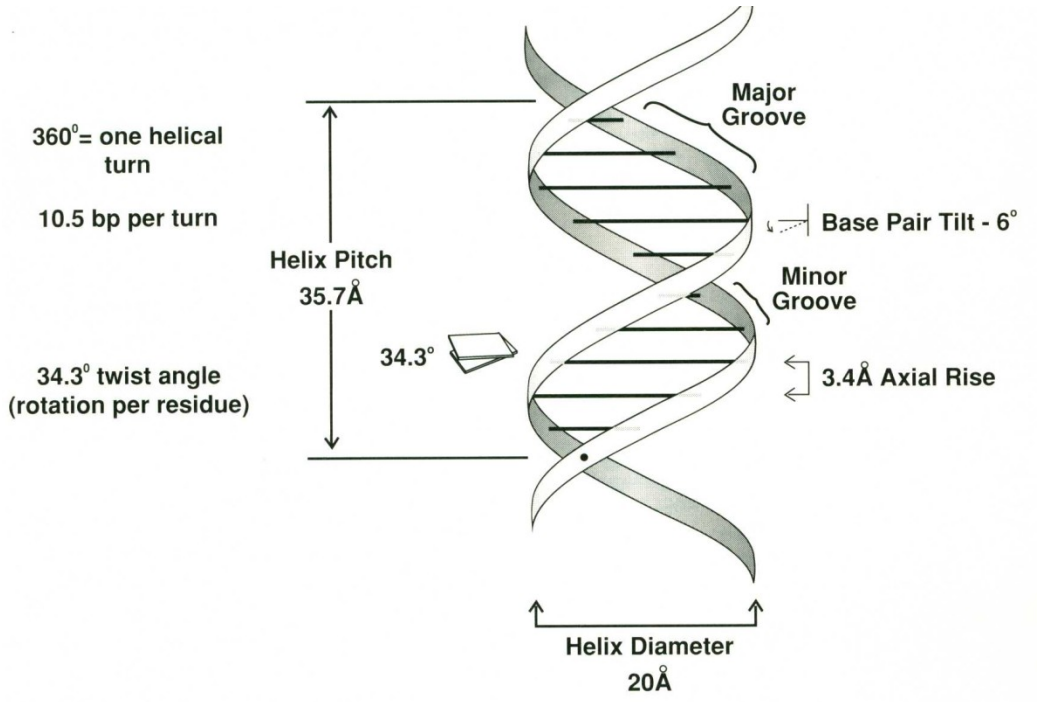

Figure 2-2: Schematic of the helical structure of B-form double-stranded DNA (Sinden, 1994)

A double stranded DNA molecule containing less than 150-200 base pairs (i.e. less than about 60 nm in total length) behaves almost as a stiff rod. Larger DNA segments, with lengths much larger than the persistence length (around 54 nm in typical

ionic environments) adopt a more flexible structure that is often described as a worm-like chain. The bends and kinks in the dsDNA structure have been described as a function of the DNA sequence using a Wedge and / or Junction model (Wu and Crothers, 1984; Bolshoy et al., 1991). The bendability of the helix allows the DNA to twist into a more compact superhelical structure. The linking number, L, is a topological attribute of dsDNA which defined as:

$$L = T + W \tag{2-1}$$

where T is the twisting number, equal to the number of complete turns in the helical structure, and W is writhing number, equal to the number of times the double-stranded helix twists around itself.

A right-handed superhelix corresponds to a negative writhing number, requiring an increase in the number of helical turns to keep the linking number constant. The superhelical density, σ, describes the extent of superhelical twisting:

$$\sigma = \frac{W}{L_0} \tag{2-2}$$

where L_0 is the linking number that a linear dsDNA naturally possesses in solution, $L_0 = \frac{N}{10.5}$ with N the total number of base pairs and 10.5 the number of base pairs per helical turn. Typical values of σ for natural plasmids obtained from eukaryotic and prokaryotic cells are between -0.05 and -0.07 (Sinden, 1994).

A relaxed plasmid is a circular ds-DNA which possesses a linking number equal to that of the linear and nicked ds-DNA (i.e. a double-stranded helix that doesn't twist around itself and has a writhing number equal to zero). However, a supercoiled plasmid

has a linking number different than L_0, with the specific linking number parameter, σ_{sp}, defined as:

$$\sigma_{sp} = \frac{L - L_0}{L_0} \tag{2-3}$$

Plasmids can be either positively or negatively supercoiled (corresponding to $L > L_0$ and $L < L_0$, respectively), due to either writhing or an alteration of the twisting angle between adjacent bases. The change in linking number causes torsional tension in the plasmid structure leading to a positive free energy of supercoiling (Sinden, 1994).

$$\Delta G = \left(1100 \frac{RT}{N}\right)(L - L_0)^2 \tag{2-4}$$

where R is the ideal gas constant, T is the absolute temperature, and N is the number of base pairs. This energy is released during replication in which the DNA must be unwound to expose the bases at the center of DNA structure. The negatively supercoiled form is the natural state of most plasmids and genomic DNA.

2.2. DNA elongation

Similar to the behavior seen with other polymers, DNA can be stretched by application of an external force. The degree of extension of a polymer in a fluid flow field is typically characterized in terms of the Deborah number (De), originally proposed by Reiner (1964) and defined as the product of the polymer relaxation time (τ) and the inverse of characteristic time of the flow, which is typically taken as the shear rate (γ). When $De = \tau \times \gamma$ is larger than a critical value (De_{crit}), the polymer becomes extended

since there is insufficient time for the polymer to relax and return to its natural and more energetically favorable state. .

2.2.1. Relaxation time

There are a number of experimental techniques that can be used to evaluate the DNA relaxation time including birefringence (Hagerman, 1981; Sturm and Weill, 1989), hydrodynamic stretching (Perkins et al., 1997) and dynamic light scattering (Berne and Pecora, 1976; Sorlie and Pecora, 1990).

In addition, several theoretical models have been developed to evaluate the relaxation time, typically based on the physical picture of DNA as a sequence of rigid beads connected by spring-like forces. In general, these models fall into two categories depending on whether intra-molecular interactions between the beads are considered.

Rouse (1953) used a free-draining model to describe the dynamics of a polymer chain in dilute solution, with the relaxation time given as:

$$\tau \cong 4 \frac{\mu R_g^3}{k_B T} \tag{2-5}$$

where μ is the solution viscosity, k_B is the Boltzmann constant, T is the absolute temperature, and R_g is the radius of gyration of the polymer. Berne and Pecora (1976) presented a slightly different form for the free-draining model:

$$\tau = \frac{R_g^2}{\pi^2 D} \tag{2-6}$$

where the diffusion coefficient, D, is typically evaluated using the Stokes-Einstein equation:

$$D = \frac{k_B T}{6\pi\mu R_H} \quad (2\text{-}7)$$

with R_H the polymer hydrodynamic radius. Note that if the hydrodynamic radius is equal to $4\pi R_g/6$, Equation (2-6) reduces to Equation (2-5).

The free-draining models ignore intra-molecular hydrodynamic interactions between the beads. Zimm (1956) modified the Rouse model to include intra-molecular interactions, typically referred to as the non-free draining model. The Zimm model has a similar form to the Rouse model (Equation 2-5) but with a proportionality coefficient of 0.69 (Latulippe, 2010).

2.2.2. Characteristic flow time

The fluid velocity profile in a membrane pore can cause elongation of DNA due to the difference in the velocity between the pore centerline and the wall. If the ultrafiltration membrane pores are modeled as well-defined cylinders with the length of L, the radial flow velocity profile inside each pore with fully developed parabolic flow regime is given as:

$$V(r) = \frac{\Delta P \times r_p^2}{4\mu L}\left(1 - \left(\frac{r}{r_p}\right)^2\right) \quad (2\text{-}8)$$

where ΔP is transmembrane pressure and r_p is the pore radius. Thus, the wall shear rate is derived as:

$$\gamma_{wall} = \frac{\Delta P \times r_p}{2\mu L} \quad (2\text{-}9)$$

The right side of Equation (2-9) can be re-written as Equation (2-11) using Hagen-Poiseuille equation (Equation (2-10))

$$Q_p = \frac{\Delta p \pi r_p^4}{8 \mu L} \tag{2-10}$$

$$\gamma_{wall} = \frac{4Q_p}{\pi r_p^3} \tag{2-11}$$

where Q_p is the volumetric filtrate flow rate through a single pore. Thus, the inverse of characteristic flow time is directly proportional to filtrate flux as (Cherkasov et al., 1993):

$$\gamma_{wall} = 4 \frac{J_v}{\varepsilon \times r_p} \tag{2-12}$$

where J_v is the filtrate flux (volumetric filtrate flow rate per total membrane area), and ε is the membrane porosity.

The converging flow field in the fluid approaching the membrane pore also creates velocity gradients that can elongate DNA, in this case because of the acceleration of the fluid as it approaches the pore. The flow velocity profile for flow into a single orifice in an infinite flat plane is given by Knudsen et al. (1996):

$$v(x) \cong \frac{Q}{2\pi x^2} \tag{2-13}$$

where x is vertical distance above the pore entrance and Q is the volumetric fluid flow rate through the pore. The inverse of characteristic time for this elongation flow can be evaluated by taking the gradient of Equation (2-13) giving:

$$\gamma_x \cong \frac{Q}{\pi x^3} = J_v \frac{r_p^2}{\varepsilon x^3} \tag{2-14}$$

In contrast to Equation (2-12), the sink-flow model predicts that the inverse of the characteristic time varies with the cube of the distance to the pore entrance (x^{-3}) and with the square of the pore radius square (r_p^2).

2.2.3. Critical flux

The converging flow field into a nanopore can cause elongation of DNA when De ≥ De_{crit}, typically with critical Deborah number set equal to 1. Daoudi and Brochard (1978) developed the first mathematical model for the critical flux for a flexible polymer chain:

$$J_{crit} \approx \left(\frac{\varepsilon R_g^3}{r_p^2}\right)\left(\frac{K_B T}{\mu R_g^3}\right) \tag{2-15}$$

based on the Rouse free-draining model for the polymer and the sink-flow model (Equation 2-14), with the critical distance from the pore set equal to the radius of gyration of the polymer. Cherkasov et al. (1993) evaluated the critical flux for flexible polymer chain transmission used the wall-shear rate model for the characteristic flow time (Equation 2-12) and the Rouse free-draining model for the characteristic elongation time (Equation 2-5) giving:

$$J_{crit} \approx \left(\varepsilon \times r_p\right)\left(\frac{K_B T}{\mu R_g^3}\right) \tag{2-16}$$

Equation (2-16) significantly over-predicted actual critical flux data obtained with dextran. Equation 2-15 predicts that the critical flux is independent of plasmid size, which is in agreement with data obtained by Latulippe and Zydney (2009). In contrast, Equation (2-16) predicts that the critical flux varies very strongly with the inverse cube of the radius of gyration of the plasmid.

Latulippe et al. (2007) obtained extensive data for the critical flux for transmission of a 3.0 kbp supercoiled plasmid DNA though different ultrafiltration membranes. They observed a significant increase of critical flux with decreasing pore

size, in good qualitative agreement with Equation (2-15) but inconsistent with Equation (2-16). Latulippe and Zydney (2009) hypothesized that the supercoiled plasmid can approach the membrane pore entrance much more closely than the radius of gyration, i.e. $x = \beta \times R_g$ giving:

$$J_{critical} = \frac{\pi}{6}\left(\frac{\varepsilon}{r_p^2}\right)\left(\frac{\beta^3 De_{critical}}{R_H/R_g}\right)\left(\frac{K_B T}{\mu}\right) \quad (2\text{-}17)$$

Equation (2-17) properly describes the dependence of the critical flux on the membrane pore size and porosity of membrane, solution viscosity and temperature, and plasmid size. It is also in qualitative agreement with data for different plasmid topology (Latulippe and Zydney, 2011), as well as type of salt and ionic strength of buffer solution (Latulippe and Zydney, 2008), both of which were thought to affect De_{crit}. Experimental data for supercoiled plasmids were well fit using $\beta = 0.12$ with $De_{crit} = 1$.

Chapter 3

Membrane fouling during ultrafiltration of plasmid DNA through semipermeable membranes

The work presented in this chapter was previously published in the Journal of Membrane Science (Borujeni, E.E., A. L. Zydney, Volume 450 (2014), pp. 189-196)

3.1. Introduction

Highly purified DNA is of interest in a number of very diverse applications. Gene therapy and DNA-based vaccines can provide novel treatment of different diseases by exploiting the ability of the DNA to code for unique proteins (Acland et al., 2001; Ginn et al., 2013). DNA provides the sensing elements in tests for genetic variations that predispose for specific diseases. DNA can also be used as a novel structural element in constructing complex nanostructures by exploiting the mechanical properties of DNA (Holzel et al., 2003; Li et al., 2011). DNA computers exploit the hybridization of complimentary DNA strands to rapidly explore a wide range of "solutions" to various optimization problems (Adleman, 1994).

The successful development of these diverse technologies requires cost-effective strategies for the large scale purification of plasmid DNA. Several studies have demonstrated the potential of using membrane ultrafiltration for DNA purification. Kahn et al. (2000) used tangential flow ultrafiltration to remove protein and RNA impurities from a DNA solution, with the purified DNA collected in the retentate solution. Nunes et

al. (2012) used microfiltration to remove cell debris and genomic DNA, with the plasmid DNA collected in the permeate. More recent studies have demonstrated that ultrafiltration can be used to separate different topological isoforms of DNA (linear, supercoiled, and open-circular) by exploiting the different extensional flexibility of the isoforms in the elongation flow field into a membrane pore (Latulippe and Zydney, 2011; Borujeni and Zydney, 2012).

Most of the previous studies of DNA ultrafiltration have been limited to relatively dilute solutions and short operating times, conditions under which the filtrate flux and DNA transmission typically remain relatively constant. In contrast, Arkhangelsky et al. (2011) obtained data for ultrafiltration of a 4.5 kbp plasmid DNA through a 20 kDa polyethersulfone membrane over longer filtration times and found that the filtrate flux and transmission both decreased with time, with an approximately linear relationship between these two quantities during a single experiment performed at constant transmembrane pressure. They attributed these changes to membrane fouling associated with the gradual blockage of the pores by the plasmid DNA, although there was no direct evidence for this fouling mechanism.

There have also been several studies of DNA fouling during microfiltration. For example, Affandy et al. (2013) examined the fouling behavior during plasmid filtration through 0.2 μm pore size sterilizing grade membranes. The flux decline data were best described by the intermediate pore blockage model during the initial stage of the fouling, with the longer term fouling best described by the standard blocking (pore constriction) model. This transition from external to internal fouling also corresponded to a reduction in plasmid transmission. However, it is not possible to extrapolate these results to the

behavior of plasmid DNA in much smaller pore size ultrafiltration membranes where the plasmid has to undergo significant elongation in order to enter into the very narrow membrane pores.

The objective of the work described in this Chapter was to obtain quantitative data for membrane fouling phenomena during ultrafiltration of more concentrated DNA solutions through semipermeable ultrafiltration membranes. Data were obtained over a variety of filtration conditions using two different pore size membranes and two different size plasmids. A new but very simple fouling model was developed to describe both the flux decline and the change in plasmid transmission based on the partial blockage of the membrane pores by individual plasmids, with these partially blocked pores allowing filtrate flow but being inaccessible to additional plasmids. The results provide important insights into the fouling behavior during ultrafiltration of plasmid DNA.

3.2. Material and Methods

3.2.1. Materials

3.2.1.1 Buffers

All the buffer solutions in this work were prepared by appropriate dilution of 100X concentrated Tris-EDTA (TE) buffer with deionized water obtained from a Barnstead Nanopure water purification system (Thermo Scientific, Dubuque, IA) with a resistivity greater than 18 MΩ. The concentrated Tris-EDTA buffer, purchased from Sigma-Aldrich (St. Louis, MO), contained 1 M Tris.HCl (pH = 8.0 ± 0.2) and 0.1 M

EDTA (Ethylenediaminetetraacetic acid) and was used to chelate metal ions like Ca^{2+} or Fe^{3+} thus preventing condensation of DNA molecules. Figure 3-1 shows the schematic structures of Tris.HCl and EDTA. The desired ionic strength of the buffer solution was adjusted by dissolving appropriate amounts of sodium chloride (NaCl) into the buffer. All buffer solutions were pre-filtered through 0.2 µm Supor®200 filters (Pall Corporation, Port Washington, NY), after which the conductivity and pH values were determined using a Thermo Orion 150A+ conductivity meter and a model 402 Thermo Orion pH meter (Beverly, MA), respectively. All buffers were stored at room temperature, 21 ± 1 ºC.

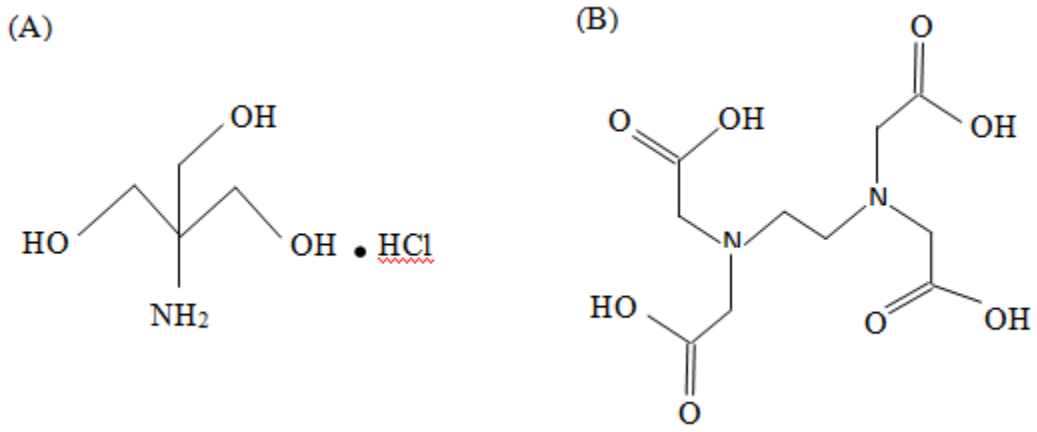

Figure 3-1: Schematic structures of (A) Tris.HCl and (B) EDTA.

3.2.1.2. Plasmid DNA solutions

The majority of data were obtained using supercoiled isoforms of a 2.9 kbp (kilo base pair) pBluescript II KS+ plasmid DNA (p-EMP) supplied by Stratagene and a 16.9 kbp plasmid (p-FDY) provided by Dr. Paula Clemens at the University of Pittsburgh.

The latter plasmid was generated by insertion of a 13.9 kbp DNA segment containing the gene sequence for human full-dystrophin into the NotI site of the pBluescript II KS- plasmid. The vectors maps and gene sequences of these plasmids are presented in Appendix. The stock solutions of plasmids, containing 200 μg/mL plasmids in Tris-EDTA buffer, were supplied by Aldevron (Fargo, ND) and stored in 110 μL aliquots at -20 ºC.

A few experiments were performed using the linear isoform of p-FDY plasmid, which was produced by enzymatic digestion of the supercoiled isoform using 2 U/μg plasmid of PaeR7I restriction enzyme (New England Biolabs, Ipswich, MA) added to 27.5 μg of the supercoiled p-FDY plasmid. The final volume of the digestion solution was adjusted to 275 μL by addition of deionized water with a resistivity greater than 18 MΩ. The digestion mixtures were incubated at 37°C for 3 hr and then purified using a QIAquick PCR purification kit (QIAGEN, Valencia, CA) which uses a silica-gel membrane to bind the DNA in high-salt buffer while the impurities are washed away. The DNA was then eluted using TE buffer without NaCl. The final concentrations were measured by a NanoDrop* 2000c UV spectrophotometer (Thermo Scientific) using the absorbance at 260 nm. The purified linear plasmids were stored at -20 °C.

The stored plasmids were thawed and then diluted with buffer to achieve to the desired final concentration. A rocker was used to mix the plasmid solutions for 20 min right before each experiment to insure complete dissolution and uniform concentration.

3.2.1.3. Membrane preparations

Omega polyethersulfone ultrafiltration disc membranes (Pall Corporation, Port Washington, NY) with 4.1 cm^2 effective filtration area and nominal molecular weight cut-off (MWCO) of 100 and 300 kDa were used in all experiments. According to the manufacturer, Omega membranes are modified composite polyethersulfone (PES) membranes that have hydrophilic characteristics with low non-specific adsorption and high flow rates. Membranes were initially flushed with 100 mL of deionized water to ensure removal of any wetting / storage agents like glycerin and sodium azide.

3.2.1.4. Filtration apparatus

Ultrafiltration experiments were conducted using an Amicon 8010 stirred cell from Millipore Co. (Billerica, MA), which was placed on a magnetic stir plate with the stirring speed adjusted to 730 rpm. The nominal hold up volume of the stirred cell was 10 mL. The cell uses 25 mm diameter membrane discs. The stirred cell was thoroughly rinsed with buffer and sonicated before each experiment. A 100 mL feed reservoir was connected to the stirred cell to maintain constant volume during the filtration experiments. The flux was adjusted by In air pressurization of the feed reservoir as shown in Figure 3-2.

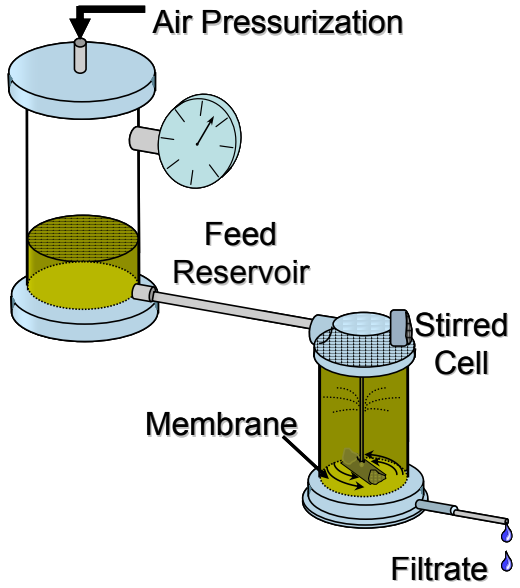

Figure 3-2: Schematic of experimental set-up used for ultrafiltration, adopted from (Latulippe, 2010).

3.2.2. Methods

3.2.2.1. Ultrafiltration experiments

The hydraulic permeability (L_p) of the membrane was evaluated from data for the filtrate flux (J_v) of the TE buffer solution as a function of applied transmembrane pressure (ΔP):

$$L_p = \frac{\mu J_v}{\Delta P} \tag{3-1}$$

In each case, permeate samples were obtained after at least 1 min of filtration to ensure stable operation. The filtrate flux was evaluated by timed collection and by weighing the permeate samples with an AG104 Mettler-Toledo analytical balance. The applied transmembrane pressure (TMP) was measured using a digital pressure gauge connected to the feed reservoir.

According to Hagen-Poiseuille equation (Zydney and Zeman, 1996), the permeability of the membrane can be used to estimate the membrane pore radius (r_p) as:

$$L_p = \frac{\mu . J_v}{\Delta P} = \frac{\varepsilon r_p^2}{8\delta} \quad (3\text{-}2)$$

where ε is the membrane porosity, δ is the membrane thickness, and μ is the solution viscosity. Equation (3-2) assumes that the membrane is composed of a parallel array of uniform cylindrical pores. All experiments were performed at room temperature, 21±1 ºC. Membranes were re-used as long as the change in membrane permeability was less than 10%.

Plasmid ultrafiltration experiments were performed immediately after evaluation of the membrane permeability by filling the stirred cell and feed reservoir with the desired plasmid solution. A feed sample initially was taken from the stirred cell before starting the experiment. Ultrafiltration experiments were performed either at constant filtrate flux, which was set using a Dynamax peristaltic pump connected to the filtrate line, or at constant transmembrane pressure (set using air pressurization). The first permeate sample was taken after flushing at least 1 mL of feed solution through the membrane to insure wash out of the dead volume beneath the membrane and in the permeate exit tube. 150-200 μL filtrate samples were collected at specific times during the course of experiment, with the filtrate flux determined as explained above.

Plasmid sieving coefficients were evaluated by measuring the plasmid concentration in samples taken from both the permeate and the retentate solution in the stirred cell (after stopping the ultrafiltration). This process was repeated for 7 to 8 different pressures.

3.2.2.2. PicoGreen assay

Total plasmid concentrations were measured using Quant-iT PicoGreen dsDNA assay kit (Life technologies, Carlsbad, CA). PicoGreen is a fluorescent dye widely used in DNA quantification; its structure is shown in Figure 3-3. The dye binds to DNA in the minor groove region through intercalation and electrostatic interactions which provides more than a 1000-fold enhancement in the intensity of the emitted fluorescence compared to the free dye (Dragan et al., 2010).

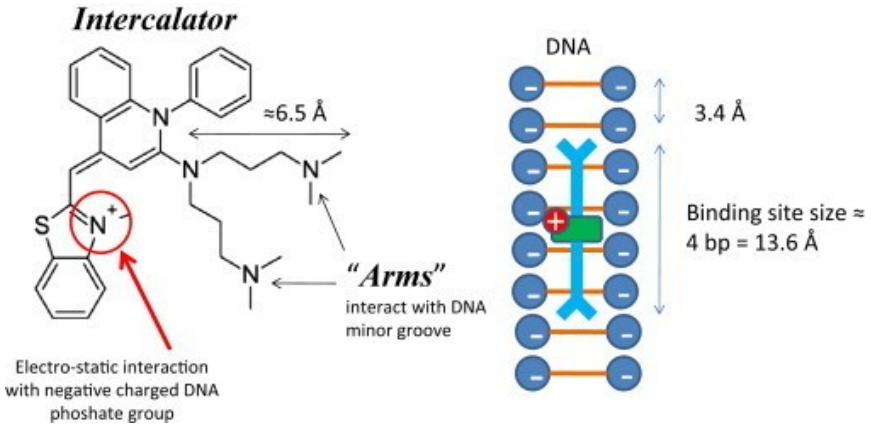

Figure 3-3: The schematic structure of PicoGreen dye showing binding sites of intercalation and electrostatic interactions with DNA, adopted from (Dragan et al., 2010).

70 µL samples were loaded into the wells of a 96-well black plate supplied by VWR (Philadelphia, PA) along with an equal amount of a 200:1 diluted solution of the PicoGreen dye and 20:1 diluted solution of the TE buffer. Several plasmid solutions having known concentrations, in the range from 0 (i.e. buffer) to 1 µg/mL, were made and loaded into the plate as internal calibration standards. Samples were mixed for 10 min at 36°C using an orbital shaker inside A GENiosFL microplate reader. Excitation

was at 485 nm and the emitted fluorescent intensity was measured at 535 nm. A calibration line of concentration versus intensity was made from the known samples, with the actual concentrations determined using the resulting calibration. Samples with concentrations greater than 1 μg/mL were diluted to insure that they were in the linear range. All dilutions were done using buffer with the same ionic strength as the sample (Latulippe, 2010).

The observed sieving coefficient, S_o, which provides a measure of the extent of plasmid transmission through the membrane was evaluated as:

$$S_o = \frac{C_{filtrate}}{C_{feed}} \tag{3-3}$$

The filtrate concentration was evaluated as the average of that obtained in multiple samples, while the feed concentration was typically determined as the average of the concentration in samples obtained from the stirred cell before and after collection of the filtrate sample(s).

3.2.2.3. Agarose gel electrophoresis (AGE)

Agarose gel electrophoresis (AGE) was used to examine the integrity of the plasmid DNA. A 0.7% (w/w) agarose solution was prepared by dissolving 0.32 g OmniPur® agarose powder (EMD Millipore, Billerica, MA) in 45 mL of Tris-Acetate-EDTA buffer (Mediatech Inc., Manassas, VA). 4.5 μL of Gel Star nucleic acid gel stain (Lonza, Allendale, NJ) was added and the resulting solution was cast into an Owl B2 EasyCast mini gel electrophoresis system with a 12-tooth comb. 15 μL samples of the plasmid DNA and 3 μL of loading dye (New England Biolabs, Ipswich, MA) were

loaded into each well. Electrophoresis was conducted using an applied electric field of 45-50 V for 1-2 hr, with the gel imaged using a Fluorchem FC2 image system.

3.3. Results and Analysis

3.3.1. Permeability evaluation

The 100 kDa Omega membranes had a permeability of $L_p = 3.6 \pm 0.2 \times 10^{-9}$ m/s/Pa while the 300 kDa membranes had $L_p = 5.0 \pm 0.2 \times 10^{-9}$ m/s/Pa both in the range reported by the manufacturer. These values correspond to pore radii of 5.0 and 6.3 nm, respectively, using a membrane porosity of $\varepsilon = 0.5$ and a membrane thickness of $\delta = 0.5$ μm using Eq. (3-2).

3.3.2. Fouling phenomena

Figure 3-4 shows typical data for the filtrate flux and the observed sieving coefficient, S_o, as a function of time during ultrafiltration of the supercoiled 16.9 kbp plasmid through a single 100 kDa membrane at a constant transmembrane pressure of 16.5 kPa giving an initial filtrate flux of 55 x 10^{-6} m/s (corresponding to 200 L/m^2/h). Results are shown for 3 separate experiments at feed concentrations of 0.28 x 10^{-3}, 1.2 x 10^{-3}, and 7.2 x 10^{-3} kg/m^3 (corresponding to 0.28, 1.2, and 7.2 μg/mL) in a Tris-EDTA buffer with 150 mM NaCl. Data obtained with other membranes under the same conditions showed similar trends, although the actual values of the filtrate flux and sieving coefficient were somewhat different due to the inherent membrane-to-membrane

variability in pore size and hydraulic permeability. The initial plasmid sieving coefficient was approximately $S_o = 0.78 \pm 0.03$ for all 3 experiments even though the average pore radius of the 100 kDa membrane (5.0 nm) is more than an order of magnitude smaller than the radius of gyration of the 16.9 kbp plasmid (estimated as 169 ± 4 nm based on static light scattering data (Latulippe and Zydney, 2010)). The high plasmid transmission is due to flow-induced elongation of the DNA in the converging flow field above the membrane pore as discussed by Latulippe and Zydney (2009). There was no evidence of any DNA fragmentation during the ultrafiltration; samples obtained from the permeate solution provided a single sharp band in the agarose gel electrophoresis at exactly the same location as a sample from the feed solution.

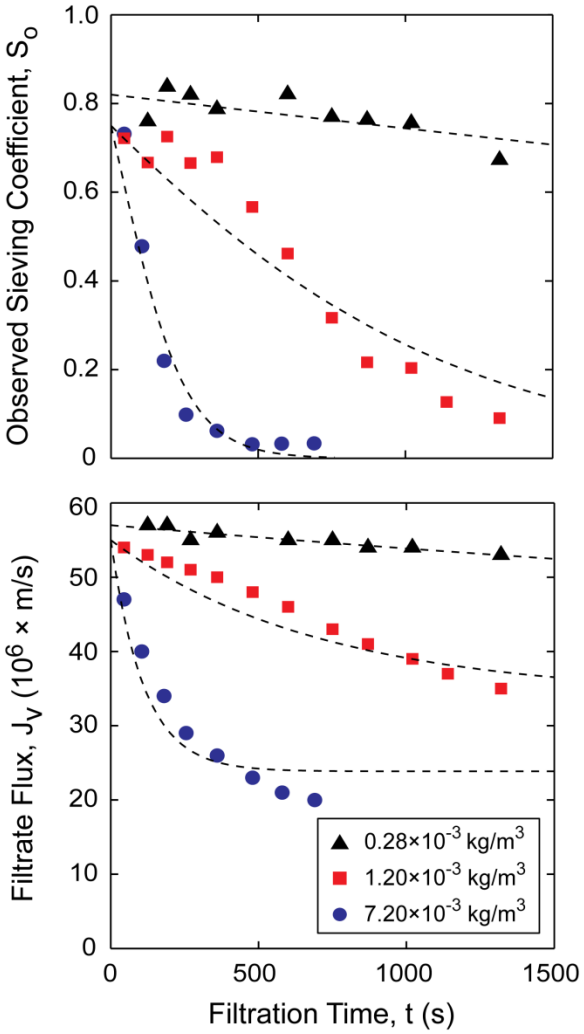

Figure 3-4: Effect of plasmid concentration on the filtrate flux and observed sieving coefficient of the 16.9 kbp supercoiled plasmid during constant pressure ultrafiltration at 16.5 kPa through a 100 kDa Omega membrane. The dashed curves are model calculations using parameters values in Table 3-1.

The filtrate flux and plasmid sieving coefficient both remained nearly constant during ultrafiltration of the most diluted plasmid solution (0.28 x 10^{-3} kg/m^3), indicating that there was no significant fouling under these conditions. This was confirmed by measurements of the membrane hydraulic permeability before and after the plasmid ultrafiltration, with these values differing by less than 3%. In contrast, the filtrate flux for

the 1.2 x 10^{-3} kg/m^3 solution decreased by more than 30% after 20 min of filtration (corresponding to 55 L/m^2 of filtrate volume per unit membrane area), while the sieving coefficient decreased by more than a factor of 3 over this same time period. The decline in flux and sieving coefficient were even more pronounced for the 7.2 x 10^{-3} kg/m^3 solution, with J_v decreasing by a factor of 2.5 and S_o dropping to nearly zero (greater than 97% retention) after only 10 min (approximately 20 L/m^2). The permeability values for the fouled membranes also showed a significant amount of irreversible fouling, with L_p/L_{po} = 0.93 after filtration of the 1.2 x 10^{-3} kg/m^3 solution and 0.88 for the 7.2 x 10^{-3} kg/m^3 solution. The dashed curves in Figure 3-4 are model calculations developed subsequently in Section 3.3.3.

The large decline in plasmid sieving coefficient seen in Figure 3-4 could be due at least in part to the flux dependence of the plasmid transmission (even in the absence of fouling) associated with the flow-induced elongation of the plasmid DNA. For example, Latulippe and Zydney (2007) evaluated the sieving coefficient of a dilute solution of the 16.9 kbp supercoiled plasmid through a 1000 kDa Ultracel membrane as a function of filtrate flux under conditions where there was no measurable fouling and found that S_o decreased from S_o = 0.45 at a flux of 40 x 10^{-6} m/s (140 L/m^2/h) to S_o = 0.08 at a flux of 16 x 10^{-6} m/s (58 L/m^2/h). In order to separate out the effects of the filtrate flux (plasmid elongation) and fouling on plasmid transmission, a series of experiments were performed at a constant filtrate flux of approximately 55 x 10^{-6} m/s (200 L/m^2/h), which was maintained by placing a pump on the permeate exit line from the stirred cell. The results for experiments using 0.24 x 10^{-3}, 1.1 x 10^{-3}, and 7.4 x 10^{-3} kg/m^3 solutions are shown in Figure 3-5. The dashed curves are again model calculations. The plasmid sieving

coefficient for the dilute solution again remained essentially constant throughout the ultrafiltration, while the transmission at the higher plasmid concentrations declined significantly over the course of the filtration. The change in sieving coefficient seen at constant filtrate flux was, however, somewhat less pronounced than that seen at constant transmembrane pressure. For example, the sieving coefficient for the 1.1 x 10^{-3} kg/m^3 solution after a volumetric throughput of 53 L/m^2 was S_o = 0.37 for the run at constant flux compared to only S_o = 0.13 at constant pressure, consistent with the drop in filtrate flux for the constant pressure filtration (from 55 x 10^{-6} m/s at the start to 37 x 10^{-6} m/s at this point in the ultrafiltration experiment). In addition, the data in the most dilute solution actually seemed to show a slight increase in sieving coefficient during the ultrafiltration. This is discussed in more detail subsequently.

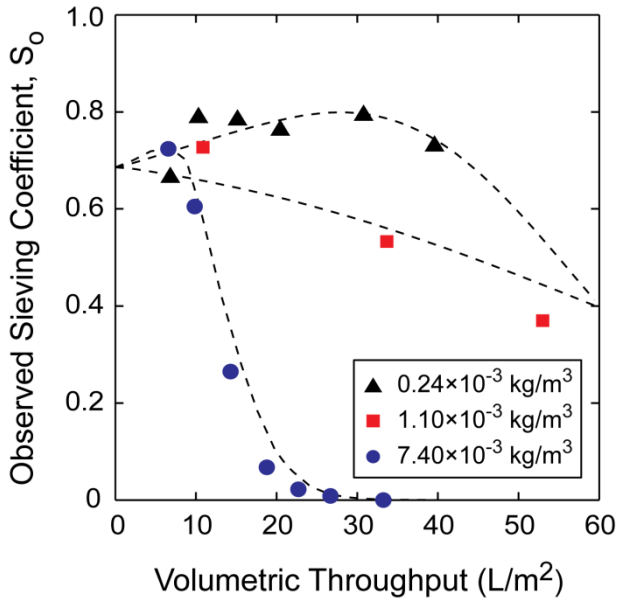

Figure 3-5: Effect of plasmid concentration on the observed sieving coefficient of a 16.9 kbp supercoiled plasmid through a 100 kDa Omega membrane at a constant filtrate flux of 55 x 10^{-6} m/s. Dashed curves are model calculations using parameter values in Table 3-1.

Figure 3-6 shows the effects of the plasmid size on the ultrafiltration behavior. The results for the 16.9 kbp plasmid (p-FDY) are taken from Figure 3-4; the curves are the model calculations. The data for the 2.9 kbp plasmid (p-EMP) were obtained with a separate membrane using a 6.8×10^{-3} kg/m^3 solution in TE buffer with 150 mM NaCl at a constant transmembrane pressure of 14 kPa, giving an initial filtrate flux of 50×10^{-6} m/s. The initial plasmid transmission was slightly greater for the 2.9 kbp plasmid, which is probably due to the small difference in initial filtrate flux (50×10^{-6} m/s for 2.9 kbp plasmid vs. 47×10^{-6} m/s for the 16.9 kbp plasmid) in combination with inherent membrane-to-membrane variability. However, the sieving coefficient of the 2.9 kbp plasmid declined much more slowly than that of the 16.9 kbp plasmid, with the sieving coefficient remaining above $S_o = 0.5$ after filtration of 23 L/m^2 while the sieving coefficient of the 16.9 kbp plasmid decreased to below $S_o = 0.05$ after only 20 L/m^2.

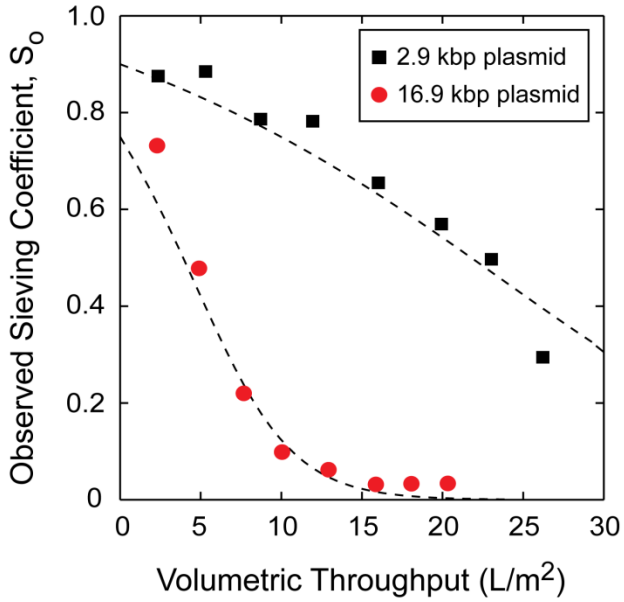

Figure 3-6: Effect of plasmid size on transmission of the supercoiled plasmid through a 100 kDa Omega membrane. Data obtained with a 7.2 x 10^{-3} kg/m3 solution of the16.9 kbp plasmid and a 6.8 x 10^{-3} kg/m^3 solution of the 2.9 kbp plasmid at constant transmembrane pressure (initial filtrate flux of approximately 50 x 10^{-6} m/s for both experiments). Dashed curves are model calculations using parameter values in Table 3-1.

3.3.3. Fouling model

It is now well established that transmission of large plasmids through relatively small pore size ultrafiltration membranes occurs by the flow-induced elongation of the plasmid DNA in the converging flow field entering into the membrane pores (Latulippe et al., 2007; Latulippe and Zydney, 2009; Arkhangelsky et al., 2011). There is also limited theoretical work (Rosa et al., 2012) demonstrating that "knots" in polymer chains like DNA can cause the polymer to become trapped or "jammed" during translocation through a nanopore, i.e., in a pore with size much less than the radius of gyration of the polymer. Rosa et al. (2012) hypothesized that the presence of topological constraints like

knots in the plasmid DNA structure could cause clogging in nanopores used for DNA sequencing, halting the translocation of the DNA and providing an upper limit on the length of the DNA sequence that can be read using nanopore technology. This physical picture is also consistent with experimental observations by Li et al. (2003) on the translocation and trapping of a linear 10 kbp through a 3-nm ion-sculpted nanopore. This type of DNA trapping could potentially be responsible for the observed reduction in DNA transmission seen in Figures 3-4 to 3-6.

A simple mathematical model for this behavior was developed as follows. The total volumetric flow rate through the membrane is given by the sum of the flow rate through the blocked and open (unblocked) pores:

$$Q = J_{blocked}A_{blocked} + J_{open}A_{open} \tag{3-5}$$

where we have assumed that the blocked or jammed pores still allow at least some pressure-driven flow around the trapped plasmid. In contrast, the blocked pores should be completely impermeable to the transport of additional plasmids; thus, the plasmid sieving coefficient is given as:

$$S_o = \frac{J_{open}A_{open}S_{open}}{Q} \tag{3-6}$$

where S_{open} is the plasmid sieving coefficient through the open pores. Equations (3-5) and (3-6) can be rewritten in terms of the fraction of open pores, $f = \frac{A_{open}}{A \times \epsilon}$, as:

$$\frac{J_v}{J_{open} \times \varepsilon} = \beta + f(1 - \beta) \tag{3-7}$$

$$\frac{S_o}{S_{open}} = \frac{f}{\beta + f(1-\beta)} \tag{3-8}$$

where A is the membrane surface area, ε is the membrane porosity (ratio of fractional pore area to membrane area), J_{open} is the filtrate flux through the open pores, and β is equal to the ratio of the flow rate through a blocked pore to that through an open pore. For operation at constant transmembrane pressure, the filtrate flux through the open pores is a constant equal to the initial flux through the membrane (J_o) divided by the membrane porosity.

Equations (3-7) and (3-8) can be combined to develop a direct relationship between the sieving coefficient and the flux decline:

$$\frac{S_o}{S_{open}} = \frac{1}{(1-\beta)} - \frac{\beta}{(1-\beta)}\left[\frac{J_o}{J_v}\right] \tag{3-9}$$

The data from Figure 3-4 for the 1.2 x 10^{-3} kg/m^3 plasmid concentration have been re-plotted in Figure 3-7 in the form suggested by Equation (3-9). The data collapse to a single line when plotted in this fashion with $r^2 = 0.96$. The best fit value of β can be calculated directly from the slope and intercept of the linear regression fit as $\beta = 0.63 \pm 0.01$. Note that Arkhangelsky et al. (2011) found a linear relationship between the observed sieving coefficient and the filtrate flux in their plasmid ultrafiltration experiments, in contrast to the dependence on $1/J_v$ given in Equation (3-9). However, the data obtained by Arkhangelsky et al. were over a fairly limited range of filtrate flux (less than 40% flux decline), which is insufficient to accurately determine the relationship between the sieving coefficient and flux. Re-plotting the data of Arkhangelsky et al. in the form given by Equation (3-9) also provided a linear relationship with $r^2 > 0.9$ (results not shown).

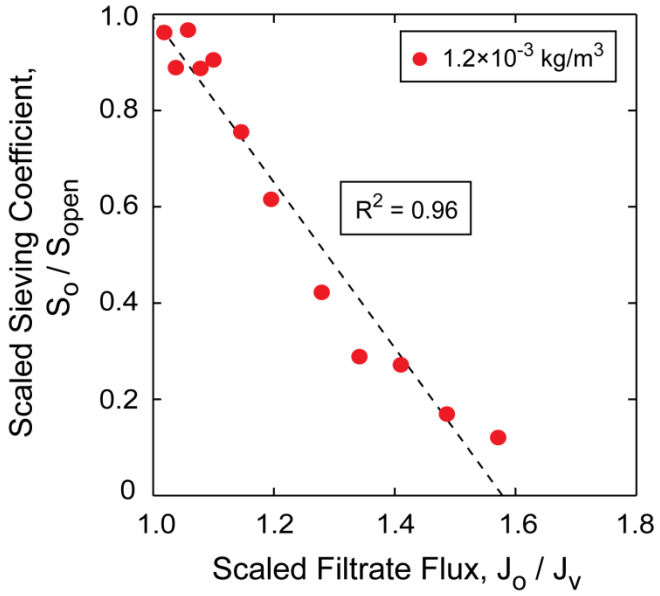

Figure 3-7: Scaled values of the observed sieving coefficient for the 1.2 x 10^{-3} kg/m3 solution of the 16.9 kbp plasmid (data from Figure 3-4) plotted in the form given by Equation (3-9).

In order to calculate the sieving coefficient and flux as a function of time, one needs to develop a relationship for the fraction of open pores during the ultrafiltration. The rate of pore blockage was assumed to be directly proportional to the rate at which the DNA enters the open pores:

$$\frac{df}{dt} = -k(J_{open} C_{feed} S_{open} f) \qquad (3\text{-}10)$$

where the flux and sieving coefficient through the open pores will both be constant during a constant pressure ultrafiltration. Although the feed concentration in the stirred cell will increase with time due to plasmid retention, this effect is negligible for the small filtration volumes (relative to the volume of the stirred cell) examined in our experiments, thus C_{feed} is also approximately constant (independent of time). Under these conditions, Equation (3-10) can be immediately integrated to give:

$$f = \exp\left[-k\,(J_o/\varepsilon)C_{feed}S_{open}t\right] \tag{3-11}$$

The dashed curves shown previously in Figures 3-4 and 3-6 show the calculated values of the observed sieving coefficient and filtrate flux given by Equations (3-7), (3-8), and (3-11), with $\varepsilon = 0.5$ and the best fit values of β and k determined by using the penalty optimization method which minimizes the weighted sum of squared residuals between the model and data for both the observed sieving coefficient and the filtrate flux. Calculations were performed with S_{open} set equal to the initial sieving coefficient in each experiment. The model calculations are in good agreement with data for both the flux and sieving coefficient throughout the ultrafiltration experiments. The model accurately captures the very rapid decay in the sieving coefficient at the highest plasmid concentration and the near absence of any fouling for the 0.28×10^{-3} kg/m^3 solution seen in Figure 3-4 as well as the different curvature in the S_o data for the 2.9 and 16.9 kbp plasmids seen in Figure 3-6. The model does tend to slightly overpredict the filtrate flux at long times; the data in Figure 3-4 for the 7.2×10^{-3} kg/m^3 solution clearly show a small continued decline in filtrate flux at long times while the partial pore blockage model predicts that the filtrate flux approaches a constant value of $J_v/J_o = \beta = 0.43$ at very long filtration times, i.e., when all of the pores are blocked. This behavior could be due to some type of additional fouling at long times, e.g., the formation of a deposited layer of retained plasmid on the external surface of the membrane over the blocked pores. This plasmid deposit would provide an additional resistance to flow, leading to a reduction in the value of β at long times. Additional data at much longer filtration times would be needed to clarify this behavior.

The best fit values of β and k for each of the ultrafiltration experiments are summarized in Table 3-1. The best fit values of β were very similar for the different plasmid concentrations as expected. The β value for the 2.9 kbp plasmid may be slightly smaller than those for the 16.9 kbp plasmid, although additional data would be required to verify this behavior. The pore blockage parameter k is also essentially independent of the plasmid concentration; the smaller value of k for the 0.28 x 10^{-3} kg/m^3 solution is not statistically significant given the very small amount of fouling seen with this dilute solution. The pore blockage parameter is greater for the larger plasmid, which is consistent with the higher probability of knot formation in larger DNA molecules as determined from Monte Carlo simulations (Rybenkov et al., 1993).

Table 3-1: Best fit values of β and k for plasmid ultrafiltration experiments in Figures 3-4 to 3-6.

Plasmid size (kbp)	**Operation**	**Plasmid Concentration (x 10^{-3} kg/m^3)**	**β**	**k (x 10^4 m^2/kg)**
16.9	Constant Pressure	7.2	0.43	1.5
16.9	Constant Pressure	1.2	0.62	1.4
16.9	Constant Pressure	0.28	0.61	0.6
2.9	Constant Pressure	6.8	0.34	0.3
16.9	Constant Flux	7.4	0.42	0.7
16.9	Constant Flux	1.1	0.65	0.9
16.9	Constant Flux	0.24	0.35	5.5

The fouling behavior is somewhat more complex during ultrafiltration at constant filtrate flow rate since the increase in transmembrane pressure will cause an increase in the filtrate flux through the open pores. However, the ratio of the filtrate flux through the blocked and open pores will remain constant, assuming that β is independent of the transmembrane pressure, with the flux through the open pores directly related to the fraction of pores remaining open:

$$\frac{J_{open}}{J_v/\varepsilon} = \frac{1}{f+\beta(1-f)} \tag{3-12}$$

In this case, the filtrate flux through the membrane (J_v) remains constant throughout the filtration. The plasmid sieving coefficient is still given by Equation (3-7), but S_{open} is now a function of time due to the increase in filtrate flux, and thus the degree of elongation, through the open pores.

A relationship between S_{open} and J_{open} was developed by conducting a set of sieving experiment using a 0.25 x 10^{-3} kg/m^3 solution of a 16.9 kbp plasmid transmitted through the 100 kDa Omega membrane. Since very dilute solutions were utilized, no fouling occurred during these experiments so that $S_{open} = S_o$ and $J_{open}=J_v/\varepsilon$. Figure (3-8) shows the resulting data which could be well-described by a simple linear relationship (for $\varepsilon = 0.5$):

$$S_{open} = 7.23 \times 10^3 J_{open} - 0.11 \tag{3-13}$$

with J_{open} in units of m/s. Equation (3-13) is valid for $J_{open} > 15\times10^{-6}$ m/s.

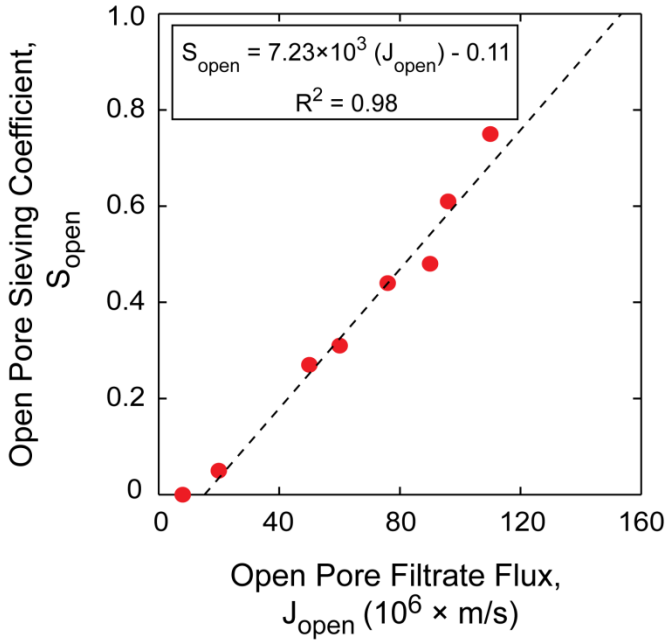

Figure 3-8: Observed sieving coefficient of the 16.9 kbp plasmid in TE buffer containing 150 mM NaCl as a function of filtrate flux during ultrafiltration through the 100 kDa Omega membranes. The dashed line is the linear regression fit to the data.

The dashed curves in Figure 3-5 are model calculations developed by numerical solution of Equations (3-6), (3-10), and (3-12) with S_{open} a function of J_{open} as given by Equation (3-13). The model calculations are in good agreement with the data at all 3 plasmid concentrations. The model predicts a small increase in the plasmid sieving coefficient at the start of the ultrafiltration due to the increase in S_{open} associated with the increase in transmembrane pressure and the corresponding increase in filtrate flux through the open pores (curves in Figure 3-5). The sieving coefficient in the most concentrated plasmid solution declines very rapidly to $S_o < 0.01$ after 30 L/m^2 due to the partial blockage of all of the membrane pores.

The sieving coefficient data from Figures 3-4 and 3-5 have been re-plotted in Figure 3-9, with the model calculations performed using a single value of the flow

parameter ($\beta = 0.46$) with the best fit values of k determined for each data set by minimizing the weighted sum of the squared residuals. The data collapse along the 45° line as expected using only a single value of β, suggesting that the flow rate parameter is independent of the plasmid concentration, the plasmid size, and the magnitude of the filtrate flux (or transmembrane pressure).

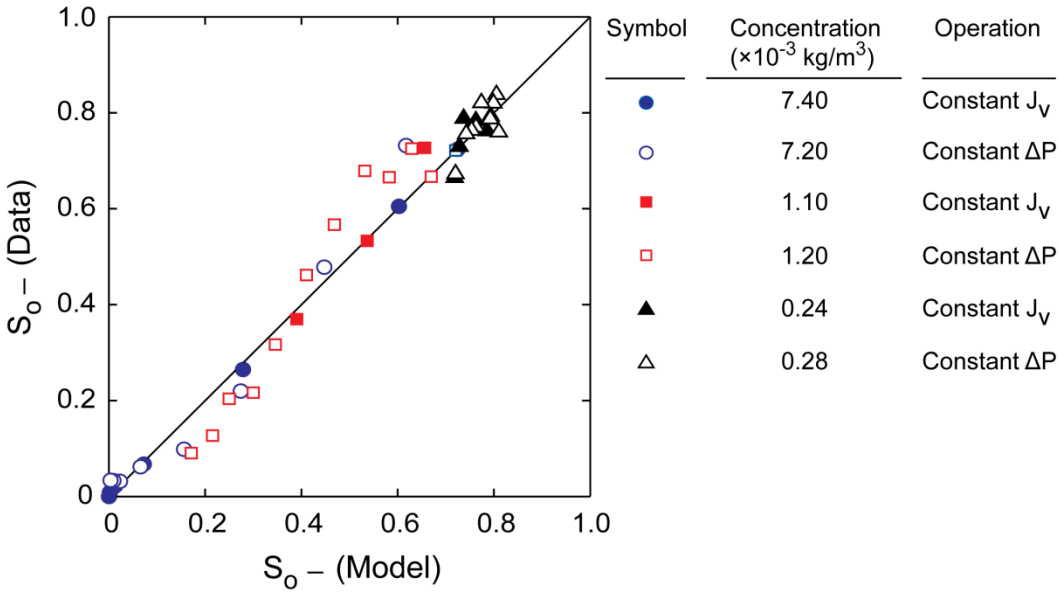

Figure 3-9: Comparison of experimental and predicted values of the plasmid sieving coefficients for the 16.9 kbp plasmid over a range of concentrations at both constant pressure and constant filtrate flux.

3.3.4. Hydrodynamic effects

Figure 3-10 shows the effects of the initial filtrate flux on the transmission of a 6.2 x 10^{-3} kg/m^3 solution of the supercoiled 16.9 kbp p-FDY plasmid through the 100 kDa Omega membrane. Data were obtained in two separate experiments, each performed with a fresh membrane, at constant filtrate flux of 30 and 55 x 10^{-6} m/s. The initial values of the observed sieving coefficients increase with increasing filtrate flux as expected due

to the greater elongation of the plasmid at high J_v. However, the rate of flux decline is much more rapid for the experiment performed with the higher filtrate flux, even when the data are plotted as a function of the volumetric throughput. Thus, the observed sieving coefficient for the experiment with $J_v = 55 \times 10^{-6}$ m/s was only $S_o = 0.05$ after filtration of approximately 19 L/m^2 (corresponding to 6 min of filtration), which is more than a factor of two smaller than the plasmid sieving coefficient at a $J_v = 30 \times 10^{-6}$ m/s after the same volumetric throughput (corresponding to 11 min of ultrafiltration). The dashed curves are the model calculations for operation at constant flux using $\beta = 0.46$ and $k = 1.1 \times 10^4$ m^2/kg at $J_v = 55 \times 10^{-6}$ m/s and $k = 1.6 \times 10^4$ m^2/kg at $J_v = 30 \times 10^{-6}$ m/s. The model is in good agreement with the data, with the small differences in the values of pore blockage parameter being statistically not significant.

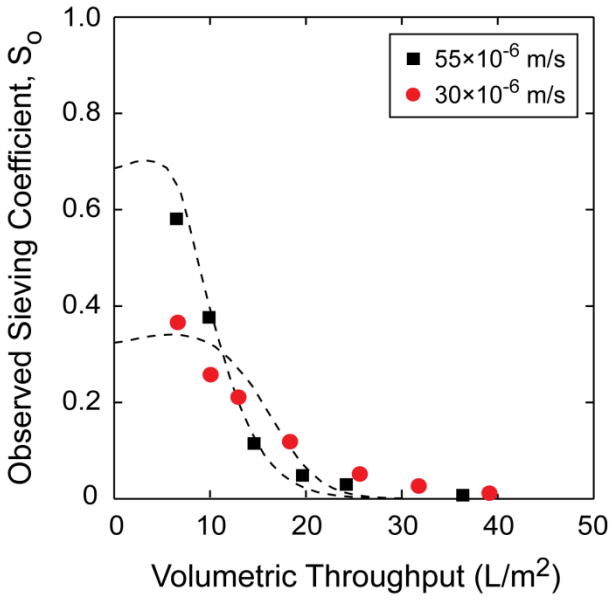

Figure 3-10: Effect of filtrate flux value on the observed sieving coefficient of a 6.2 x 10^{-3} kg/m3 solution of the 16.9 kbp plasmid in TE buffer with 150 mM NaCl during constant flux filtration through two separate 100 kDa Omega membranes. Dashed curves are model calculations with $\beta = 0.46$ and $k = 1.1 \times 10^4$ m^2/kg and 1.6×10^4 m^2/kg at $J_v = 55$ and 30×10^{-6} m/s, respectively.

The increased fouling seen at high filtrate flux could be due to concentration polarization effects, i.e., the accumulation of retained plasmid at the upstream surface of the membrane. In order to examine this effect in more detail, a set of experiments was performed at constant filtrate flux using a 7.4×10^{-3} kg/m^3 solution of the 16.9 kbp plasmid, one with a stirring speed of 730 rpm and one with the stirrer turned off (Figure 3-11). The observed sieving coefficients for the two experiments were essentially identical, with S_o declining from around $S_o = 0.3$ to essentially zero after filtration of 20 L/m^2. The lack of any effect of stirring on the initial values of the sieving coefficient is consistent with the flow-induced elongation model presented by Latulippe et al. (2007), which was developed using data for very dilute plasmid solutions in which the flux and sieving coefficient remained constant throughout the filtration. The similarity in the filtrate flux and sieving coefficient data at 0 and 730 rpm throughout the ultrafiltration suggests that concentration polarization has no effect on plasmid fouling in these experiments, i.e., the flow and pore blockage parameters (β and k) appear to be independent of stirring. In contrast to the results in Figure 3-11, Morao et al. (2009; 2011) observed a small decrease in transmission of both linear and supercoiled plasmid DNA with increasing stirring speed for ultrafiltration of a 6.05 kbp plasmid through a 0.03 μm pore size polycarbonate membrane and also through a polyacrylonitrile XM300 (300 kDa) membrane. The reason for this discrepancy is unclear, although it is worth noting that Morao et al. found no effect of stirring on the sieving coefficient of the supercoiled plasmid through a cellulosic YM100 (100 kDa) membrane (Morao et al., 2011) .

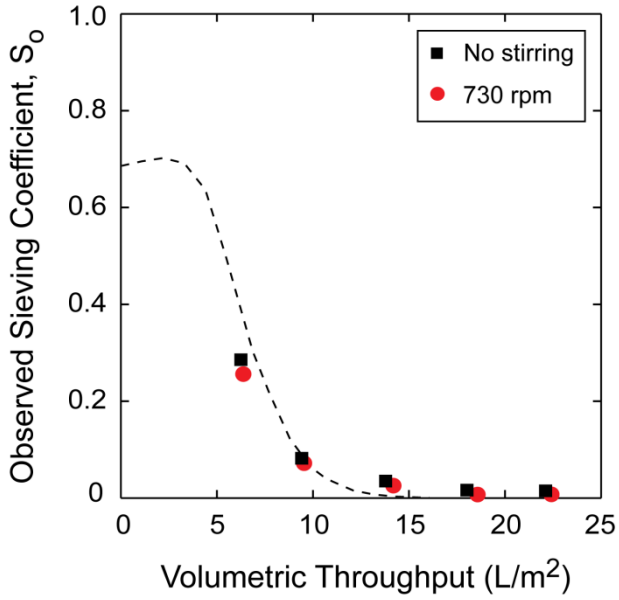

Figure 3-11: Effect of stirring on the ultrafiltration of a 7.4 x 10^{-3} kg/m3 solution of the 16.9 kbp supercoiled plasmid through a 100 kDa Omega membrane at a constant filtrate flux of 55 x 10^{-6} m/s. Dashed curves are model calculations using $\beta = 0.46$ and $k = 1.6 \times 10^4$ m^2/kg.

The data in Figure 3-11 were obtained with the same membrane but in two separate experiments performed on different days; the permeability of the membranes were within 5%. The somewhat smaller values of the initial sieving coefficients seen in Figure 3-11 (compared to the data in Figure 3-4) could be associated with small changes in the effective membrane pore size after multiple ultrafiltration experiments. An additional experiment was thus performed in which the ultrafiltration began without stirring but the stirrer was then turned on at some point during the experimental run (without stopping the filtration). Results are shown in Figure 3-12 for a 1.0 x 10^{-3} kg/m^3 solution of the 16.9 kbp plasmid at a constant transmembrane pressure of 11 kPa. The small increase in the sieving coefficient at the start of the experiment (which was seen only in some experiments) is due in part to dilution of the initial samples by the hold-up

volume beneath the membrane and in the filtrate exit line. It is also possible that there is a small time lag in the development of the flow field upon application of the air pressure.

The initiation of stirring (after filtration of 18 L/m^2) caused a small but significant increase in the plasmid sieving coefficient (upper panel), but there was no measurable effect on the filtrate flux (lower panel). The plasmid sieving coefficient decreased quickly (after initiation of the stirring) and then appears to follow the same basic trend seen during the initial ultrafiltration in the absence of stirring. The transient increase in the plasmid sieving coefficient seen upon application of stirring is likely due to plasmids that were originally retained in a thin deposit formed above the "blocked" pores. The tangential flow associated with the stirring could move these plasmids away from the "blocked" pores so that they are now able to elongate and pass through the open pores. Once this "bolus" of plasmid DNA passes through the membrane, the measured sieving coefficient should return to the expected value (determined by the fraction of open pores), consistent with the experimental data in Figure 3-12. The absence of any measurable effect of the stirring on the decline in plasmid sieving coefficient provides further support for the physical picture that the fouling is due to plasmids becoming trapped within the pore structure, a phenomenon that would be expected to depend on the geometry of the pore and the properties of the plasmid (and not the device hydrodynamics).

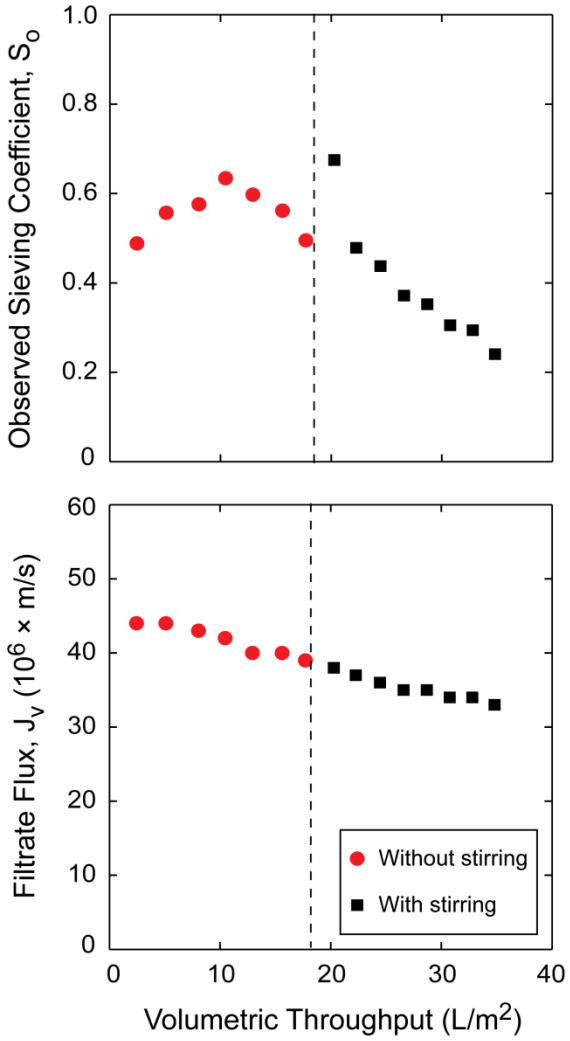

Figure 3-12: Ultrafiltration of a 1.0 x 10^{-3} kg/m3 solution of the 16.9 kbp supercoiled plasmid through a 100 kDa Omega membrane at a constant transmembrane pressure of 11 kPa first without and then with stirring. Stirring was initiated after filtration of 18 L/m^2 as shown by the dashed vertical line.

Figure 3-13 shows data for the ultrafiltration of a 7.2 x 10^{-3} kg/m^3 solution of the 16.9 kbp plasmid through Omega ultrafiltration membranes with nominal molecular weight cut-offs of 100 and 300 kDa, corresponding to mean pore size of approximately 10 and 35 nm, respectively, as reported by manufacturer. The transmembrane pressure was adjusted so that the initial filtrate flux was J_o = 55 x 10^{-6} m/s for both experiments.

The initial plasmid sieving coefficient is greater for the 300 kDa membrane, consistent with predictions of the flow elongation model (Latulippe and Zydney, 2009). The plasmid transmission declined much more rapidly with the smaller pore size (100 kDa) membrane, with the sieving coefficient through the 100 kDa membrane decreasing to zero after filtration of only 15 L/m^2 while S_o for the 300 kDa membrane remained above 0.5 even after a volumetric throughput of more than 25 L/m^2. The best fit value of k for the 100 kDa membrane (k = 1.5 x 10^4 m^2/kg) is approximately 7 times larger than that for the 300 kDa membrane (k = 0.2 x 10^4 m^2/kg), indicating that the plasmids are more likely to get "trapped" in the smaller pores.

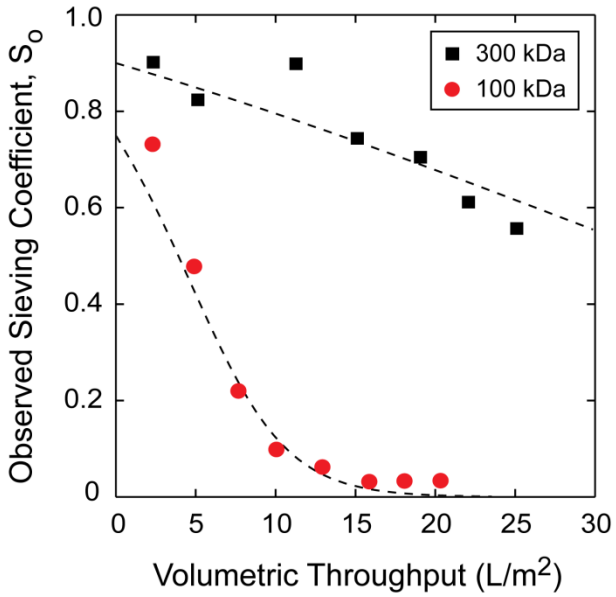

Figure 3-13: Effect of membrane pore size on the observed sieving coefficient of a 16.9 kbp supercoiled plasmid. Data were obtained at constant transmembrane pressure using a 7.2 x 10^{-3} kg/m^3 solution with an initial filtrate flux of 55 x 10^{-6} m/s. Dashed curves are model calculations with β = 0.46 and k = 1.5 x 10^4 m^2/kg for the 100 kDa membrane and k = 0.2 x 10^4 m^2/kg for the 300 kDa membrane.

3.3.5. Plasmid topology effects

A set of ultrafiltration experiment was also performed using 1.2 x 10^{-3} and 7.2 x 10^{-3} kg/m^3 solutions of the linear isoform of the 16.9 kbp plasmid through a 100 kDa membrane at constant filtrate flux. Results are shown in Figure 3-14, with the observed sieving coefficient plotted as a function of the volumetric throughput. In contrast to the results with the supercoiled isoform (Figure 3-4), there is very small decline in the sieving coefficient (< 10%) even for the more highly concentrated solution; the supercoiled plasmid was nearly completely rejected after a throughput of only 20 L/m^2. The low fouling behavior indicates that the linear isoform does not get trapped in the pores, possibly due to the small diameter of the linear DNA even in the presence of a small number of knots. This hypothesis is in agreement with data obtained by Li et al. (2003) for a 10 kb linear DNA showing that the plasmid only became stuck in nanopores with diameter ≤ 3 nm.

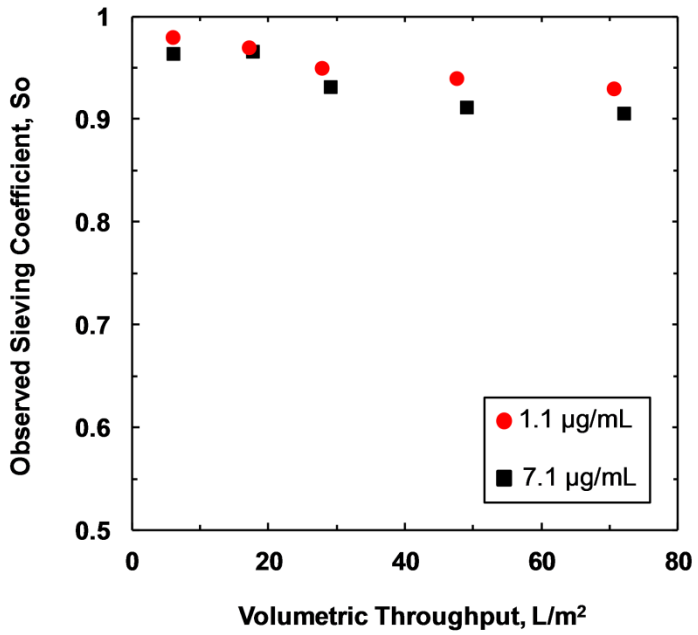

Figure 3-14: Effect of plasmid concentration on the observed sieving coefficient of the linear isoform of a 16.9 kbp plasmid. Data were obtained at constant filtrate flux using 1.1 and 7.1 x 10^{-3} kg/m^3 solutions with an initial filtrate flux of 55 x 10^{-6} m/s.

3.4. Discussion

The results presented in this Chapter provide one of the first detailed analyses of the fouling behavior of plasmid DNA during ultrafiltration through semipermeable ultrafiltration membranes, i.e., membranes that have a small enough pore size that plasmid transmission can only occur by significant elongation of the plasmid in the flow field. Fouling was negligible during ultrafiltration of dilute solutions, with negligible decline in filtrate flux or plasmid transmission for a 0.28 x 10^{-3} kg/m^3 solution up to volumetric throughputs of more than 70 L/m^2. However, there was a significant decline

in both flux and plasmid sieving coefficients with more concentrated solutions. For example, the filtrate flux during constant pressure filtration of a 7.2 x 10^{-3} kg/m^3 solution declined by more than a factor of three while the plasmid sieving coefficient decreased to essentially zero after filtration of only 20 L/m^2. This decline in flux and plasmid transmission was not due to any concentration polarization effects, with nearly identical behavior observed in the presence / absence of stirring.

A simple mathematical model was developed for the decline in flux and sieving coefficient based on the capture and partial blockage of the membranes pores by the large plasmid DNA. The model calculations are in good agreement with the experimental results, properly capturing the effect of membrane pore size, plasmid concentration, and plasmid size on the fouling behavior. The model accounts for two distinct phenomena: the partial blockage of the pores as described by the parameter β, equal to the ratio of the filtrate flux through a blocked pore to that through an open pore, and the rate at which the pores are blocked, which is described by the parameter k. The probability of a plasmid blocking a pore increased with increasing plasmid size, which is consistent with theoretical calculations showing a greater probability of knot formation in longer plasmids (Rybenkov et al., 1993). Additional studies with a broader range of plasmids and membranes would be needed to quantify the dependence of the blocking probability on the key physical properties of the plasmid and membrane, including both the membrane pore size and pore morphology.

Chapter 4

Application of periodic backpulsing to reduce membrane fouling during ultrafiltration of plasmid DNA

The work presented in this chapter was previously published in the Journal of Membrane Science (Borujeni, E.E., Y. Li, A. L. Zydney, Volume 473 (2014), pp. 102-108)

4.1. Introduction

As discussed in Chapter 3, one of the major challenges in using membrane systems for DNA purification is membrane fouling, which can cause a large reduction in filtrate flux, plasmid transmission, and membrane selectivity during the ultrafiltration process. Affandy et al. (2013) observed significant flux decline during sterile filtration of DNA through 0.2 μm pore size microfiltration membranes, with the data well described by a standard blocking (pore constriction) fouling model. Similar behavior was seen by Watson et al. (2006) over a range of plasmid sizes, conformations, and concentrations. The data in Chapter 3 showed a reduction in DNA transmission by more than 10-fold after only 500 s of ultrafiltration of a 16.9 kbp plasmid at a concentration of 7.2×10^{-3} kg/m^3 due to the "trapping" of plasmids in the membrane pores.

A variety of approaches have been used to reduce fouling during membrane filtration, including a wide range of membrane surface modifications and the use of appropriate hydrodynamic methods to increase back-transport (Yong Chung et al., 1993; Kuruzovich and Piergiovanni, 1996; Ma et al., 2000; Zhao et al., 2010). A number of investigators have explored the use of periodic backpulsing, in which short pulses of

reverse filtration are used to clear the pores and membrane surface of any captured foulants. For example, Wen et al. (2005) and Meacle et al. (1999) demonstrated the application of periodic backpulsing for the removal of unreacted polysaccharide during ultrafiltration for the purification of polysaccharide-protein conjugate vaccines. Mores and Davis (2002) examined the use of backpulsing to enhance the performance of crossflow microfiltration of yeast cell suspensions.

The objective of the work described in this Chapter was to examine the use of periodic backpulsing to reduce fouling during plasmid ultrafiltration by "releasing" the previously trapped plasmids from the membrane pores. Data were obtained with ultrafiltration membranes that allowed the supercoiled plasmid to be collected in the permeate solution, i.e., with membranes that would be appropriate for removing cell debris and genomic DNA, the open-circular isoform, and any plasmid dimers or higher order oligomers. Experiments were performed over a range of backpulse frequency, amplitude, and duration to develop a more fundamental understanding of the key factors governing the fouling / cleaning process and to identify optimal backpulse conditions. Data were also compared with predictions of the theoretical framework presented in Chapter 3. The results clearly demonstrate the potential of using periodic backpulsing to significantly improve the performance of DNA ultrafiltration and diafiltration processes.

4.2. Material and methods

4.2.1. Materials

4.2.1.1. Buffers

Tris-EDTA (TE) buffer solutions containing 150 mM NaCl were prepared as explained in Section 3.2.1.1.

4.2.1.2. Plasmid DNA

A 9.8 kilo base pair (kbp) plasmid (p-MDY), produced by Dr. Jeffrey Chamberlain at the University of Washington, was used in all the filtration experiments in this chapter. It was originally generated by insertion of a 6.84 kbp fragment as the complementary gene sequence for human mini-dystrophin into the SalI site of the pBluescript® II KS+ plasmid vector. The gene sequence map of this plasmid is shown in Appendix. New batches of 200 μg/mL stock solutions of this plasmid were obtained from Aldevron (Fargo, ND) and stored frozen at -20º C. Plasmid solutions with final concentrations of approximately 3.2 ± 0.2 μg/mL were prepared following the procedure explained in Section 3.2.1.2.

4.2.1.3. Ultrafiltration membrane

Ultrafiltration experiments were performed with a hollow fiber polysulfone (PS) membrane obtained from GE Healthcare (Niskayuna, NY) with nominal molecular

weight cutoff of 500 kDa (UFP-500-C-03M). Figure 4-1 shows the image of a cross section of the PS membrane. The hollow fiber is self-supporting, with sufficient mechanical stability for filtration in either direction (lumen to shell or shell to lumen). The selective membrane skin is on the lumen surface of the hollow fiber.

Figure 4-1: Cross-sectional image of a PS ultrafiltration hollow fiber membrane provided by GE Healthcare.

All experiments were performed with the same module to minimize variability in results. The module contained 30 hollow fibers with 0.5 mm ID and 30 cm length, giving 140 cm^2 of membrane area. The hold-up volume in the retentate (primarily inside the fiber lumens) was 2 mL while that in the permeate region was 9 mL (as reported by the manufacturer). The membrane was initially flushed with buffer for a minimum of 30 min to remove any storage or wetting agents. The module was cleaned immediately after each ultrafiltration experiment by flushing with 0.5 M NaOH at 45 ºC for one hour followed by 2 L of deionized (DI) water. It was stored at 4 º C between experiments.

4.2.1.4. Filtration set-up

Figure 4-2 shows a schematic of the apparatus used in the filtration experiments performed in this Chapter. The feed reservoir, containing either buffer or the plasmid solution, was placed on a stirring plate maintain uniform concentration throughout the filtration process. The feed solution was pumped from the reservoir through the lumen side of the membrane module using a Masterflex peristaltic pump. Initial experiments were performed in total recycle mode, with the retentate and permeate solution both returned to the feed reservoir. Permeate was collected in a separate tank in the diafiltration experiments described at the end of the Chapter. A three-way valve (valve 2) was installed on the permeate line to obtain periodic samples of the filtrate and to apply backpulses by air-pressurization of the collected permeate. Transmembrane pressure was adjusted using a ball valve (valve 1) installed on the retentate line. The feed, retentate, and permeate pressures (P_1, P_2, and P_3, respectively) were measured using pressure sensors on the flow lines. The pressure data were analyzed using Logger Lite 1.6.1 software supplied by Vernier (Beaverton, OR).

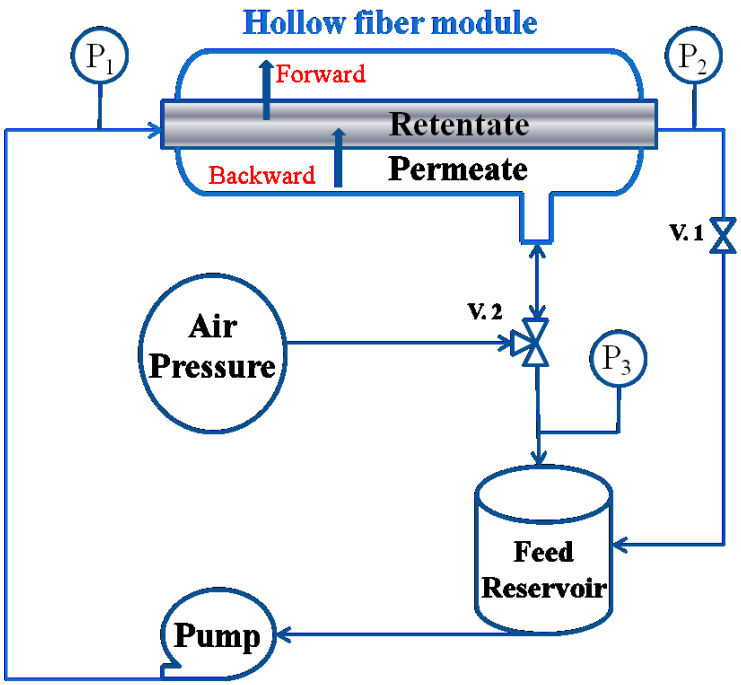

Figure 4-2: Schematic of the set-up used in the ultrafiltration experiments with periodic backpulsing

4.2.2. Methods

4.2.2.1. Ultrafiltration experiments

The permeability (L_p) of the hollow fiber membrane was evaluated from data for the filtrate flux (J_v) as a function of the transmembrane pressure (ΔP) as:

$$L_p = \frac{\mu J_v}{\Delta P} \tag{4-1}$$

Data were obtained with TE buffer containing 150 mM NaCl. The buffer solution was pumped through the module at a feed flow rate of 100 mL/min. The transmembrane pressure was adjusted using a ball valve installed on the retentate line and evaluated as

$$\Delta P = \frac{P_{feed}+P_{retentate}}{2} - P_{filtrate} \quad (4\text{-}2)$$

with pressures measured using the installed sensors. The volumetric filtrate flow rate was measured by timed collection of the permeate using an AG104 Mettler-Toledo analytical balance. The permeability of the module was fully restored upon cleaning with NaOH.

Ultrafiltration experiments were conducted over a range of feed flow rates. Each filtration cycle consisted of a period of forward filtration (positive transmembrane pressure) followed by a period of backpulsing (application of negative transmembrane pressure) or a period of pulsing (continued crossflow but with the permeate line closed to eliminate filtration). Samples were taken from the feed at the beginning of experiment and from the filtrate at specific times during forward filtrations. The transmembrane pressure and filtrate flux were evaluated as explained earlier. Permeate and feed samples were stored at 4 ^{o}C until they could be analyzed to evaluate the plasmid concentration.

Plasmid diafiltration was performed using the same apparatus except that only the retentate was recycled back to the feed reservoir; the permeate was collected in a separate vessel. Plasmid-free buffer was continuously added to the feed reservoir at a flow rate equal to the filtrate flow rate using another Dynamax peristaltic pump to maintain a constant feed volume.

4.2.2.2. Assays

Plasmid concentrations were determined using the PicoGreen dsDNA assay described in Section 3.2.2.2 with the observed sieving coefficients calculated using Equation (3-3). The integrity of the plasmid DNA was examined by agarose gel electrophoresis (AGE) following the procedures described in Chapter 3 (Section 3.2.2.3).

4.3. Results and analysis

4.3.1. Backpulsing

Figure 4-3 shows typical data for the filtrate flux (bottom panel) and the plasmid sieving coefficient (top panel), defined as the ratio of the plasmid concentration in the filtrate to that in the feed solution, as a function of time during two separate ultrafiltration experiments, both performed at a feed flow rate of 100 mL/min. Data were obtained at a transmembrane pressure of 55 kPa (8 psi), determined using Equation 4-2. The triangles represent data without any backpulsing while the squares are for a run in which a 55 kPa backpulse was applied every 180 s for a duration of 20 s. Data in the backpulsing experiment are plotted as a function of the forward filtration time, which is defined as the cumulative time during only the periods of forward (normal) filtration. Thus, the sieving coefficient appears to jump instantaneously upon application of the backpulse. The initial filtrate flux was slightly higher for the run without backpulsing, 45 μm/s (corresponding to 160 L/m^2/hr) versus 42 μm/s. This higher flux gave a slightly higher initial sieving coefficient; the flux dependence of the plasmid sieving coefficient is discussed in more

detail by Latulippe and Zydney (2007) and in Chapter 3. There was no evidence of any DNA damage during the ultrafiltration; agarose gels of DNA samples obtained from the permeate showed no degradation in DNA size or any change in DNA topology.

The filtrate flux in the absence of backpulsing declined by about 10% during the ultrafiltration, while the sieving coefficient decreased from $S_o \approx 0.7$ to $S_o \approx 0.1$. This behavior is consistent with the partial pore blockage model discussed in Chapter 3, with the "blocked" pores becoming impermeable to subsequent plasmid transport while still allowing significant filtrate flow. The solid curve in Figure 4-3 is a model calculation based on this partial pore blockage model using $\beta = 0.95$ and $k = 0.15$ m^2/kg as determined by minimizing the sum of the squared residuals between the experimental data and model calculations. The larger value of β compared to the values presented in Chapter 3 is due to the larger pore size of the 500 kDa membrane – all of the experiments performed in Chapter 3 used smaller pore size Omega 100 and 300 kDa membranes. The behavior in the presence of backpulsing was very different, with the application of each backpulse causing a significant increase in the plasmid sieving coefficient. For example, the sieving coefficient at the end of the first cycle was $S_o \approx 0.45$, but this increased to $S_o = 0.58$ in the first sample obtained immediately after the 20 s backpulse. This behavior continued throughout the ultrafiltration, although there was a continual decline in the value of the sieving coefficient at the start of each filtration cycle from $S_o = 0.65$ for the very first cycle to $S_o = 0.41$ at the beginning of the 5^{th} cycle. The filtrate flux remained nearly constant throughout the ultrafiltration experiment; the final filtrate flux at the end of the backpulsing experiment was 41 μm/s, which is only 5% smaller than the initial flux.

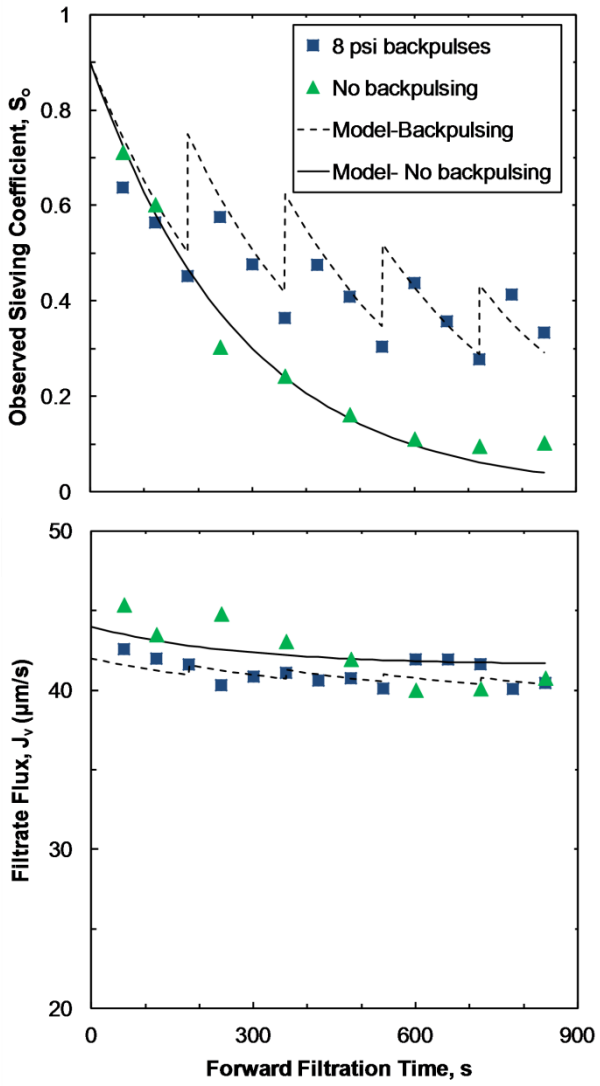

Figure 4-3: Effect of backpulsing on the observed sieving coefficient (top panel) and filtrate flux (bottom panel) during ultrafiltration of 3.2 ± 0.2 µg/mL solutions of a 9.8 kbp plasmid through a 500 kDa GE hollow fiber membrane at a feed flow rate of 100 mL/min and a positive transmembrane pressure of 55 kPa. Backpulsing was performed every 180 s for 20 s at a backpressure of 55 kPa. Solid and dashed curves are model calculations described subsequently.

4.3.2. Model development

The effect of fouling on the filtrate flux and DNA transmission during plasmid ultrafiltration was discussed in Chapter 3. This framework was extended to the backpulsing experiments by accounting for the "un-blockage" of the pores in response to the backpressure. The effectiveness of the backpulsing was defined as:

$$\propto = \frac{f_i}{f_{i-1}} \tag{4-1}$$

where f_i is the initial value of f at the start of the i^{th} cycle of forward filtration. α was assumed to be constant throughout a given ultrafiltration experiment. The best fit value of $\alpha = 0.83 \pm 0.01$ for the conditions examined in Figure 4-3 was determined by minimizing the sum of the squared residuals between the model and data using the previously determined values of β and k. A somewhat better fit to the data could have been obtained by simultaneously fitting α, β, and k to the backpulsing data, although the values of the parameters were only slightly different. The resulting model calculations (dashed lines in Figures 4-3) are in very good agreement with the experimental data throughout the backpulsing experiment, properly capturing both the decline in sieving coefficient during each cycle as well as the partial recovery after application of the backpulse. The calculated value of f at the end of the backpulsing experiment was $f = 0.31$, indicating that around 69% of the pores become blocked with trapped plasmids even in response to the backpulsing. Calculations using the same conditions but without backpulsing give $f = 0.04$ at the end of the ultrafiltration.

4.3.3. Optimization of backpulse conditions

The effectiveness of backpulsing is typically a function of the frequency, amplitude, and duration of the backpulses [14, 16], with the optimal conditions dependent upon the fouling characteristics of the feed. Figure 4-4 shows results from a series of experiments with different backpulse amplitudes of 0, 28, 55, and 83 kPa (0, 4, 8, and 12 psi), with the backpulsing performed every 180 s for a duration of 20 s. The results at a backpulse amplitude of 8 psi were shown previously in Figure 4-3. All experiments were performed at a feed flow rate of 100 mL/min, with the positive transmembrane pressure during the forward filtration maintained at 55 kPa (8 psi) yielding an initial filtrate flux of 43 ± 1 μm/s. The 0 psi backpulse was obtained by simply closing the permeate line for 20 s, with the feed flow rate maintained at 100 mL/min. The results for the four experiments were very similar; the small differences between the observed sieving coefficients were all within the typical variability seen between repeat experiments performed under the same conditions using a single module. The final values of the observed sieving coefficient at the end of the ultrafiltration were all $S_o = 0.32 \pm 0.02$, which is about 53% smaller than the initial values ($S_o = 0.68 \pm 0.04$). The best fit values of α determined from the data in Figure 4-4 (using $\beta = 0.95$ and $k = 0.15$ m^2/kg) were $\alpha = 0.83 \pm 0.01$ for all of the backpulse amplitudes. These values are all statistically identical, i.e., the effectiveness of backpulsing is independent of the backpulse amplitude, suggesting that the removal of trapped plasmids from the membrane pores occurs primarily by the drag force (or shear stress) associated with the tangential flow and not the backflow through the membrane.

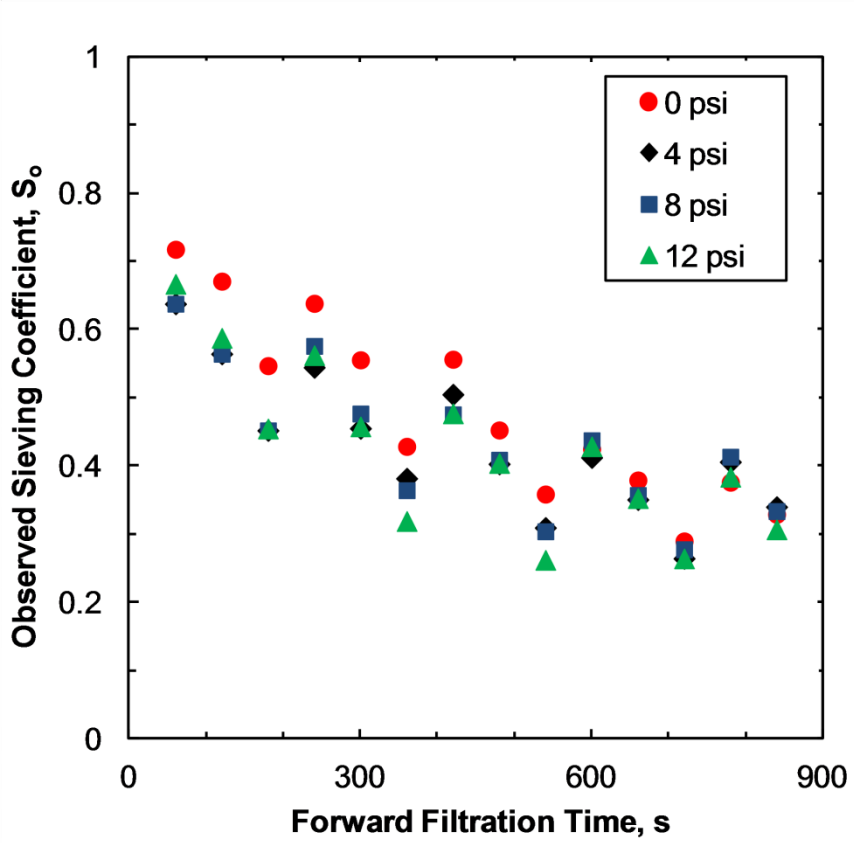

Figure 4-4: The effects of backpulse amplitude on the observed sieving coefficient during ultrafiltration of 3.2 ± 0.2 µg/mL solutions of a 9.8 kbp plasmid through a 500 kDa GE hollow fiber membrane at a feed flow rate of 100 mL/min and a positive transmembrane pressure of 55 kPa (giving an initial filtrate flux of 43 ± 1 µm/s). Backpulses were applied every 180 s for a fixed duration of 20 s.

A separate experiment was performed in which the backpulsing was done in the absence of any crossflow (by turning off the feed pump when the backpressure was applied). Application of a 20 s backpulse at a back-pressure of 82.5 kPa caused a significant increase in the plasmid sieving coefficient. Thus, the trapped plasmids can be removed from the pores by backflow through the membrane (in the absence of any

crossflow), although no backflow is required when the module was operated at moderately high tangential flow rates.

Figure 4-5 shows the effect of the pulse duration on the observed sieving coefficient for a series of experiments in which pulsing was done without any applied backpressure (i.e., with the permeate line closed for a set period of time). Data were obtained at a constant feed flow rate of 100 mL/min with a positive pressure of 55 kPa. The permeate line was clamped after 180 s of forward filtration for 5, 10, and 20 s, corresponding to crossflow volumes of approximately 8.5, 17, and 33 mL (compared to the 2 mL hold-up volume within the fiber lumens). The use of a 5 s pulse provided only a small improvement in the sieving coefficient, with S_o declining to below 0.2 by the end of the ultrafiltration. The use of a 10 s pulse provided significantly better recovery of the sieving coefficient, with a small further improvement seen with a 20 s pulse. The best fit values of α for these experiments ranged from $\alpha = 0.66 \pm 0.01$ for the 5 s pulse to $\alpha = 0.79 \pm 0.01$ for 10 s and $\alpha = 0.85 \pm 0.01$ for the 20 s pulse.

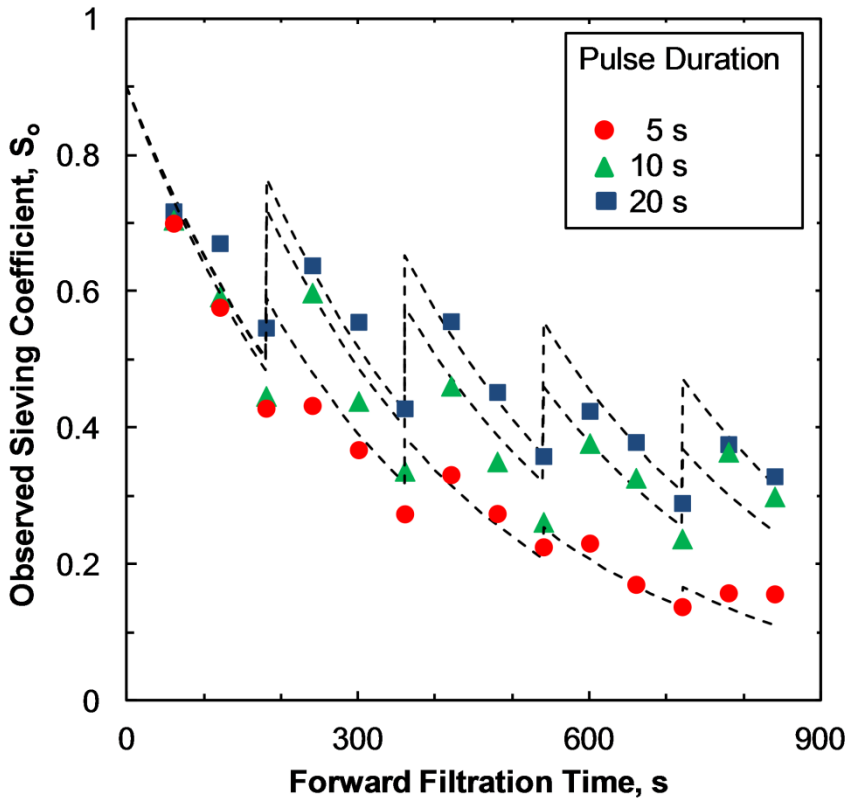

Figure 4-5: The effects of pulse duration (at 0 kPa backpulse) on the observed sieving coefficient during ultrafiltration of 3.2 ± 0.2 μg/mL solutions of a 9.8 kbp plasmid through a 500 kDa GE hollow fiber membrane at a feed flow rate of 100 mL/min with an initial filtrate flux of 43 ± 1 μm/s. Pulses were applied every 180 s. Dashed curves are model calculations using α = 0.66, 0.79, and 0.85 for the experiments with 5, 10, and 20 s pulses, respectively.

In order to study plasmid removal due to crossflow in more detail, ultrafiltration experiments were performed at feed flow rates of 50, 100, and 150 mL/min (corresponding to Reynolds numbers of 73, 145 and 220 and wall shear rates of 1700, 3300, and 5000 s^{-1} assuming fully developed parabolic flow in the 0.5 mm diameter fibers). In each case, the forward filtration was performed at a constant pressure of 55 kPa for 180 s following by a 10 s pulse with the permeate line closed (i.e., no forward

filtration). The best fit values of α determined from the plasmid sieving coefficient data for these experiments are shown in Figure 4-6, with the error bars representing the standard deviations determined from the regression analysis. All fits were performed using the same values of β and k during the forward filtration; there was no indication that the rate or extent of fouling was dependent on the feed flow rate. The α values increase slightly with increasing feed flow rate, going from α = 0.79 ± 0.02 at 50 mL/min to α = 0.87 ± 0.01 at 150 mL/min, suggesting that the higher drag force and or shear stress is more effective at removing plasmids from the membrane pores.

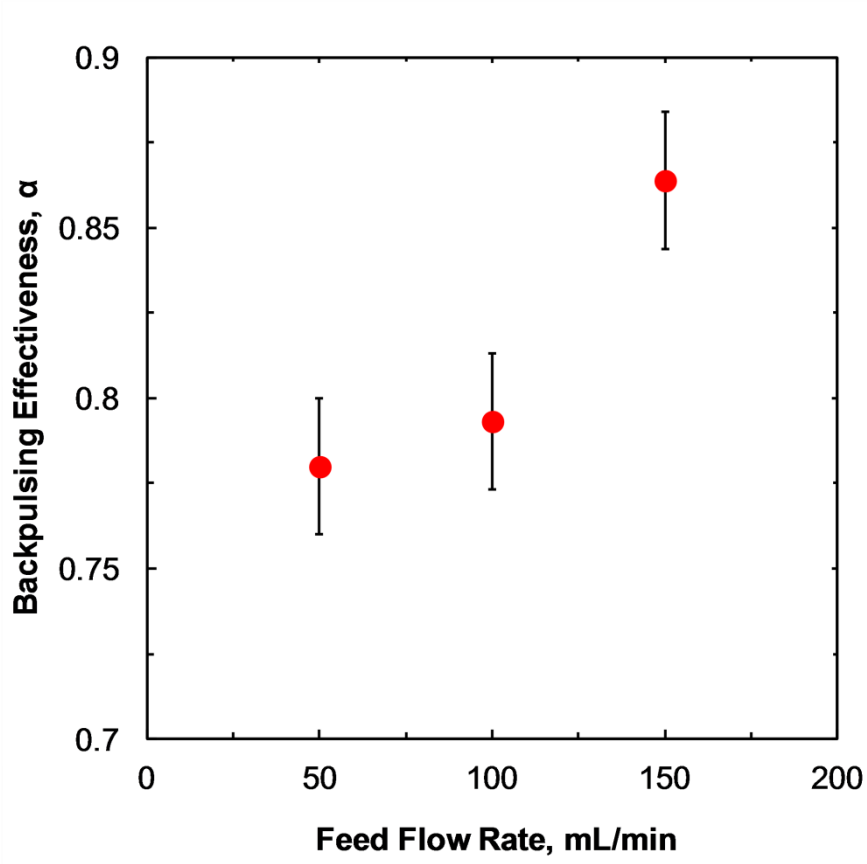

Figure 4-6: The effects of volumetric feed (cross) flow rate on the best fit value of α during ultrafiltration of 3.2 ± 0.2 µg/mL solutions of a 9.8 kbp plasmid using a 500 kDa GE hollow fiber membrane with an initial filtrate flux of 43±1 µm/s. 10 s pulses (with no filtration) were applied every 180 s.

Figure 4-7 shows results from two separate ultrafiltration experiments, one in which the pulsing was applied every 90 s and one in which the pulsing was applied every 180 s (data shown previously in Figure 4-5). In both cases, the pulsing was done by clamping the permeate exit for 10 s (with no filtration) with the feed flow rate maintained at 100 mL/min throughout the experiment. The initial sieving coefficients were similar for both experiments as expected. However, the plasmid sieving coefficient declined much more rapidly for the run with the lower pulse frequency (i.e. one pulse every 180 s). The final value of the plasmid sieving coefficient for the run with pulsing every 90 s is $S_o = 0.50$, which is significantly higher than the $S_o = 0.33$ for the run with pulsing every 180 s. The model calculations for these experiments (dashed curves in Figure 4-7) gave $\alpha = 0.79$ for pulsing every 180 s and $\alpha = 0.96$ for pulsing every 90 s, with the latter corresponding to almost complete recovery of the plasmid transmission after each pulse.

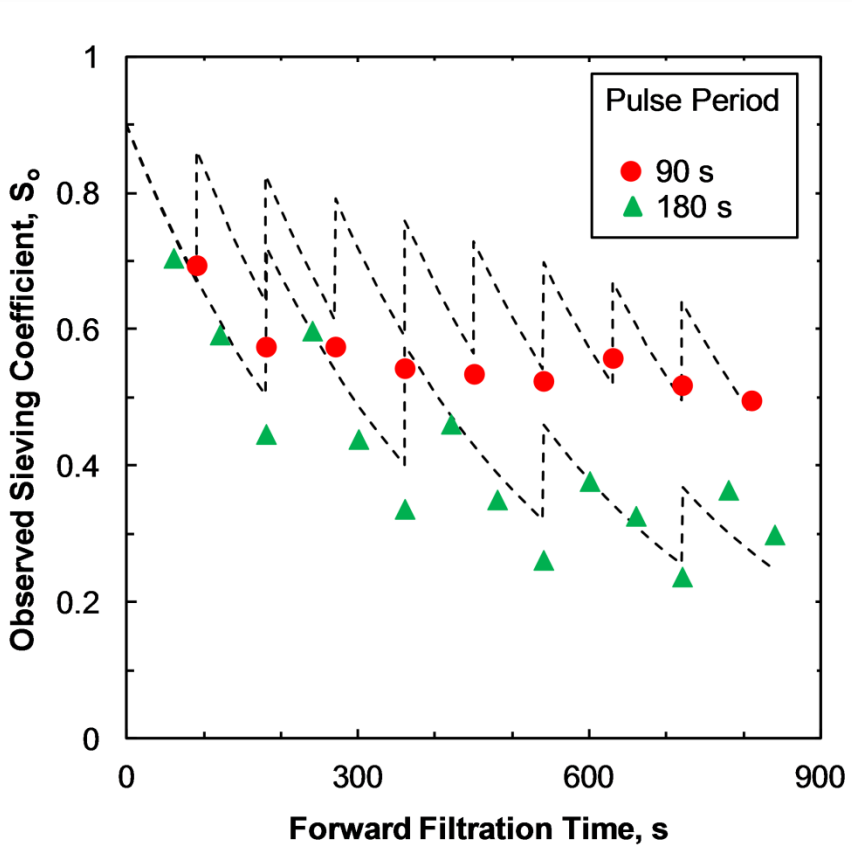

Figure 4-7: The effects of pulse frequency (at 0 kPa backpulse) on the observed sieving coefficient during ultrafiltration of 3.2 ± 0.2 µg/mL solutions of a 9.8 kbp plasmid through a 500 kDa hollow fiber membrane at a feed flow rate of 100 mL/min with an initial filtrate flux of 43±1 µm/s. Pulses were applied for a duration of 10 s. Dashed curves are the model calculations using $\alpha = 0.79$ and 0.96 for the experiments with 180 and 90 s pulse periods, respectively.

4.3.4. Diafiltration

In order to demonstrate the effectiveness of pulsing, data were obtained during a constant volume diafiltration in which the plasmid product was to be recovered in the collected permeate, i.e. for a process that might be used to remove small cellular debris, genomic DNA, and / or the open-circular isoform. Experiments were performed with a

300 mL feed tank initially containing a 3.2 ± 0.2 μg/mL solution of the 9.8 kbp plasmid. The feed was pumped through the 500 kDa hollow fiber module at a flow rate of 100 mL/min with a transmembrane pressure of 55 kPa. The volume of solution in the feed tank was kept constant by continually adding TE buffer containing 150 mM NaCl to the feed tank at a flow rate equal to the filtrate flow rate. One run was performed without any pulsing, while the other run used a 10 s pulse (permeate line shut, zero back-pressure) every 90 s. Samples were obtained directly from the feed tank and the collected permeate throughout the diafiltration.

Results from the two diafiltration experiments are shown in Figure 4-8 as the fractional plasmid recovery, defined as the ratio of the mass of plasmid in the collected permeate divided by the initial mass of plasmid in the feed. Data are plotted as a function of the number of diavolumes, which is equal to the ratio of the cumulative filtrate volume to the (constant) feed volume. The fractional recovery increases with increasing number of diavolumes, but levels off at F = 0.37 for the run without pulsing after only 2.5 diavolumes since the plasmid transmission dropped to essentially zero at this point in the diafiltration. In contrast, the fractional recovery continued to increase throughout the run with pulsing, with F = 0.98 after approximately 6 diavolumes.

The solid and dashed curves in Figure 4-8 are the model calculations with and without pulsing using the previously determined values of the model parameters: k = 0.15 m^2/kg, $\alpha = 0.96$ and $\beta = 0.95$. In this case, Equations (3-7), (3-8), (3-10), and (4-1) were combined with a mass balance on the plasmid in the feed reservoir:

$$V\frac{dC}{dt} = -qS_oC - (A_m\varepsilon N_{pore}\frac{\partial f}{\partial t}\theta)(\frac{M_w}{N_{Avogadro}}) \quad (4\text{-}2)$$

where q is the volumetric permeate flow rate. The first term on the right hand side in Equation (4-2) represents the flux of plasmid into the permeate while the second term represents the loss of plasmid due to trapping within the membrane pores assuming that θ, defined as the number of plasmids per "blocked" pores, is equal to one. The dashed curve is developed by numerical integration of Equation (4-2) with $N_{pore} = \frac{1}{\pi \times r_p^2} = 5.1 \times 10^{14}$ per m^2 of porous membrane area (using $r_p = 25 \times 10^{-9}$ m as given by Bakhshayeshi et al. (2011)). The membrane porosity was assumed to be ε = 0.5 based on results with other porous ultrafiltration membranes [20]. M_W is plasmid molecular weight, estimated using 660 Da per base pair. The solid curve (in the presence of pulsing) is developed using the same approach but with a fraction of the trapped plasmids returned to the bulk solution during each pulse. The model calculations clearly show the benefit of pulsing, although for the run without pulsing a somewhat better fit to the data can be obtained by assuming multiple trapped plasmids per blocked pore (different θ values in dashed curves), consistent with the formation of a layer of deposited plasmids on the membrane surface.

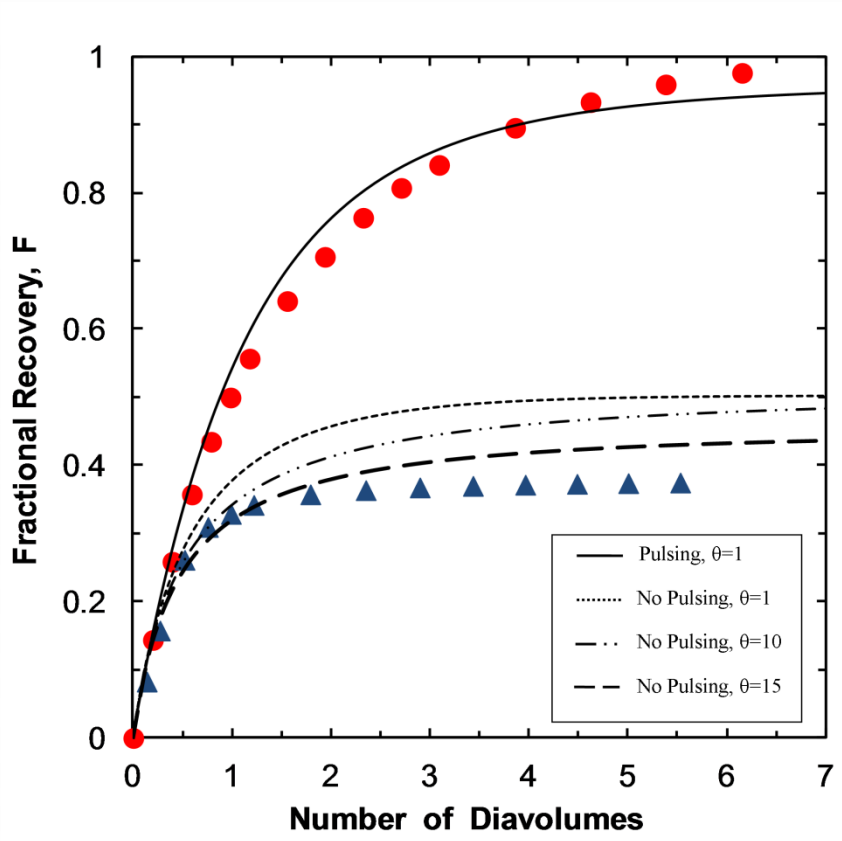

Figure 4-8: Diafiltration of 3.2 ± 0.2 µg/mL solutions of a 9.8 kbp plasmid through a 500 kDa hollow fiber membrane but with (●) and without (▲) pulsing. Data obtained at a feed flow rate of 100 mL/min and a transmembrane pressure of 55 kPa. Pulses with 10 s duration (with no filtration) were applied every 90 s. The solid and dashed lines are model calculations for the runs with and without pulsing, respectively, using various θ values.

4.4. Conclusion

The results presented in this Chapter provide the first demonstration that periodic backpulsing can significantly improve the performance of plasmid ultrafiltration processes by the partial release of plasmids that become "stuck" or "trapped" in the

membrane pores. In contrast to the behavior seen in most studies of backpulsing in protein ultrafiltration or cell microfiltration, plasmid removal from the pores was due primarily to the shear or drag forces exerted on the trapped plasmid. Very high recovery of the plasmid transmission and filtrate flux could thus be achieved by simply closing the permeate line (pulsing with zero back-pressure) for a short period of time as long as the crossflow velocity was sufficiently large.

A simple mathematical model was developed for the plasmid sieving coefficient and filtrate flux based on an extension of the partial pore blockage framework presented in Chapter 3. In this case, the fraction of membrane pores that are blocked by a trapped plasmid is reduced by each pulse, with the backpulse effectiveness (α) defined as the ratio of the open pore area at the beginning of a forward filtration cycle to that at the beginning of the previous cycle. The effectiveness of the backpulsing was largely independent of the backpulse pressure, but it increased with increasing pulse duration, pulse frequency, and crossflow velocity. Model calculations were in very good agreement with the experimental data for both the filtrate flux and the plasmid sieving coefficient over a wide range of pulsing conditions. The theoretical framework could also be applied to a diafiltration process by combining the fouling / pulsing model with an appropriate mass balance for the plasmid concentration in the constant volume feed tank. Plasmid recovery after 6 diavolumes was greater than 98% with pulsing compared to only 37% for a constant pressure ultrafiltration (without pulsing). These results clearly demonstrate the potential of using pulsed ultrafiltration to enhance the separation and purification of plasmid DNA for a variety of applications.

Chapter 5

Effect of membrane pore structure on transmission of plasmid DNA

Note: The work described in this Chapter was performed in collaboration with Ying Li.

5.1 Introduction

As explained in Chapter 2, DNA transmission through ultrafiltration membranes with pores that are smaller than the radius of gyration of the DNA occurs by flow-induced elongation. DNA transmission tends to be minimal at low filtrate flux but becomes significant above a critical value of the flux at which the hydrodynamic forces are sufficient to cause significant DNA elongation (Latulippe et al., 2007; Latulippe and Zydney, 2009; Borujeni and Zydney, 2012). In addition, it is possible to exploit differences in the elongational flexibility of the different DNA isoforms to use ultrafiltration for the purification of the desired (typically supercoiled) isoform.

There have also been a number of fundamental studies showing that the initial conformation of the DNA can affect the rate of DNA transmission through narrow pores. For example, Perkins et al. (1997) demonstrated that even at a 300-fold strain in an elongational flow field, there are different topological forms of DNA molecules in solution which show different dynamics and degrees of extension. They also found out that a dumbbell shaped DNA stretches more easily than a folded structure.

Several studies have demonstrated that "pre-elongation" of DNA, e.g., by pre-shearing (Larson, 2000; Larson et al., 2006; Hsieh and Liou, 2009), passing through an array of obstacles (Trahan and Doyle, 2009) or a gel matrix (Randall et al., 2006), or by application of an alternating extensional flow (Hsieh and Lin, 2011), facilitates the subsequent elongation of the DNA, reducing the strain rate required for full elongation of the DNA molecule. This phenomenon is of particular importance in microfluidic systems for gene sequencing where linear DNA molecules must be completely extended to accurately determine the base sequence.

There have, however, been no previous studies on the possible effect of pore shape or morphology on the transmission of plasmid DNA during ultrafiltration. The objective of the work described in this Chapter was to examine the effect of pore shape on the transmission of plasmid DNA during ultrafiltration. Data were obtained with asymmetric ultrafiltration membranes in both the forward and reverse orientation, i.e., with the flow entering through either the tight skin or the more open support structure. Additional experiments were performed with microfiltration and ultrafiltration membranes used in series, with flow through the microfiltration membrane used to pre-elongate the DNA. The results clearly indicate the potential of controlling DNA transmission through narrow pore size ultrafiltration membranes by tailoring the membrane pore morphology.

5.2. Materials and method

5.2.1. Materials

5.2.1.1. Buffer

Tris-EDTA (TE) buffer containing 150 mM NaCl was prepared as explained in Section 3.2.1.1.

5.2.1.2. Plasmid DNA

Data were obtained with both a 2.9 kbp (p-EMP) and a 16.9 kbp (p-FDY) supercoiled plasmid (provided by Dr. Paula Clemens at the University of Pittsburgh), prepared according to the procedures described in Section 3.2.1.2. Limited experiments were also conducted using the linear isoform of the 2.9 kbp plasmid, produced using 4 U/μg plasmid of BamHI enzyme (Life technologies, Grand Island, NY) as explained in Section 3.2.1.2.

5.2.1.3. Membranes

Ultrafiltration experiments were performed using hollow fiber polysulfone (PS) membranes obtained from GE Healthcare (Niskayuna, NY) with nominal molecular weight cutoff (MWCO) of 500 kDa (UFP-500-C-03M) and 50 kDa (UFP-50-C-3MA). Section 4.2.1.3 describes the procedures used for membrane preparation and cleaning with 0.5 N NaOH.

Data were also obtained with Ultracel® flat sheet ultrafiltration membranes (a composite regenerated cellulose membrane) with MWCO of 100 kDa supplied by EMD Millipore Co. (Bedford, MA). The Ultracel membranes were initially soaked in 90% isopropanol solution, followed by flushing with 100 mL deionized water, to remove any wetting/storing agents from the membrane. The Ultracel membranes were also used in series with a 0.22 μm Durapore® polyvinylidene fluoride (PVDF) membrane from Millipore to further examine the effects of membrane morphology on DNA transmission.

5.2.1.4. Filtration apparatus

The apparatus and procedures used for the hollow fiber membranes were described previously in Chapter 4. Feed solution was pumped through the module by a peristaltic pump, with the permeate and retentate lines recycled back to the feed reservoir. The desired transmembrane pressure was applied by adjusting a ball valve installed on the retentate line. Permeate samples were collected periodically for subsequent analysis of the DNA concentration, with the filtrate flux, J_v, evaluated by timed collection.

The apparatus and procedures used for the flat sheet membranes were described in Section 3.2.1.4.

5.2.2. Methods

5.2.2.1. Ultrafiltration experiments

The hydraulic permeability was evaluated using Tris-EDTA buffer. Ultrafiltration experiments were then conducted over a range of filtrate flux by adjusting the transmembrane pressure (TMP). A 100 mL plasmid solution was pumped from the feed reservoir into either the lumen side of hollow fiber module (forward filtration) or the shell side (reverse filtration) at a flow rate of 100 mL/min. An initial feed sample was taken with permeate samples obtained throughout the ultrafiltration.

Data with the flat sheet membranes were obtained at constant transmembrane pressure using a 10 mL stirred cell as described in Section 3.2.2.1.

5.2.2.2. Assays

The DNA concentration for experiments performed with single isoforms was determined using the PicoGreen assay with the observed sieving coefficient, S_o, calculated using Equation (3-3). Samples containing a mixture of plasmid isoforms were analyzed using AGE as described in Section 3.2.2.3.

5.3. Results and analysis

5.3.1. Hydraulic membrane permeability

The hydraulic permeability of the 500 kDa hollow fiber membrane was 0.97×10^{-6} m/(s.kPa) while that of the 50 kDa membrane was 0.42×10^{-6} m/(s.kPa). The 100 kDa Ultracel and 0.22 μm Durapore membranes had permeability values of 2.5×10^{-6} m/(s.kPa) and 21.4×10^{-6} m/(s.kPa), respectively.

5.3.2. Ultrafiltration experiments

The effect of membrane orientation on the transmission of a 16.9 kbp plasmid through a 500 kDa PS hollow fiber membrane is shown in Figure 5-1. In each case, data were obtained with increasing filtrate flux, set by adjusting the transmembrane pressure. DNA transmission increases with increasing filtrate flux as expected, with much greater transmission (at a given filtrate flux) when the filtration is in the reverse direction (through the membrane substructure and then through the skin). For example, at a filtrate flux of 10 μm/s, the sieving coefficient in the reverse direction was slightly more than 0.8 compared to a value of less than 0.2 in the forward direction. In addition, the critical filtrate flux for DNA transmission (evaluated by extrapolation of the data to zero transmission) was more than 6 μm/s in the forward direction but decreased to less than 3 μm/s for reverse filtration. It appears that the sieving coefficient has a sharper dependence on the flux in the reverse orientation, which might also be related to the preconditioning effect in the large micron-size pores of the membrane support layer.

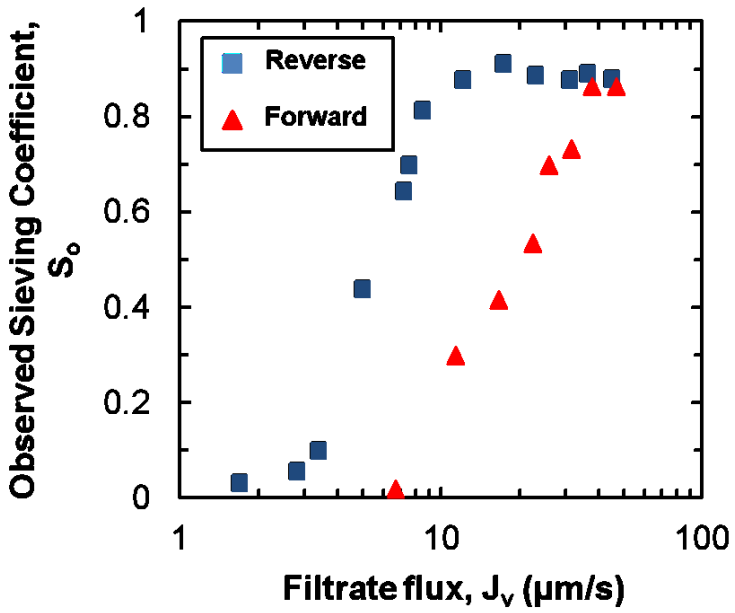

Figure 5-1: The effect of membrane orientation on the observed sieving coefficient of a 16.9 kbp supercoiled plasmid transmitted through a 500 kDa PS hollow fiber membrane.

In order to verify that the increase in plasmid transmission was due to the pre-conditioning of the plasmid during ultrafiltration through the more open porous support in the hollow fiber membrane, a separate set of experiments were conducted using flat sheet Ultracel membranes in the 10 mL stirred cell. Data were obtained with 0.25 µg/mL solutions of a 2.9 kbp plasmid at filtrate flux values of 40 and 60 µm/s. The first experiment used the 100 kDa Ultracel ultrafiltration membrane in its normal orientation (skin-side up). The second used the same 100 kDa membrane but in the reverse orientation, with the flow through the membrane substructure and then through the skin. The third used to same 100 kDa membrane (placed skin-side up) but in a double-layer configuration with a 0.22 µm Durapore microfiltration membrane placed directly on top

of the skin layer of the ultrafiltration membrane in the base of the stirred cell. The observed sieving coefficient data are summarized in Table 5-1.

Table 5-1: Plasmid sieving coefficients through the 100 kDa Ultracel membrane in three configurations: skin-side up, skin-side down, and in a double layer with a 0.22 μm PVDF membrane.

Configuration	**S_o (J_v = 40 μm/s)**	**S_o (J_v = 60 μm/s)**
Skin-Side Up	0.01	0.03
Skin-Side Down	0.17	0.32
Double-Layer	0.15	0.32

Plasmid transmission through the Ultracel membrane in the normal (skin-side up) orientation was very low at both values of the filtrate flux; higher transmission could only be achieved by operating at significantly higher filtrate flux. In contrast, data obtained with the same membrane but in the reverse orientation (skin-side down) showed considerably higher plasmid transmission, with values of S_o = 0.17 and 0.32 at filtrate flux of 40 and 60 μm/s, respectively. Results with the Ultracel membrane in a "double-layer" configuration with a Durapore membrane were nearly identical to that for the Ultracel membrane in the skin-side down orientation. The Durapore is a symmetric (homogeneous) membrane with pore size of 0.22 μm, which is similar to the pore size in the substructure of the Ultacel membrane. These results clearly indicate that filtration of the plasmid through a relatively large pore size region, either the substructure in an

asymmetric membrane or the Durapore membrane in the double-layer configuration, makes it easier for the plasmids to elongate and pass through the small nanopores in the skin layer of an ultrafiltration membrane. This finding is in agreement with a theoretical work presented by Daoudi and Brochard (1978) in which they showed that the frictional force required for extending a polymer chain into a conical pore is significantly less than the force needed for transmission of the polymer through a cylindrical pore. A slower reduction in the pore diameter (i.e. a smaller cone angle) allows the polymer chain to extend gradually as it approaches the narrow exit, with the "pre-conditioning" enabling the polymer to pass through the pore at a smaller value of the filtrate flux.

In order to examine the effect of the pore size in the skin-layer on plasmid transmission, ultrafiltration experiments were conducted using a 16.9 kbp plasmid with 50 kDa and 500 kDa hollow fiber membranes with flow in the reverse orientation (skin-side away from the feed). Results are shown in Figure 5-2; the data for the 500 kDa membrane were previously shown in Figure 5-1. Plasmid transmission was significantly reduced for the smaller pore size 50 kDa membrane, demonstrating that the overall rate of plasmid transmission is determined by both the pre-elongation of the plasmid in the membrane substructure and the final elongation required to pass through the very small pores in the skin layer of the membrane.

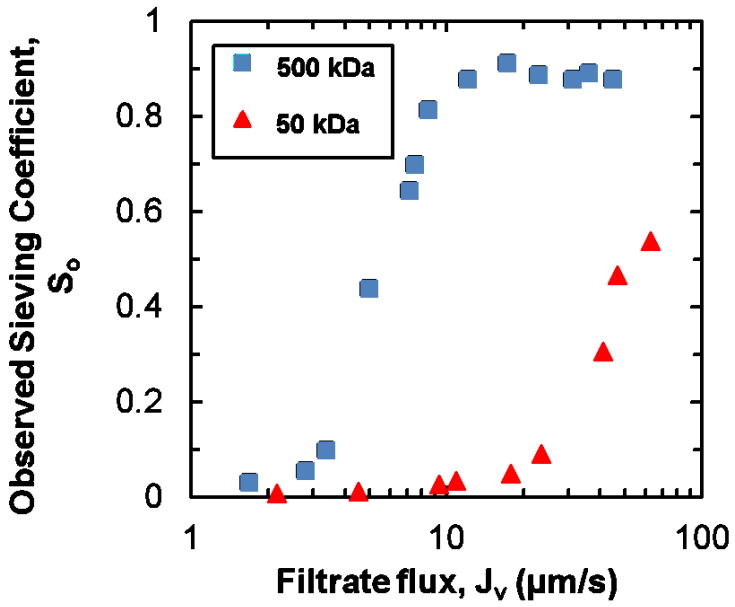

Figure 5-2: The observed sieving coefficient of a 16.9 kbp plasmid filtered through a 50 kDa and 500 kDa PS hollow fiber membrane in the reverse orientation.

Figure 5-3 shows data obtained with both the linear and supercoiled isoforms of a 2.9 kbp plasmid using a 50 kDa hollow fiber ultrafiltration membrane. Operation of the membrane in the reverse orientation caused a significant reduction of the critical flux and a corresponding increase in plasmid transmission for both isoforms. The selectivity for the isoform separation is similar in the two flow directions, with the data in Figure 5-3 suggesting that it would be possible to separate a mixture of linear and supercoiled plasmid isoforms using either membrane orientation but with a lower filtrate flux in the reverse orientation.

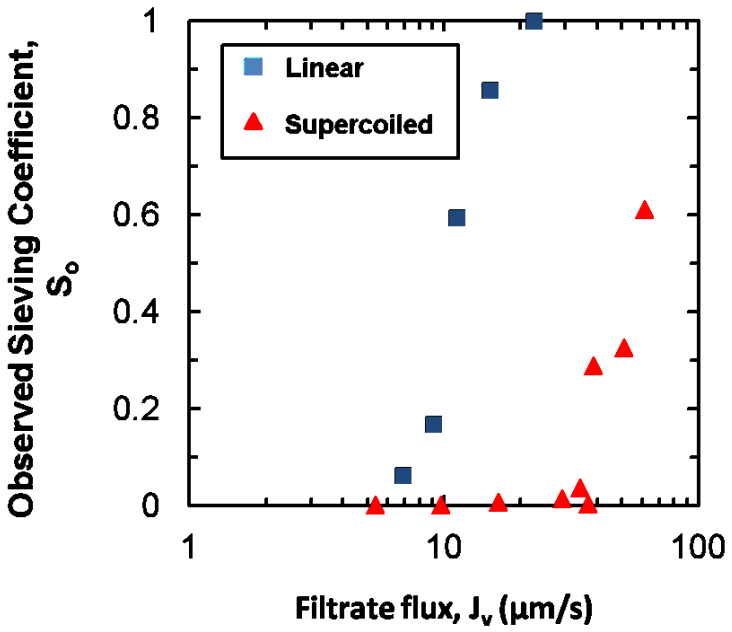

Figure 5-3: Ultrafiltration of the linear and supercoiled isoforms of a 2.9 kbp plasmid through a 50 kDa PS hollow fiber membrane using both the forward and reverse orientations.

Figure 5-4 shows data for the 2.9 and 16.9 kbp plasmids using the 50 kDa hollow fiber membrane in the reverse orientation. Similar to the results reported previously by Latulippe and Zydney for ultrafiltration in the normal orientation, plasmid transmission in the reverse orientation is essentially independent of the plasmid size (Latulippe et al., 2007). Both plasmids show a critical filtrate flux of between 20 and 30 µm/s, with the plasmid sieving coefficient increasing to more than 60% above a filtrate flux of approximately 65 µm/s.

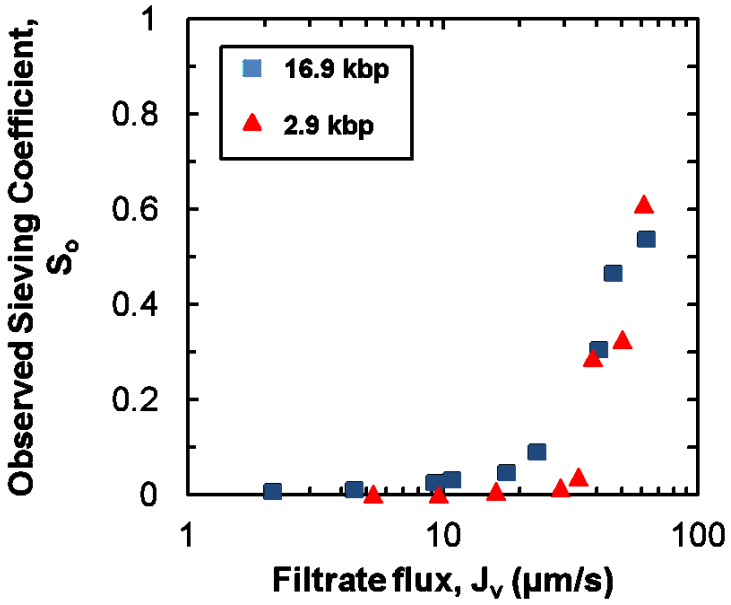

Figure 5-4: Observed sieving coefficient of the 2.9 and 16.9 kbp supercoiled plasmids through a 50 kDa PS hollow fiber membrane in the reverse orientation.

In order to examine the potential of using reverse filtration for the separation of the plasmid isoforms in more detail, an experiment was performed using a mixture containing equal concentrations of the linear and supercoiled isoforms of the 2.9 kbp plasmid (total concentration of 0.5 µg/mL). Data were obtained with the 50 kDa membrane hollow fiber membrane in the reverse orientation at filtrate fluxes of 10 and 20 µm/s based on the results in Figure 5-3. Permeate and feed samples were analyzed using agarose gel electrophoresis (AGE), with a typical gel image shown in Figure 5-5. Lane 2 shows the feed sample with the linear (top band) and supercoiled (bottom band) isoforms. Lane 3 is the filtrate sample obtained at 10 µm/s while Lane 4 shows the filtrate sample obtained at 20 µm/s. Neither of the plasmid isoforms passed through the membrane at a flux of 10 µm/s; increasing the filtrate flux to 20 µm/s caused a significant increase in transmission of the linear isoform (very bright band) while the supercoiled isoform was

nearly completely retained by the membrane. These results are very consistent with the data obtained with the single isoforms in Figure 5-3, with the flux of 20 μm/s lying between the critical flux values of the linear and supercoiled isoforms.

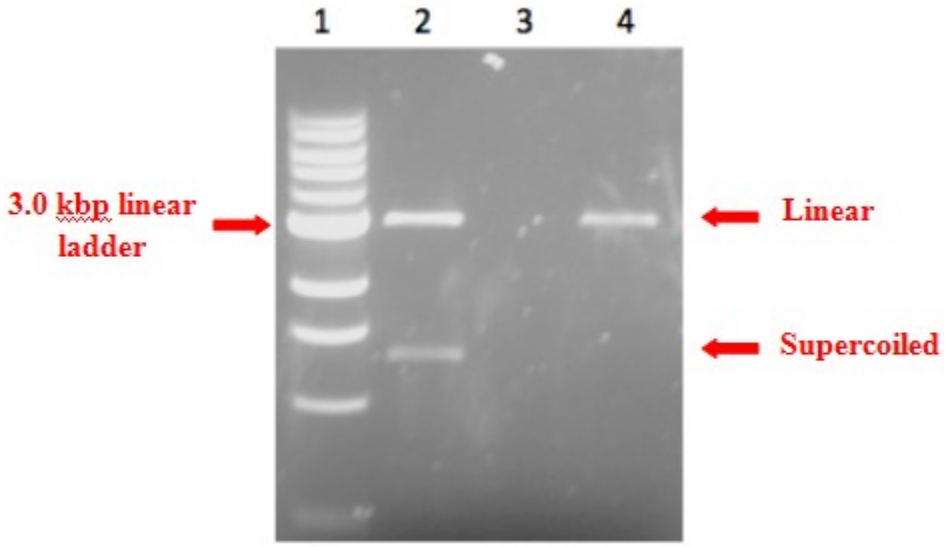

Figure 5-5: AGE image of a mixture of the linear and supercoiled isoforms of the 2.9 kbp plasmid using a 50 kDa PS hollow fiber membrane. Lane 1 is a calibration standard constructed using a DNA ladder with different size of linear DNA. Lane 2 is the feed solution containing equal amounts of the two isoforms. Lane 3 is the permeate sample obtained at a filtrate flux of 10 μm/s, while Lane 4 is the filtrate sample at 20 μm/s.

5.3.3. Fouling

All of the data reported in the previous sections were obtained with dilute solutions of the plasmid DNA, i.e., under conditions where membrane fouling would be expected to be minimal as discussed in Chapter 3. In order to examine the effect of membrane orientation on the fouling behavior, experiments were performed with a 3.0

μg/mL solution of the 16.9 kbp plasmid using a 500 kDa hollow fiber membrane in both the normal and reverse orientations. Data were obtained at a constant transmembrane pressure of 55 kPa giving an initial filtrate flux of 45±1 μm/s in both orientations. The filtrate flux was nearly constant throughout the ultrafiltration in both orientations, consistent with results reported in Chapter 3 for these relatively large pore size ultrafiltration membranes. The observed sieving coefficient data in the two orientations are shown in Figure 5-6. The observed sieving coefficient in the normal (forward) orientation declined significantly during the ultrafiltration. In contrast, the plasmid transmission in the reverse orientation was stable at $S_o \approx 0.8$ throughout the filtration even in the absence of any pulsing.

The absence of any fouling in the reverse orientation is likely related to the pre-extension of the plasmid molecules in the larger pores of the membrane support layer. For example, Rosa et al. (2012) previously demonstrated that the translocation of a knotted chain through a small pore is strongly force-dependent. They predicted that a trefoil-knotted chain can "un-knot" and pass though a small pore as long as the extensional force is smaller than a critical value (~ 30 pN). At higher force, the knots become "tighter", with the net result that the polymer chain can no longer un-knot and is instead trapped by the pore. It is possible that the weak extensional forces in the membrane support layer allow the plasmids to un-knot, minimizing the trapping of plasmids during ultrafiltration through the small pores in the membrane skin layer when the hollow fiber is used in the reverse orientation. This behavior is not seen in the normal flow orientation since the plasmids have to pass directly through the small pores in the membrane skin.

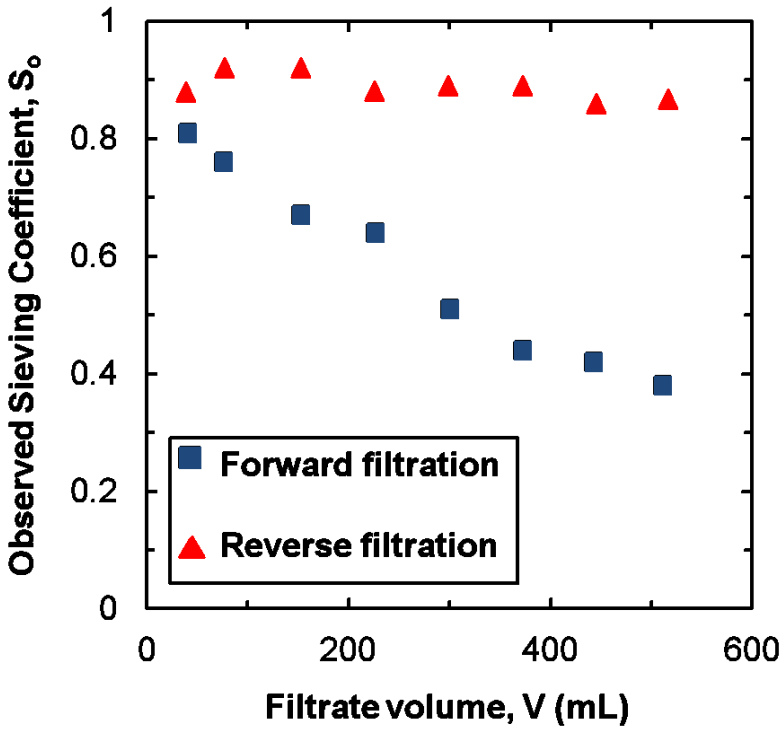

Figure 5-6: Effect of membrane orientation on fouling of a 3.0 µg/mL solution of the 16.9 kbp plasmid using a 500 kDa PS hollow fiber membrane at an initial flux of 46 ± 1 um/s.

5.4. Conclusions

The data obtained in this Chapter provide the first demonstration that the use of a "reverse" ultrafiltration can significantly enhance the performance of ultrafiltration processes for the purification of plasmid DNA. Plasmid transmission in the reverse flow direction, i.e., with the filtration directed through the membrane support structure before the skin, is significantly greater than that in the normal orientation. This behavior appears to be directly related to the "pre-extension" of the DNA during transmission through the relatively large pores in the membrane support. This was confirmed with

data obtained using a "double-layer" configuration in which a 0.22 μm pore size microfiltration membrane was placed directly on top of the skin of an ultrafiltration membrane; this double-layer membrane had much larger transmission of a 3.0 kbp plasmid than the ultrafiltration membrane alone, with the overall behavior being very similar to that of the ultrafiltration membrane when used in the reverse flow direction. This effect of membrane orientation on plasmid transmission was essentially independent of the plasmid size and was seen with both the linear and supercoiled isoforms. Data obtained using a mixture of the two isoforms showed good separation in the reverse orientation, similar to that seen in the forward orientation but at a much lower filtrate flux.

In addition, data obtained with a more concentrated solution of the supercoiled 16.9 kbp plasmid DNA showed nearly steady transmission in the reverse orientation without any measurable fouling, in sharp contrast to the nearly 50% reduction in transmission seen in the normal (forward) orientation. This behavior is also likely related to the pre-elongation of the DNA in the microporous support layer, which allows the plasmids to effectively "un-knot" and pass through the small pores in the skin layer without getting trapped. This behavior is in good qualitative agreement with results obtained in microfluidic devices for gene sequencing in which a pre-conditioning step before the nanopores can be used to partially extend the DNA molecules so that they can subsequently become fully elongated in the nanopores. These results demonstrate the potential of designing ultrafiltration membranes with tailored pore geometries for the high resolution purification of plasmid isoforms with dramatically reduced fouling.

Further studies will be required to fully investigate the effects of the membrane pore morphology on the separation and fouling characteristics during plasmid ultrafiltration.

Chapter 6

Purification of plasmid DNA isoforms using centrifugal ultrafiltration

The work presented in this Chapter was previously published in Biotechniques (Borujeni, E.E., A. L. Zydney, 53 (2012) pp. 49-56)

6.1. Introduction

Centrifugal ultrafiltration (UF) is used extensively for laboratory-scale purification, concentration, and isolation of a variety of biomolecules. This includes the use of centrifugal UF for rapid concentration of *Legionella* antigen in urine (Blanco et al., 2004), the isolation of free benzalkonium chloride (BAC) molecules from micelle solutions (Liu et al., 2009), the analysis of low-molecular weight proteins in the human plasma proteome (Greening and Simpson, 2011) and saliva (Lin et al., 2008), and the analysis of plant extracts (Sanchez, 2008).

Centrifugal UF is also a well-established method for concentrating and purifying DNA. Krowczynska and Henderson (1992) described the use of centrifugal UF for removal of unincorporated nucleotides and PCR primers after DNA amplification by the polymerase chain reaction. Schratter et al. (1993) summarized the use of centrifugal UF in construction of cosmid libraries (hybrid plasmids containing cos sequences), removal of restriction enzymes, and concentration of RNA. Centrifugal UF is also widely used in forensics for isolation and concentration of genomic DNA (McNevin, 2005).

All of these applications of centrifugal UF involve recovery of the large DNA in the retentate, with smaller molecules, impurities, and buffer components passed through the membrane and into the filtrate. However, previous works (Latulippe et al., 2007; Latulippe and Zydney, 2009; Latulippe and Zydney, 2010) has demonstrated that large DNA molecules with lengths of 3 – 17 kbp (kilobase pairs) can actually be transmitted through the small pores in traditional ultrafiltration membranes under certain conditions due to flow-induced elongation of the DNA. This opens up exciting opportunities for DNA purification, e.g., for removal of large cell debris, viruses, or bacteriophage, with the DNA recovered in the filtrate. In addition, Latulippe and Zydney (2011) demonstrated that pressure-driven ultrafiltration could also be used to separate the linear, supercoiled, and open circular isoforms of a given plasmid based on differences in elongational flexibility of these topological isoforms.

The objective of the work described in this Chapter was to demonstrate the feasibility of using centrifugal UF for small-scale DNA purification, including the identification of appropriate conditions for removal of unwanted plasmid isoforms. Initial experiments were performed using the individual isoforms to identify the critical centrifugal conditions for retention / transmission of the plasmid. DNA separations were then performed using commercially available centrifugal UF devices, with the composition of the DNA in the filtrate and retentate analyzed by agarose gel electrophoresis (AGE). The results clearly demonstrate that centrifugal UF can be used as a high-throughput screening technique for identification of the optimal ultrafiltration conditions that lead to an improved resolution of the plasmid isoforms separation.

6.2. Materials and Methods

6.2.1. Materials

6.2.1.1. Buffer

The Tris-EDTA (TE) buffer containing 10 mM NaCl was prepared according to the procedures described in Chapter 3 (Section 3.2.1.1).

6.2.1.2. Plasmids

Experiments were performed using linear, open circular and supercoiled isoforms of the 9.8 kbp plasmid (p-MDY) as discussed in Chapter 4 (see Section 4.2.1.2). Stock solutions of the supercoiled plasmid were provided by Dr. Jeffrey Chamberlain at the University of Washington. The linear and open circular isoforms were obtained by enzymatic digestion using 2 U/μg of respectively KpnI and Nt.AlwI enzymes (New England Biolabs, Ipswich, MA, USA). The digestion process along with the clean-up step was performed according to the procedure explained in Chapter 3 (Section 3.2.1.2). The final concentrations of digested plasmids were measured using the absorbance at 260 nm. The purified plasmid solutions were stored at -20 °C.

6.2.1.3. Centrifugal ultrafiltration membrane

Experiments were performed using NanoSep® centrifugal UF tubes obtained from Pall Corporation (Ann Arbor, MI). Each tube contains a feed reservoir with an

encapsulated Omega polyethersulfone ultrafiltration membrane with an effective filtration area of 0.28 cm^2 and a nominal molecular weight cutoff of 100 kDa. Membranes were initially flushed with 450 µL of 0.05 N NaOH followed by 1 mL of deionized water.

6.2.1.4. Centrifugation

Centrifugations were performed using a 5424 Eppendorf microcentrifuge with a fixed-angle rotor (FA 45-24-11) of 45°. The centrifugal speed could be varied up to 15,000 rpm, which corresponds to approximately 16,520×g (for a centrifuge tube filled with 450 µL of liquid) based on the rotor arm length of 0.066 m.

6.2.2. Methods

6.2.2.1. Filtration

Figure 6-1 shows a schematic diagram of the centrifugal ultrafiltration system. This type of filtration is driven by the hydrostatic force exerted by the liquid column over the membrane surface as determined by the key operational parameters in the centrifugation. Reduction of the liquid column height throughout the process leads to a declining transmembrane pressure and therefore a reduction in the filtrate flux.

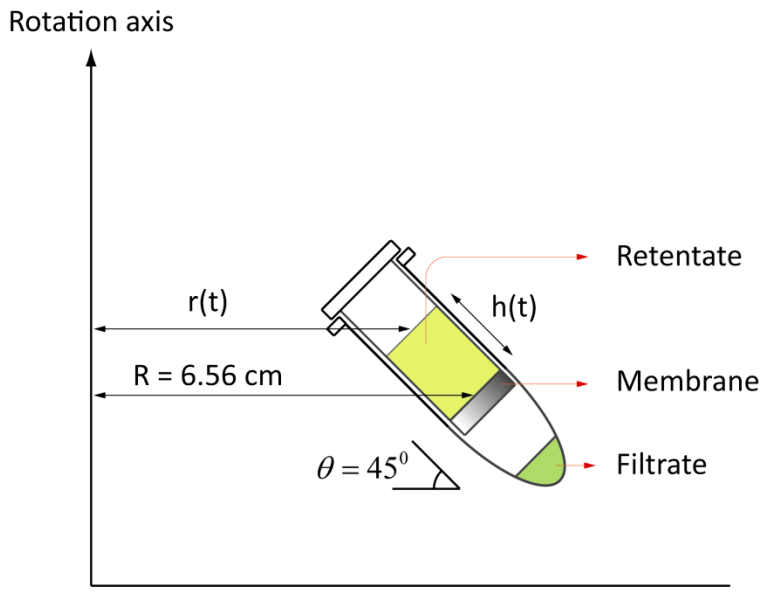

Figure 6-1: Schematic diagram of the centrifugal ultrafiltration (UF) system

A simple model was developed for selecting the proper operational conditions for the centrifugal UF (angular velocity and centrifugation time) in order to achieve a desired cumulative filtrate volume and average filtrate flux during the process. The instantaneous filtrate flux, J_v, through the membrane is given as:

$$J_v = L_p \Delta P \tag{6-1}$$

where, L_p is the hydraulic membrane permeability and ΔP is the transmembrane pressure driving force. The pressure in the liquid within the centrifuge tube increases as one moves down into the liquid:

$$\frac{dP}{dz} = \rho\omega^2 r\cos(\theta) \tag{6-2}$$

where z is the distance into the liquid (measured along the axis of the centrifuge tube), ρ is the liquid density, ω is the angular velocity, r is the distance measured from the rotor

axis to the position within the liquid, and θ is the fixed rotor angle. Equation (6-2) can be integrated over z to evaluate the pressure at the bottom of the liquid (of height h):

$$P_{z=h} = P_0 + \rho\omega^2\cos(\theta)\left[Rh - \frac{h^2}{2}\cos(\theta)\right] \tag{6-3}$$

where P_o is the pressure at the top interface (assumed to be atmospheric), h is the height of liquid in the tube, and R is the mean distance from the rotor axis to the location of the membrane. Equations (6-1) and (6-3) are combined with the mass balance to give:

$$\frac{dm}{dt} = \rho A\frac{dh}{dt} = -\rho A_0 J_v = -\rho^2\omega^2\cos(\theta)\left[Rh - \frac{h^2}{2}\cos(\theta)\right]L_p A_0 \tag{6-4}$$

where A is the cross-sectional area of the centrifuge tube (a function of h for a tapered tube) and A_o is the cross-sectional area of the membrane. Equation (6-4) can be integrated numerically to account for the slight taper at the bottom of the centrifuge tube and the acceleration of the rotor at the start of the centrifugation. In this case, ω was assumed to increase linearly from 0 to the specified rpm over the first 2 – 6 s. Equation (6-4) can also be integrated analytically assuming that $A = A_o$ and constant ω to give:

$$\ln\left(\frac{h}{h_0}\right) - \ln\left(\frac{R-\frac{h}{2}\cos(\theta)}{R-\frac{h_0}{2}\cos(\theta)}\right) = -\left[L_p\omega^2 R\rho\cos(\theta)\right]t \tag{6-5}$$

The cumulative filtrate volume under these conditions can be calculated using Equation (6-6):

$$V = A(h_0 - h) \tag{6-6}$$

where h is evaluated using Equation (6-5). Then, the average filtrate flux during a centrifugal ultrafiltration is obtained as:

$$\bar{J} = \frac{V}{A.t} \tag{6-7}$$

The membrane permeability in Equations (6-4) and (6-5) can be evaluated by performing a set of centrifugation ultrafiltration experiments with pure buffer with the results for the cumulative filtrate volume fit to the data using the least squared residuals method to determine the best fit value of L_p.

Centrifugal ultrafiltration experiments were conducted by filling the NanoSep® centrifuge tube with 450 μL of the feed (buffer or plasmid solutions), the rotation speed was set at the desired value, and the tube was spun for a given period of time. The tube was then removed from the microcentrifuge, with the filtrate collected and weighed using a MS104S analytical balance (Mettler Toledo, Columbus, OH) with an accuracy of 10^{-4} g. A small sample of the filtrate and retentate were collected for analysis of the plasmid concentration and composition.

Several multistep discontinuous diafiltration experiments were also performed as follows. The NanoSep® centrifuge tube was prepared and a centrifugal UF was performed to reduce the volume from 450 μL to approximately 50 μL. The tube was then removed from the centrifuge with the filtrate collected and weighed. The retentate remaining within the tube was then diluted with additional TE buffer back to the initial volume. This entire procedure was repeated multiple times using the same centrifugal conditions, with the filtrate removed at the end of each UF step. A final sample was obtained from the retentate sample at the end of the experiment.

6.2.2.2. Assays

The total DNA concentration was evaluated using Quant-iT^{TM} PicoGreen® dsDNA assay (see Section 3.2.2.2), and the composition of solutions containing mixtures of the different isoforms was determined by agarose gel electrophoresis (AGE) (see Section 3.2.2.3). AGE was also used in order to verify the successful plasmid isoform digestions.

6.3. Results and analysis

Figure 6-2 shows a plot of the experimental and predicted values of the cumulative filtrate volume as a function of time during a set of centrifugal ultrafiltration experiments performed with a plasmid-free buffer at different angular velocities, with the centrifuge tube cross-sectional area and initial liquid column height over the membrane taken as $A = 0.41$ cm^2 and $h_0 = 1.1$ cm. The dashed curves are the model calculations given by Equation (6-5) using the best fit value of the membrane permeability, $L_p = 1.9 \times 10^{-6}$ m/(s.kPa), as determined by minimizing the sum of the squared residuals between the model and data. The solid curves were developed by numerical integration of Equation (6-4) using the same value of L_p but accounting for the slight taper in the centrifuge tube. The model calculations are in very good agreement with the experimental data, with only slight differences between the analytical and numerical results. Equation (6-5) can thus be used to estimate the angular velocity and centrifugation time required to achieve a given total filtrate volume and average filtration velocity (via Equation (6-7)).

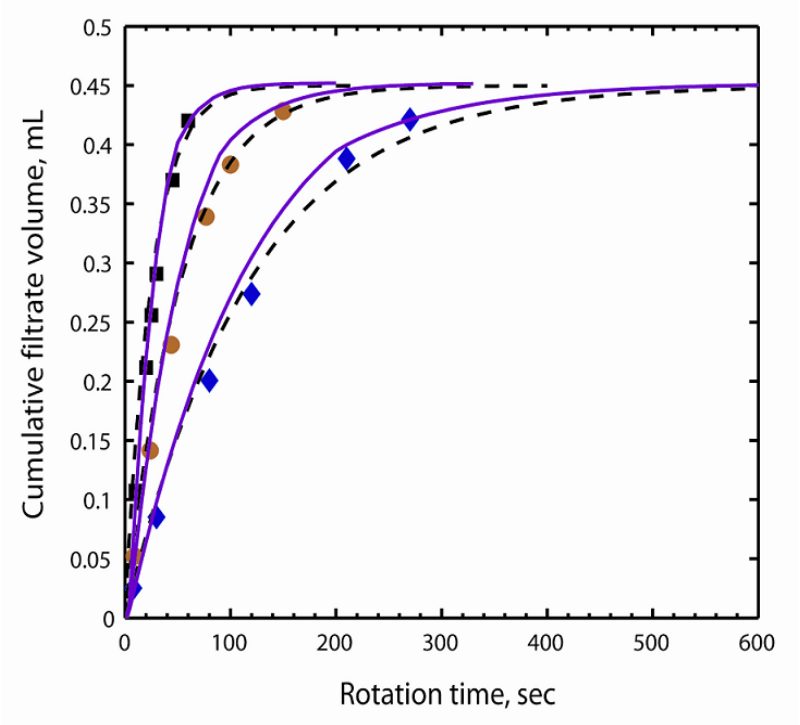

Figure 6-2: Cumulative filtrate volume as a function of time during centrifugal ultrafiltration. The symbols (♦), (●), and (■) represent experimental data obtained at angular velocities of 3000, 4500, and 6500 rpm, using TE buffer with 10 mM NaCl using the 100 kDa Omega membrane. Solid and dashed curves are numerical and analytical solutions as described in text using $L_p = 1.9 \times 10^{-6}$ m/(s.kPa).

Figure 6-3 shows typical experimental data obtained in centrifugal UF. The tubes were initially filled with 450 µL of the supercoiled, linear, or open circular isoform of a 9.8 kbp plasmid suspended in TE buffer containing 10 mM NaCl at a concentration of 1 µg/mL. Each data point represents results from a separate centrifugation. In each case, the centrifugation time was adjusted to collect 160 ± 10 µL of filtrate based on the models presented earlier in this Chapter (Section 6.2.2.1). The y-axis shows the concentration of the plasmid isoform collected in the filtrate solution for each centrifugation, determined using the measured fluorescence of the PicoGreen stain. The

x-axis is the set value of the angular velocity used for the centrifugation. At any given angular velocity, the filtrate concentration for the linear isoform was significantly greater than that of the supercoiled isoform, with relatively little of the open circular isoform transmitted through the membrane out to even 5500 rpm.

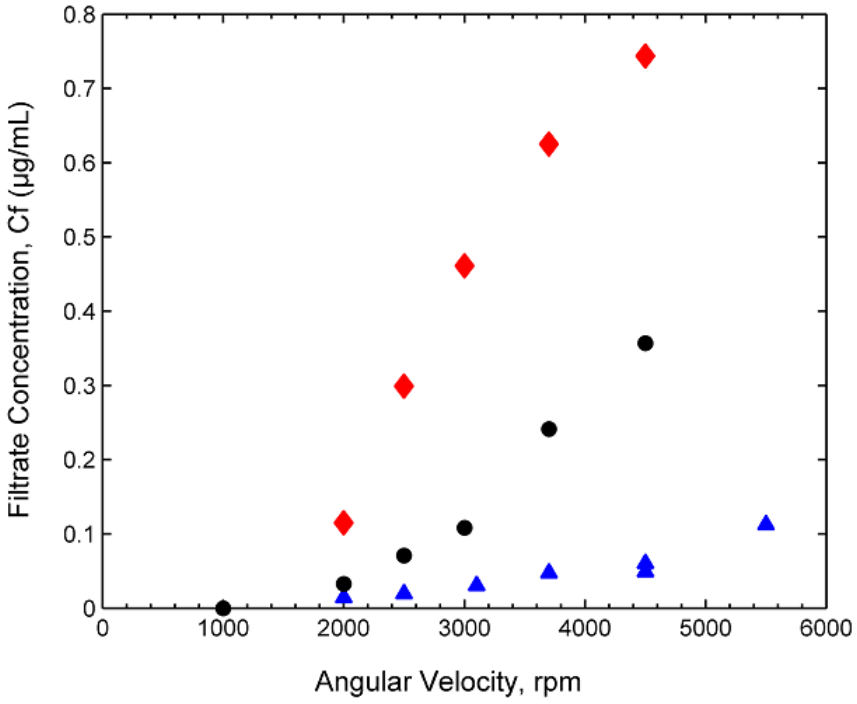

Figure 6-3: Concentration of linear (♦), supercoiled (•), and open circular (▲) isoforms of a 9.8 kbp plasmid collected during centrifugal ultrafiltration through a 100 kDa Omega membrane as a function of the angular velocity.

The data for the supercoiled isoform show no measurable DNA in the filtrate (concentration ≤ 0.03 µg/mL) for angular velocities below about 1500 rpm, consistent with complete retention of the 9.8 kbp plasmid by the small pores of the 100 kDa membrane under these conditions. Plasmid transmission increased with increasing centrifugal speed, with greater than 0.35 µg/mL (corresponding to 64 ng) of the

supercoiled plasmid collected in the filtrate for centrifugation at 4500 rpm. This high degree of plasmid transmission occurs even though the radius of gyration of the supercoiled 9.8 kbp plasmid is 117 ± 3 nm in a Tris–EDTA buffer containing 200 mM NaCl (Latulippe and Zydney, 2010), which is approximately 20 times larger than the 6.4 nm pore size of a typical 100 kDa ultrafiltration membrane (Latulippe et al., 2007). The transmission of the linear DNA isoform was even greater, with a filtrate concentration of 0.75 μg/mL at 4500 rpm, even though the linear isoform has a radius of gyration of more than 200 nm (Latulippe and Zydney, 2010).

There was no evidence of any plasmid degradation during the centrifugal UF; agarose gel electrophoresis of samples obtained from the initial feed, final retentate, and filtrate solutions showed bands corresponding to the linear, supercoiled, and open-circular plasmids as expected. As discussed by Latulippe at al. (2007), and Latulippe and Zydney (2009), the high degree of plasmid transmission through the small membrane pores is due to the flow-induced elongation of the plasmid in the converging flow-field into the membrane pores.

Figure 6-4 shows a comparison of results from the centrifugal UF with data obtained during pressure-driven ultrafiltration through a 100 kDa composite regenerated cellulose membrane (Latulippe et al., 2007). In this case, the data are plotted as a function of the average filtrate flux ($\bar{J}$), which was calculated using Equation (6-7). The y-axis is the scaled filtrate concentration, equal to the plasmid concentration in the filtrate sample collected at the end of the centrifugation divided by the arithmetic mean of the initial (feed) and final (retentate) plasmid concentrations in the solution above the membrane ($\overline{C}$). The scaled concentration is equivalent to the average value of the

observed sieving coefficient (see Section 3.2.2.2). The results from the centrifugal and pressure-driven UF are in good qualitative agreement, with the data for the pressure-driven experiment shifted to slightly higher filtration velocities. In both cases, plasmid transmission was negligible below a critical filtration velocity between 40 and 60 µm/s.

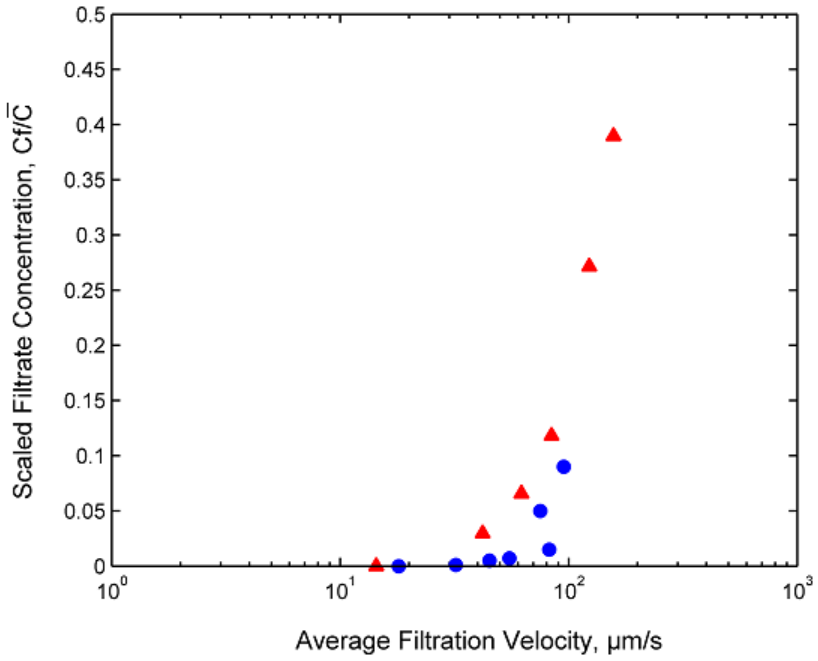

Figure 6-4: Scaled filtrate concentration as a function of the average filtration velocity for centrifugal (▲) and pressure-driven (●) ultrafiltration of the supercoiled 9.8 kbp plasmid through a 100 kDa membrane.

Based on the results with the individual isoforms, a centrifugal UF experiment was performed to separate 450 µL of a binary mixture containing 0.7 µg/mL of the supercoiled plasmid and 0.3 µg/mL of the linear isoform (lane 2 in the agarose gel electrophoresis in Figure 6-5-A). Data were obtained at 1350, 2350, and 2750 rpm, with the time adjusted to collect 160 ± 10 µL of filtrate. The supercoiled isoform migrates furthest through the gel, consistent with results from previous studies (Moreau et al.,

1987; Latulippe and Zydney, 2010). The faint band, seen slightly above the linear isoform, is likely due to the presence of a small quantity of a dimer of the supercoiled isoform or possibly trace amounts of the open-circular isoform initially present in the stock solution of the supercoiled plasmid. This species was fully retained by the membrane in all experiments.

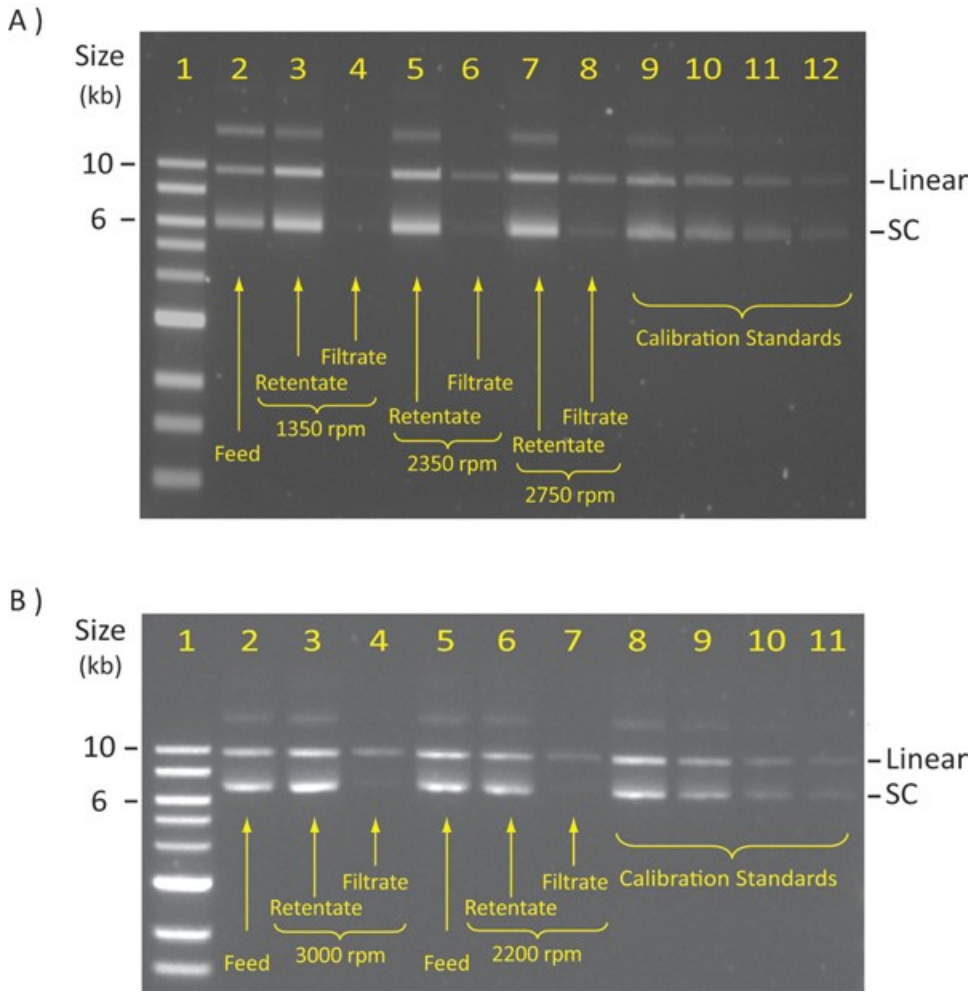

Figure 6-5: AGE image of feed, retentate, and filtrate samples obtained during centrifugal ultrafiltration after collection of A) 160 ± 10 µL and (B) 370 ± 10 µL filtrate. Feed solutions are binary mixtures containing 0.7 µg/ml of the supercoiled (SC) 9.8 kbp plasmid and 0.3 µg/ml of the linear isoform in TE buffer containing 10 mM NaCl. Images were taken after running the gels for 2 hours at 75 V.

The centrifugal UF at 1350 rpm showed complete retention of both plasmid isoforms (Lane 4). The filtrate sample for the run at 2350 rpm shows a significant amount of the linear isoform with only trace levels of the supercoiled isoform (Lane 6), consistent with the results shown previously in Figure 6-3. The use of a larger centrifugal speed (2750 rpm) led to greater transmission of the linear isoform with a small but measureable amount of the supercoiled isoform collected in the filtrate (Lane 8). The bands corresponding to the supercoiled isoform in the final retentate samples (Lanes 3, 5, and 7) are significantly brighter than those in the feed (Lane 2), consistent with an increase in concentration of the highly retained supercoiled plasmid in these experiments.

Figure 6-5-B shows corresponding results for centrifugal UF experiments with the same feed (Lanes 2 and 5) performed with higher degrees of filtration. Data were obtained at 2200 and 3000 rpm, providing V = 380 and 360 μL of filtrate (compared to the initial volume of 450 μL); these experiments yielded average filtration velocities of $\bar{J}$ = 37 and 66 μm/s, respectively. The filtrate samples (Lanes 4 and 7) show negligible amounts of the supercoiled isoform, consistent with operation near or below the critical average filtration velocity for transmission of this plasmid. The retentate samples (Lanes 3 and 6) show very bright bands for both isoforms due to the concentration of the retained plasmid.

The results in Figure 6-5-B can be analyzed more quantitatively by integrating the appropriate mass balances for an ultrafiltration process (Zydney and Zeman, 1996) . The final expressions are conveniently expressed in terms of the observed sieving coefficient (S_o), which is equal to the fractional transmission of the plasmid through the membrane

(see Section 3.2.2.2). The plasmid concentrations in the final retentate (C_R) and filtrate (C_f) are given as (Zydney and Zeman, 1996).

$$\frac{C_R}{C_o} = \left(\frac{V_o}{V}\right)^{1-S_o} \tag{6-8}$$

$$\frac{C_f}{C_o} = \frac{1-\left(\frac{V}{V_o}\right)^{S_o}}{1-\left(\frac{V}{V_o}\right)} \tag{6-9}$$

where V_o/V is the concentration factor for the centrifugal UF. The predicted final retentate concentrations for the centrifugal UF experiments in Figure 6-5-B are C_R/C_o = 3.0 and 4.6 using S_o = 0.33 and 0.07, respectively, for the linear and supercoiled isoforms at 3000 rpm. These values are consistent with the results in the AGE images, based on the comparison of the intensity of the bands for the calibration standards (Lanes 9, 10, 11, and 12 in Figure 6-5-A and Lanes 8, 9, 10, and 11 in Figure 6-5-B at concentrations of 1, 0.5, 0.2, and 0.1 μg/mL).

The purity of the retained (i.e., supercoiled) isoform can be increased by using a discontinuous diafiltration as described in Section 6.2.2.1. In this case, a three-step diafiltration was performed, with the feed volume reduced from 450 μL to approximately 50 μL during each UF step (followed by removal of the filtrate and re-dilution of the retentate to 450 μL using fresh TE buffer). Figure 6-6-A shows results for the separation of a mixture containing 0.3 μg/mL of the linear and 0.7 μg/mL of the supercoiled isoform (Lane 2) at 3000 rpm, providing an average filtration velocity of approximately 64 ± 5 μm/s. The filtrate solutions (Lanes 3, 4, and 5) are primarily the linear DNA isoform, with the concentration decreasing after each step in the discontinuous diafiltration as the linear DNA is removed from the centrifuge tube. The final retentate (Lane 6) has a bright

band corresponding to the supercoiled DNA, with a relatively small amount of the remaining linear DNA, along with some DNA dimer, visible as distinct bands near the top of the gel.

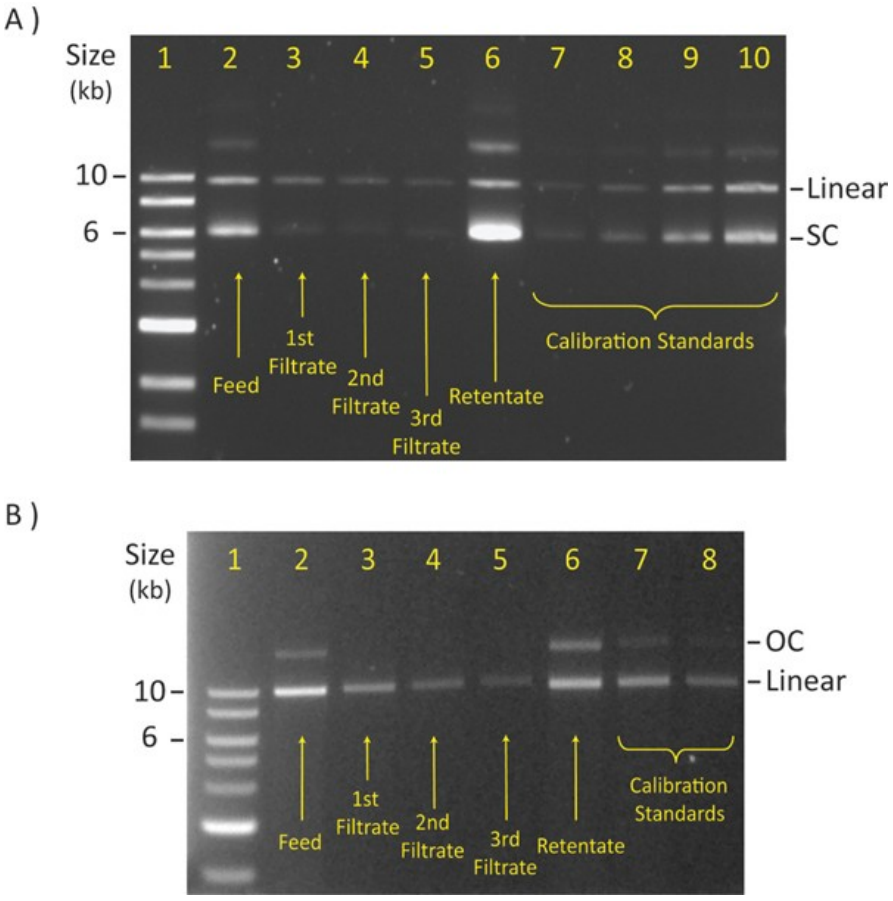

Figure 6-6: AGE image of feed, retentate, and filtrate samples obtained during three-step discontinuous diafiltrations which were performed to separate binary mixtures of the different isoforms of a 9.8 kbp plasmid in TE buffer containing 10 mM NaCl. 100 kDa Omega centrifugal UF membranes were used and images were taken after running the gels for 130 min at 75 V. (A) Separation of a feed containing 0.7 µg/mL of the supercoiled and 0.3 µg/mL of the linear isoform at 3000 rpm. (B) Separation of a mixture of 0.2 µg/mL of the open circular and 0.8 µg/mL of the linear isoform at 3300 rpm.

The final concentrations of the linear and supercoiled DNA at the end of the discontinuous diafiltration can be calculated as (Zydney and Zeman, 1996):

$$\frac{C_R}{C_o} = \left(\frac{V_o}{V} \right)^{1-n S_o} \tag{6-10}$$

where n is the number of steps in the discontinuous diafiltration (n = 1 corresponds to a simple ultrafiltration while n = 2 corresponds to a UF, dilution back to the initial volume, and then a second UF). If the observed sieving coefficients of the linear and supercoiled isoforms are assumed to be S_o = 0.33 and 0.07, respectively (consistent with the results in Figure 6-4), Equation (6-10) predicts that the final retentate would contain 3.6 μg/mL of the supercoiled plasmid and only 0.3 μg/mL of the linear isoform (assuming a concentration factor of V_o/V = 9 for each UF step). Further purification could be achieved using additional diafiltration steps. Model calculations indicate that the concentration of the linear isoform could be reduced by more than a 100-fold using n = 6 diafiltration steps.

Corresponding results for the separation of a mixture of 0.2 μg/mL open circular and 0.8 μg/mL linear isoforms (Lane 2) are shown in Figure 6-6-B. The discontinuous diafiltration was performed at 3300 rpm yielding an average filtration velocity of 69 ± 2 μm/s. The filtrate samples for the 3 diafiltrations (Lanes 3, 4, and 5) contain only the linear isoform, leaving a final retentate solution (Lane 6) that is significantly more concentrated in the open circular isoform than the feed. Lanes 7 and 8 are calibration standards at concentrations of 0.45 and 0.2 μg/mL, respectively.

6.4. Discussion

The data presented in this Chapter provide the first demonstration that centrifugal ultrafiltration can be used for the separation of plasmid DNA isoforms. The behavior of the centrifugal UF process is very similar to that in pressure-driven ultrafiltration, with the filtrate flux determined by the magnitude of the centrifugal speed and the height of the liquid column in the centrifuge tube (in contrast to the applied pressure). However, the variation of the liquid height in the centrifuge tube means that the filtrate flux varies with time during the ultrafiltration. Appropriate equations were developed that makes it possible to predict the variation of the flux and liquid height with time during the centrifugal ultrafiltration process, with the model is excellent agreement with experimental data under conditions in which the flux was limited by the membrane permeability.

There are several distinct advantages to the use of centrifugal UF for plasmid purification. Centrifugal UF is fast, requiring only a few minutes compared to the several hours needed for agarose gel electrophoresis and density gradient centrifugation. Centrifugal UF requires no staining or visualization agents, eliminating the need to remove these dyes before subsequent processing steps. Centrifugal UF is readily performed using existing equipment and is easily incorporated into multi-step processes for DNA purification and handling. Scale-up can be achieved using larger volume centrifugal UF tubes; for example, Pall JumboSep tubes can handle up 60 mL of DNA solution. Note that purification of the supercoiled DNA from both the linear and open circular isoforms would require a multi-step process: the linear DNA would first be

removed using a discontinuous diafiltration at relatively low centrifugal speed, with the supercoiled plasmid then recovered in the filtrate using a second discontinuous diafiltration at higher centrifugal speed (Figure 6-3). The latter separation is the more challenging due to the small difference in critical filtration velocity for the supercoiled and open circular isoforms and the presence of intermolecular interactions between these plasmids.

Centrifugal UF is also highly attractive for initial screening studies to identify appropriate conditions for plasmid isoform separation. This would include both the filtrate flux as well buffer conditions. For example, multiple centrifuge tubes with different solution pH or ionic strength could be run simultaneously in a given centrifuge rotor, with the effectiveness of the separation determined from the plasmid concentrations in the final filtrate and retentate. This type of screening could be done with very small volumes of plasmid, greatly facilitating the optimization of the plasmid separation process.

Chapter 7

Conclusions and recommendations for future works

7.1 Conclusions

There is increasing interest in the use of purified plasmid DNA in a variety of applications including both gene therapy and DNA vaccination. Membrane-based processes are attractive alternatives for plasmid purification with applications in primary isolation (e.g., microfiltration for removing genomic DNA, large impurities, and precipitates) and for higher resolution separations (e.g., ultrafiltration for removal of small impurities and unwanted plasmid isoforms). Previous works by Latulippe et al. (2007), and Latulippe and Zydney (2009) demonstrated that DNA transmission through small pore ultrafiltration membranes occurs by elongation of the DNA due to the hydrodynamic force associated with the filtration. The overall goals of this dissertation were to significantly extend the current understanding of key phenomena that govern the development and application of ultrafiltration processes for the purification of plasmid DNA.

The results reported in Chapter 3 showed that membrane fouling leads to a dramatic reduction in plasmid transmission, but only a small reduction in filtrate flux, during ultrafiltration of more concentrated plasmid solutions. This fouling was due to the trapping of large plasmids in the membrane pores. This blockage eliminated the transmission of subsequent plasmids, but it still allowed significant fluid flow through the pore due to the very open structure of the DNA molecule. A simple theoretical model was

developed based on this physical picture, with very good agreement between the experimental data and model calculations. The model had only two fitted parameters: one describing the rate of pore blockage (k) and one describing the rate of fluid flow through the blocked pore (β). The rate of pore blockage increased with increasing plasmid size, which was likely due to the greater probability of knot formation in the long DNA molecule, making them more likely to get trapped in the pores during ultrafiltration. These studies provide the first quantitative description of the fouling behavior during ultrafiltration of plasmid DNA through small pore size membranes.

In order to overcome the problems with membrane fouling, the studies in Chapter 4 examined the use of periodic backpulsing to "release" the previously trapped plasmids from the membrane pores. Experiments were performed over a range of backpulse frequency, amplitude, and duration using self-supported hollow fiber membranes in order to characterize the process and determine the optimal backpulsing conditions. The results clearly demonstrated that the removal of trapped plasmids from the membrane pores under typical filtration conditions was dominated by the shear / drag associated with the tangential flow. Thus, it was possible to maintain good plasmid transmission throughout the ultrafiltration process simply by periodically closing the permeate exit line (without any backpressure). The fouling model developed in Chapter 3 was extended to account for the effects of pulsing by including a single additional parameter (α), which describes the effectiveness of the pulse at releasing trapped plasmids from the membrane pores. Model calculations were in good agreement with experimental data, providing a framework for identifying the optimal pulsing conditions. A pulsed diafiltration process provided 98% recovery of a supercoiled plasmid in the filtrate compared to only 35%

recovery without backpulsing. These results clearly demonstrate the potential advantages of using pulsed ultrafiltration systems for plasmid separations. In addition, the ability to effectively release the trapped plasmids simply by clamping the permeate line (i.e., turning off the filtrate flow) for short periods of time should facilitate the use of this approach even in large scale ultrafiltration systems.

The experimental studies in Chapter 5 examined the effects of pore structure or morphology on DNA ultrafiltration, using both asymmetric membranes in the forward and reverse orientations and composite membranes produced by placing a large pore size microfiltration directly on top of the skin layer in a small pore ultrafiltration membrane. Plasmid transmission was significantly increased when the plasmid passed through a large pore region prior to the tight ultrafiltration membrane. This increase in transmission occurs because transmission of the plasmids through the large pores partially extends the plasmid molecules greatly facilitating their elongation and subsequent transmission through the nanopores in the skin layer of the ultrafiltration membrane. In addition to the increase in plasmid transmission, membrane fouling was reduced when the membrane was used in the reverse orientation, most likely due to the "un-knotting" of the DNA in the large pores within the support structure of the membrane. This behavior is very similar to results obtained in microfluidic gene sequencing devices in which the DNA is "pre-elongated" to facilitate transmission of individual DNA molecules through the pores used for sequencing.

The effective design of high resolution membrane systems for plasmid separations can be greatly facilitated using high-throughput methods for screening operating conditions (e.g.., filtrate flux and membrane pore size) as well as buffer conditions. The

studies in Chapter 6 examined the design and operation of a centrifugal ultrafiltration process both for high-throughput screening studies and laboratory-scale separations of plasmid DNA. A simple theoretical model was developed to evaluate the filtrate flux in centrifugal ultrafiltration as a function of the rotation speed, rotor length, and liquid height in the centrifuge tube. These results clearly demonstrate that centrifugal ultrafiltration can provide a rapid, safe (no hazardous chemicals), and reliable method for DNA purification that can also be used for high-throughput screening for larger-scale DNA separations.

Overall, the work presented in this dissertation has provided significant new insights into the development and application of ultrafiltration processes for the purification of plasmid DNA, including the separation of DNA isoforms based on differences in elongational flexibility in response to the hydrodynamic flow field into the small membrane pores.

7.2. Recommendations for future work

The results presented in this dissertation have also opened up new avenues of research that should be pursued to further the development of membrane-based processes for plasmid DNA purification. The recommended directions for future work are discussed below, considering both fundamental studies of DNA elongation and transmission through small nanopores and more practically oriented studies focused on the application of ultrafiltration systems for DNA separations.

7.2.1. Fundamental studies

A number of recent studies have used micro/nano fluidic devices with well-defined pore shapes, including slits and more complex arrays of pores and posts, to track the elongation of individual DNA molecules using fluorescent techniques (Levy and Craighead, 2010; Fyta et al., 2011; Dorfman et al., 2013). These studies have been focused almost entirely on understanding the behavior of linear ds-DNA molecules due to their importance in gene sequencing; there are no similar studies on the behavior of DNA with different topologies including the supercoiled, circular, or concatemer isoforms. It would be very interesting to apply these nanofluidic and single molecule techniques to study the elongational characteristics of these different plasmid isoforms, including the possible use of complex pore geometries to "pre-extend" the DNA and thereby facilitate transmission through very small pores. These studies would help in developing a more complete understating of the factors controlling the initiation of plasmid elongation as a function of plasmid size and conformation, nanopore dimension, and solution conditions. They could also be used to examine the distribution of elongational properties across a population of DNA molecules (e.g., based on their initial configuration). These results could also inform existing theoretical models of DNA elongation, possibly leading to the development of more complete descriptions of this phenomenon. It might also be possible to use these systems to study intermolecular interactions between DNA molecules, both in systems containing single isoforms and in mixtures of the different isoforms. The behavior in these more concentrated solutions has been largely unexplored in gene sequencing applications (which typically use very dilute solutions), but is likely

to be critical in applications of ultrafiltration processes for high-resolution separation of plasmid isoforms.

7.2.2. Practical studies

The difference in elongational flexibility of the different DNA isoforms provides an opportunity for separation of these isoforms using ultrafiltration by operation at a filtrate flux between the critical flux values of the isoforms (Latulippe and Zydney, 2011; Borujeni and Zydney, 2012). However, in many cases this operating window is small and may provide low resolution in the separation.

One approach that is worth examining in the future is the possibility of enhancing the separation using metal cations or polyamines to selectively interact with specific plasmid conformations thereby altering their structure and elongation characteristics. For example, Latulippe and Zydney (2008) showed that increasing the NaCl concentration from 1 to 150 mM provided an 80-fold increase in transmission of the supercoiled plasmid. They attributed this behavior to a reduction in the persistence length caused by Na^+ cations shielding the negative phosphate groups and therefore reducing the intramolecular repulsive interactions. Similar effects were achieved with addition of only 10 mM $MgCl_2$ due to the divalent character of the Mg^{2+} cations. No studies were performed with either the linear or open-circular isoforms; thus, it is not currently known whether these ions could improve the selectivity of the isoform separation. However, Mg^{2+} is known to preferentially bind to DNA at locations where there is a sharp bend or loop in the double helix that creates a region with a high concentration of negative charge

(Bloomfield et al., 1999). Braunlin et al. (1992) showed that Ca^{2+} binding to DNA is also sensitive to the local structure of the DNA. Thus, it might be possible to exploit these binding interactions to control and enhance DNA separations.

There are also a number of compacting agents that can alter the size and twist of DNA. For example, $[Co(NH_3)_6]^{3+}$ has been shown to increase the supercoiling and twisting of supercoiled isoform (Bloomfield, 1997). Crystallographic studies of spermine-DNA complexes showed that the major grooves in the DNA are more favorable targets for interaction (Bloomfield et al., 1999) while Deng et al. (2000) has shown that guanine and thymine bases for this polyamine. There is thus considerable evidence that the conformation of the plasmid can affect the binding interactions with different cations. Bloomfield et al. (1999) has provided a review of DNA condensation from a thermodynamic perspective; only tri- and higher-valent cations are able to induce DNA condensation. It would be very interesting to perform extensive studies of the effects of di- and multivalent cations and polyamines on the transmission of individual DNA isoforms during ultrafiltration, with the goal of identifying conditions that provide enhanced resolution in DNA separations. These studies could be very effectively performed using the centrifugal ultrafiltration system described in Chapter 6, with multiple centrifuge tubes examined simultaneously, each loaded with DNA in the presence of different cations (at different concentrations).

Actual separations of the supercoiled isoform would need to be conducted using a two-stage ultrafiltration process in which the linear isoform is collected in the permeate during the first step (with supercoiled and open circular isoforms retained by the membrane) followed by recovery of the supercoiled plasmid in the permeate of the

second stage. Additional studies would be needed to optimize the design of this two-stage process, possibly using different concentrations of specific cations to enhance the individual separations. In this case, a diafiltration at low filtrate flux, i.e., under conditions where all DNA isoforms are fully retained, could be used to change the buffer conditions in the two stages to enhance the overall resolution of the separation.

Most of the fouling studies presented in Chapters 3 and 4 were performed with solutions of the supercoiled isoform – limited data with the linear isoform showed minimal fouling under typical experimental conditions. It will be critically important to extend these studies to the open circular isoform and to solutions containing high loads of plasmid dimers and other conformational impurities. This work should also include more detailed studies of pulsing and the use of membranes with reverse orientation (similar to the work described in Chapters 4 and 5) to demonstrate whether these techniques can be effectively used to control fouling for the full range of isoforms and experimental conditions encountered in DNA purification. For example, although the use of reverse filtration significantly reduced membrane fouling (Chapter 5), experiments performed over long times did show some loss of plasmid transmission. Future studies are needed to quantify this behavior and to determine whether backpulsing might also be effective in this configuration. Note that it is unlikely that simple pulsing would be able to remove trapped plasmids in the reverse flow orientation since the plasmids would be stuck in pores deep within the membrane support structure and thus inaccessible to the shear / drag associated with crossflow. However, an actual backpulse might be able to remove such trapped plasmids, although the optimal conditions for backpulsing in such a system would need to be determined.

In addition to the different plasmid isoforms, there are a wide range of other cellular impurities that need to be removed during DNA purification including host cell proteins, RNA, genomic DNA, and endotoxins. Kahn et al. (2000) and Nunes et al. (2014) have provided limited data on the use of ultrafiltration for removal of cellular impurities, although these studies examined only a relatively narrow range of impurities and experimental conditions. Future studies should be focused on the optimization of these separations, including the choice of filtrate flux, membrane pore size, plasmid specifications (size, isoform, and concentration), and the type and concentration of impurities. Membrane fouling is likely to be a critical issue in the development and operation of membrane systems for purification of DNA from these more complex feed streams.

References

(2014) "Gene therapy clinical trials worldwide." The Journal of Gene Medicine.

Acland, G. M., Aguirre, G. D., Ray, J., Zhang, Q., Aleman, T. S., Cideciyan, A. V., Pearce-Kelling, S. E., Anand, V., Zeng, Y., Maguire, A. M., Jacobson, S. G., Hauswirth, W. W. and Bennett, J. (2001). "Gene therapy restores vision in a canine model of childhood blindness." Nature Genetics **28**(1): 92-95.

Adleman, L. M. (1994). "Molecular computation of solutions to combinatorial problems." Science **266**(5187): 1021-1024.

Affandy, A., Keshavarz-Moore, E. and Versteeg, H. K. (2013). "Application of filtration blocking models to describe fouling and transmission of large plasmids DNA in sterile filtration." Journal of Membrane Science **437**(0): 150-159.

Ager, K., Latulippe, D. R. and Zydney, A. L. (2009). "Plasmid DNA transmission through charged ultrafiltration membranes." Journal of Membrane Science **344**(1-2): 123-128.

Arkhangelsky, E., Sefi, Y., Hajaj, B., Rothenberg, G. and Gitis, V. (2011). "Kinetics and mechanism of plasmid DNA penetration through nanopores." Journal of Membrane Science **371**(1-2): 45-51.

Arkhangelsky, E., Steubing, B., Ben-Dov, E., Kushmaro, A. and Gitis, V. (2008). "Influence of ph and ionic strength on transmission of plasmid DNA through ultrafiltration membranes." Desalination **227**(1-3): 111-119.

Bai, J. S., Bai, S., Shi, Q. H. and Sun, Y. (2014). "Purification of supercoiled plasmid DNA from clarified bacterial lysate by arginine-affinity chromatography: Effects of spacer arms and ligand density." Journal of Separation Science **37**(12): 1386-1395.

Bakhshayeshi, M., Zhou, H. Y., Olsen, C., Yuan, W. and Zydney, A. L. (2011). "Understanding dextran retention data for hollow fiber ultrafiltration membranes." Journal of Membrane Science **385**(1-2): 243-250.

Berg, M., Blom, H. and Lemmens, R. (2009). Method of separation of deoxyribonucleic acids, Google Patents.

Berne, B. J. and Pecora, R. (1976). Dynamic light scattering : With applications to chemistry, biology, and physics, Wiley.

Birnboim, H. C. and Doly, J. (1979). "Rapid alkaline extraction procedure for screening recombinant plasmid DNA." Nucleic Acids Research **7**(6): 1513-1523.

Blanco, S., Prat, C., Pallares, M. A., Matas, L. and Dominguez, J. (2004). "Centrifugal ultrafiltration method for rapid concentration of legionella pneumophila urinary antigen." Journal of Clinical Microbiology **42**(9): 4410.

Bloomfield, V. A. (1997). "DNA condensation by multivalent cations." Biopolymers **44**(3): 269-282.

Bloomfield, V. A., Crothers, D. M. and Tinoco, I. (1999). Nucleic acids Structures, Properties, and Functions, University Science Books.

Bolshoy, A., McNamara, P., Harrington, R. E. and Trifonov, E. N. (1991). "Curved DNA without A-A : Experimental estimation of all 16 DNA wedge angles." Proceedings of the National Academy of Sciences of the United States of America **88**(6): 2312-2316.

Borujeni, E. E. and Zydney, A. L. (2012). "Separation of plasmid DNA isoforms using centrifugal ultrafiltration." Biotechniques **53**(1): 49-56.

Braunlin, W. H., Drakenberg, T. and Nordenskiold, L. (1992). "Ca^{2+} binding environments on natural and synthetic polymeric DNAs." Journal of Biomolecular Structure & Dynamics **10**(2): 333-343.

Cai, Y., Rodriguez, S. and Hebel, H. (2009). "DNA vaccine manufacture: Scale and quality." Expert Review of Vaccines **8**(9): 1277-1291.

Camps, M. (2010). "Modulation of cole 1-like plasmid replication for recombinant gene expression." Recent Pat DNA Gene Seq. **4**(1): 16.

Cherkasov, A. N., Samokhina, G. D. and Petrova, V. N. (1993). "Ultrafiltration of flexible-chain polymers based on the theory of unfolding of polymer-chains " Colloid Journal of the Russian Academy of Sciences **55**(3): 488-492.

Clemson, M. and Kelly, W. J. (2003). "Optimizing alkaline lysis for DNA plasmid recovery." Biotechnology and Applied Biochemistry **37**(3): 235-244.

Daoudi, S. and Brochard, F. (1978). "Flows of flexible polymer solutions in pores " Macromolecules **11**(4): 751-758.

Deng, H., Bloomfield, V. A., Benevides, J. M. and Thomas, G. J. (2000). "Structural basis of polyamine-DNA recognition: Spermidine and spermine interactions with

genomic B-DNAs of different GC content probed by Raman spectroscopy." Nucleic Acids Research **28**(17): 3379-3385.

Ding, Y., Jiang, Z., Saha, K., Kim, C. S., Kim, S. T., Landis, R. F. and Rotello, V. M. (2014). "Gold nanoparticles for nucleic acid delivery." Molecular Therapy **22**(6): 1075-1083.

Diogo, M. M., Queiroz, J. A. and Prazeres, D. M. F. (2005). "Chromatography of plasmid DNA." Journal of Chromatography A **1069**(1): 3-22.

Donnelly, J. J., Friedman, A., Martinez, D., Montgomery, D. L., Shiver, J. W., Motzel, S. L., Ulmer, J. B. and Liu, M. A. (1995). "Preclinical efficacy of a prototype DNA vaccine: Enhanced protection against antigenic drift in influenza virus." Nature Medicine **1**(6): 583-587.

Dorfman, K. D., King, S. B., Olson, D. W., Thomas, J. D. P. and Tree, D. R. (2013). "Beyond gel electrophoresis: Microfluidic separations, fluorescence burst analysis, and DNA stretching." Chemical Reviews **113**(4): 2584-2667.

Dragan, A. I., Casas-Finet, J. R., Bishop, E. S., Strouse, R. J., Schenerman, M. A. and Geddes, C. D. (2010). "Characterization of picogreen interaction with dsDNA and the origin of its fluorescence enhancement upon binding." Biophysical Journal **99**(9): 3010-3019.

Errampalli, D., Leung, K., Cassidy, M. B., Kostrzynska, M., Blears, M., Lee, H. and Trevors, J. T. (1999). "Applications of the green fluorescent protein as a molecular marker in environmental microorganisms." Journal of Microbiological Methods **35**(3): 187-199.

Feliciello, I. and Chinali, G. (1993). "A modified alkaline lysis method for the preparation of highly purified plasmid DNA from escherichia coli." Analytical Biochemistry **212**(2): 394-401.

Ferreira, G. N. M., Monteiro, G. A., Prazeres, D. M. F. and Cabral, J. M. S. (2000). "Downstream processing of plasmid DNA for gene therapy and DNA vaccine applications." Trends in Biotechnology **18**(9): 380-388.

Froger, A. and Hall, J. E. (2007). "Transformation of plasmid DNA into E. Coli using the heat shock method." Journal of Visualized Experiments. **253**(6): e253.

Fyta, M., Melchionna, S. and Succi, S. (2011). "Translocation of biomolecules through solid-state nanopores: Theory meets experiments." Journal of Polymer Science Part B-Polymer Physics **49**(14): 985-1011.

Ghanem, A., Healey, R. and Adly, F. G. (2013). "Current trends in separation of plasmid DNA vaccines: A review." Analytica Chimica Acta **760**: 1-15.

Ginn, S. L., Alexander, I. E., Edelstein, M. L., Abedi, M. R. and Wixon, J. (2013). "Gene therapy clinical trials worldwide to 2012 – an update." The Journal of Gene Medicine **15**(2): 65-77.

Gray, G. S. and Fitch, W. M. (1983). "Evolution of antibiotic resistance genes; the DNA sequence of a kanamycin resistance gene from staphylococcus aureus." Molecular Biology and Evolution **1**(1): 57-66.

Greening, D. W. and Simpson, R. J. (2011). "Low-molecular weight plasma proteome analysis using centrifugal ultrafiltration." Methods in Molecular Biology **728**: 109-124.

Hagerman, P. J. (1981). "Investigation of the flexibility of DNA using transient electric birefringence." Biopolymers **20**(7): 1503-1535.

Holovics, H. J., He, Y., Lacher, N. A. and Ruesch, M. N. (2010). "Capillary gel electrophoresis with laser-induced fluorescence of plasmid DNA in untreated capillary." Electrophoresis **31**(14): 2436-2441.

Holzel, R., Gajovic-Eichelmann, N. and Bier, F. F. (2003). "Oriented and vectorial immobilization of linear M13 dsDNA between interdigitated electrodes - towards single molecule DNA nanostructures." Biosensors & Bioelectronics **18**(5-6): 555-564.

Hsieh, C. C. and Lin, T. H. (2011). "Simulation of conformational preconditioning strategies for electrophoretic stretching of DNA in a microcontraction." Biomicrofluidics **5**(4): 044106-1 – 044106-17.

Hsieh, S. S. and Liou, J. H. (2009). "DNA molecule dynamics in converging-diverging microchannels." Biotechnology and Applied Biochemistry **52**: 29-40.

Iuliano, S., Fisher, J. R., Chen, M. and Kelly, W. J. (2002). "Rapid analysis of a plasmid hydrophobic-interaction chromatography with a non-porous resin." Journal of Chromatography A **972**(1): 77-86.

Jaoko, W., Nakwagala, F. N., Anzala, O., Manyonyi, G. O., Birungi, J., Nanvubya, A., Bashir, F., Bhatt, K., Ogutu, H., Wakasiaka, S., Matu, L., Waruingi, W., Odada, J., Oyaro, M., Indangasi, J., Ndinya-Achola, J., Konde, C., Mugisha, E., Fast, P., Schmidt, C., Gilmour, J., Tarragona, T., Smith, C., Barin, B., Dally, L., Johnson, B., Muluubya, A., Nielsen, L., Hayes, P., Boaz, M., Hughes, P., Hanke, T., McMichael, A., Bwayo, J. and Kaleebu, P. (2008). "Safety and immunogenicity of recombinant low-dosage HIV-1 a vaccine candidates vectored by plasmid

pTHr DNA or modified vaccinia virus AnKara (MVA) in humans in East Africa." Vaccine **26**(22): 2788-2795.

Jiang, Y., Rabbi, M., Mieczkowski, P. A. and Marszalek, P. E. (2010). "Separating DNA with different topologies by atomic force microscopy in comparison with gel electrophoresis." Journal of Physical Chemistry B **114**(37): 12162-12165.

K.H., K. (2013). "DNA vaccines: Roles against diseases." GERMS. **3**(1).

Kahn, D. W., Butler, M. D., Cohen, D. L., Gordon, M., Kahn, J. W. and Winkler, M. E. (2000). "Purification of plasmid DNA by tangential flow filtration." Biotechnology and Bioengineering **69**(1): 101-106.

Knudsen, K. D., Martinez, M. C. L. and delaTorre, J. G. (1996). "Fracture of DNA in transient extensional flow: A numerical simulation study." Biopolymers **39**(3): 435-444.

Kong, S., Rock, C. F., Booth, A., Willoughby, N., O'Kennedy, R. D., Relton, J., Ward, J. M., Hoare, M. and Levy, M. S. (2008). "Large-scale plasmid DNA processing: Evidence that cell harvesting and storage methods affect yield of supercoiled plasmid DNA." Biotechnology and Applied Biochemistry **51**: 43-51.

Krowczynska, A. M., Henderson, M. B. (1992). "Efficient purification of PCR products using ultrafiltration." Biotechniques **13**(2): 286-289.

Kuruzovich, J. N. and Piergiovanni, P. R. (1996). "Yeast cell microfiltration: Optimization of backwashing for delicate membranes." Journal of Membrane Science **112**(2): 241-247.

Larson, J. W., Yantz, G. R., Zhong, Q., Charnas, R., D'Antoni, C. M., Gallo, M. V., Gillis, K. A., Neely, L. A., Phillips, K. M., Wong, G. G., Gullans, S. R. and Gilmanshin, R. (2006). "Single DNA molecule stretching in sudden mixed shear and elongational microflows." Lab on a Chip **6**(9): 1187-1199.

Larson, R. G. (2000). "The role of molecular folds and 'pre-conditioning' in the unraveling of polymer molecules during extensional flow." Journal of Non-Newtonian Fluid Mechanics **94**(1): 37-45.

Latulippe, D. R. (2010). "Purification of plasmid DNA therapeutics: New opportunities for membrane processes" **PhD** dissertation, Department of Chemical Engineering, The Pennsylvania State University.

Latulippe, D. R., Ager, K. and Zydney, A. L. (2007). "Flux-dependent transmission of supercoiled plasmid DNA through ultrafiltration membranes." Journal of Membrane Science **294**(1-2): 169-177.

Latulippe, D. R. and Zydney, A. L. (2008). "Salt-induced changes in plasmid DNA transmission through ultrafiltration membranes." Biotechnology and Bioengineering **99**(2): 390-398.

Latulippe, D. R. and Zydney, A. L. (2009). "Elongational flow model for transmission of supercoiled plasmid DNA during membrane ultrafiltration." Journal of Membrane Science **329**(1-2): 201-208.

Latulippe, D. R. and Zydney, A. L. (2010). "Radius of gyration of plasmid DNA isoforms from static light scattering." Biotechnology and Bioengineering **107**(1): 134-142.

Latulippe, D. R. and Zydney, A. L. (2011). "Separation of plasmid DNA isoforms by highly converging flow through small membrane pores." Journal of Colloid and Interface Science **357**(2): 548-553.

Lessard, J. C. (2013). Chapter twenty seven - transformation of E. Coli via electroporation. Laboratory Methods in Enzymology:DNA. L. Jon, Academic Press. **529:** 321-327.

Levy, M. S., Collins, I. J., Yim, S. S., Ward, J. M., Titchener-Hooker, N., Shamlou, P. A. and Dunnill, P. (1999). "Effect of shear on plasmid DNA in solution." Bioprocess Engineering **20**(1): 7-13.

Levy, S. L. and Craighead, H. G. (2010). "DNA manipulation, sorting, and mapping in nanofluidic systems." Chemical Society Reviews **39**(3): 1133-1152.

Li, J., Pei, H., Zhu, B., Liang, L., Wei, M., He, Y., Chen, N., Li, D., Huang, Q. and Fan, C. H. (2011). "Self-assembled multivalent DNA nanostructures for noninvasive intracellular delivery of immunostimulatory CpG oligonucleotides." ACS Nano **5**(11): 8783-8789.

Li, J. L., Gershow, M., Stein, D., Brandin, E. and Golovchenko, J. A. (2003). "DNA molecules and configurations in a solid-state nanopore microscope." Nature Materials **2**(9): 611-615.

Li, Y., Dong, X. Y. and Sun, Y. (2005). "High-speed chromatographic purification of plasmid DNA with a customized biporous hydrophobic adsorbent." Biochemical Engineering Journal **27**(1): 33-39.

Lin, C. Y., Liu, C. H., Chang, H. C. and Tseng, W. L. (2008). "Enrichment and separation of acidic and basic proteins using the centrifugal ultrafiltration followed by nanoparticle-filled capillary electrophoresis." Electrophoresis **29**(14): 3024-3031.

Liu, D., Satoh, E. and Knapp, J. E. (2001). Naked DNA in Gene Therapy, John Wiley & Sons, Ltd.

Liu, J., Lu, G. W., Sandoval, M., Ciringh, Y., Xue, G., Jaeger, D., Kompanik, K., Jiao, J. and Gelotte, K. M. (2009). "Determination of benzalkonium chloride partition in micelle solutions using ultrafiltration method." AAPS PharmSciTech **10**(4):1216-1223

Ma, H., Bowman, C. N. and Davis, R. H. (2000). "Membrane fouling reduction by backpulsing and surface modification." Journal of Membrane Science **173**(2): 191-200.

Matos, T., Queiroz, J. A. and Bulow, L. (2014). "Plasmid DNA purification using a multimodal chromatography resin." Journal of Molecular Recognition **27**(4): 184-189.

McNevin, D., Wilson-Wilde, L., Robertson, J., Kyd, J., Lennard, C. (2005). "Short tandem repeat (STR) genotyping of keratinised hair. Part 2. An optimised genomic DNA extraction procedure reveals donor dependence of STR profiles." Forensic Science International **153**(2-3): 247-259.

Meacle, F., Aunins, A., Thornton, R. and Lee, A. (1999). "Optimization of the membrane purification of a polysaccharide-protein conjugate vaccine using backpulsing." Journal of Membrane Science **161**(1-2): 171-184.

Molloy, M. J., Hall, V. S., Bailey, S. I., Griffin, K. J., Faulkner, J. and Uden, M. (2004). "Effective and robust plasmid topology analysis and the subsequent characterization of the plasmid isoforms thereby observed." Nucleic Acids Research **32**(16): e129.

Morao, A., Nunes, J. C., Sousa, F., de Amorim, M. T. P., Escobar, I. C. and Queiroz, J. A. (2009). "Development of a model for membrane filtration of long and flexible macromolecules: Application to predict dextran and linear DNA rejections in ultrafiltration." Journal of Membrane Science **336**(1-2): 61-70.

Morao, A. M., Nunes, J. C., Sousa, F., de Amorim, M. T. P., Escobar, I. C. and Queiroz, J. A. (2011). "Ultrafiltration of supercoiled plasmid DNA: Modeling and application." Journal of Membrane Science **378**(1-2): 280-289.

Moreau, N., Tabary, X. and Le Goffic, F. (1987). "Purification and separation of various plasmid forms by exclusion chromatography." Analytical Biochemistry **166**(1): 188-193.

Mores, W. D. and Davis, R. H. (2002). "Yeast foulant removal by backpulses in crossflow microfiltration." Journal of Membrane Science **208**(1-2): 389-404.

Nies, D. H. (2003). "Efflux-mediated heavy metal resistance in prokaryotes." FEMS Microbiology Reviews **27**(2-3): 313-339.

Norrander, J., Kempe, T. and Messing, J. (1983). "Construction of improved M13 vectors using oligodeoxynucleotide-directed mutagenesis." Gene **26**(1): 101-106.

Nunes, J. C., Morao, A. M., Nunes, C., de Amorim, M. T. P., Escobar, I. C. and Queiroz, J. A. (2012). "Plasmid DNA recovery from fermentation broths by a combined process of micro- and ultrafiltration: Modeling and application." Journal of Membrane Science **415**: 24-35.

Nunes, J. C., Pessoa de Amorim, M. T., Escobar, I. C., Queiroz, J. A. and Morão, A. M. (2014). "Plasmid DNA-RNA separation by ultrafiltration: Modeling and application study." Journal of Membrane Science **463**(0): 1-10.

Ornstein, R. L., Rein, R., Breen, D. L. and Macelroy, R. D. (1978). "An optimized potential function for the calculation of nucleic acid interaction energies I. Base stacking." Biopolymers **17**(10): 2341-2360.

Perkins, T. T., Smith, D. E. and Chu, S. (1997). "Single polymer dynamics in an elongational flow." Science **276**(5321): 2016-2021.

Prather, K. J., Sagar, S., Murphy, J. and Chartrain, M. (2003). "Industrial scale production of plasmid DNA for vaccine and gene therapy: Plasmid design, production, and purification." Enzyme and Microbial Technology **33**(7): 865-883.

Przybylowski, M., Bartido, S., Borquez-Ojeda, O., Sadelain, M. and Riviere, I. (2007). "Production of clinical-grade plasmid DNA for human phase I clinical trials and large animal clinical studies." Vaccine **25**(27): 5013-5024.

Quaak, S. G. L., van den Berg, J. H., Toebes, M., Schumacher, T. N. M., Haanen, J., Beijnen, J. H. and Nuijen, B. (2008). "GMP production of pDERMATT for vaccination against melanoma in a phase I clinical trial." European Journal of Pharmaceutics and Biopharmaceutics **70**(2): 429-438.

Randall, G. C., Schultz, K. M. and Doyle, P. S. (2006). "Methods to electrophoretically stretch DNA: Microcontractions, gels, and hybrid gel-microcontraction devices." Lab on a Chip **6**(4): 516-525.

Reiner, M. (1964). "The deborah number." Physics today **17**(1): 62.

Rosa, A., Di Ventra, M. and Micheletti, C. (2012). "Topological jamming of spontaneously knotted polyelectrolyte chains driven through a nanopore." Physical Review Letters **109**(11):118301-1 – 118301-5.

Rouse, P. E. (1953). "A theory of the linear viscoelastic properties of dilute solutions of coiling polymers." Journal of Chemical Physics **21**(7): 1272-1280.

Rybenkov, V. V., Cozzarelli, N. R. and Vologodskii, A. V. (1993). "Probability of DNA knotting and the effective diameter of the DNA double helix." Proceedings of the National Academy of Sciences of the United States of America **90**(11): 5307-5311.

Sanchez, A. M., Carmona, M., Prodanov, M., Alonso, G. L. (2008). "Effect of centrifugal ultrafiltration on the composition of aqueous extracts of saffron spice (Crocus sativus L.)." Journal of Agricultural and Food Chemistry **56**(16): 7293-7301.

Schleef, M. (2001). Plasmids for Therapy and Vaccination, Wiley-VCH.

Schmidt, T., Friehs, K., Schleef, M., Voss, C. and Flaschel, E. (1999). "Quantitative analysis of plasmid forms by agarose and capillary gel electrophoresis." Analytical Biochemistry **274**(2): 235-240.

Schmitz, A. and Riesner, D. (2006). "Purification of nucleic acids by selective precipitation with polyethylene glycol 6000." Analytical Biochemistry **354**(2): 311-313.

Schratter, P., Krowczynska, A. M. and Leonard, J. T. (1993). "Ultrafiltration in molecular biology." American Biotechnology Laboratory **11**(12): 16.

Shin, M. J., Tan, L., Jeong, M. H., Kim, J.-H. and Choe, W.-S. (2011). "Monolith-based immobilized metal affinity chromatography increases production efficiency for plasmid DNA purification." Journal of Chromatography A **1218**(31): 5273-5278.

Sinden, R. R. (1994). DNA structure and function. Academic Press.

Smrekar, F., Podgornik, A., Ciringer, M., Kontrec, S., Raspor, P., Štrancar, A. and Peterka, M. (2010). "Preparation of pharmaceutical-grade plasmid DNA using methacrylate monolithic columns." Vaccine **28**(8): 2039-2045.

Sorlie, S. S. and Pecora, R. (1990). "A dynamic light scattering study of four DNA restriction fragments." Macromolecules **23**(2): 487-497.

Sousa, A., Sousa, F. and Queiroz, J. A. (2011). "Impact of lysine-affinity chromatography on supercoiled plasmid DNA purification." Journal of Chromatography B **879**(30): 3507-3515.

Sousa, F., Freitas, S., Azzoni, A. R., Prazeres, D. M. F. and Queiroz, J. (2006). "Selective purification of supercoiled plasmid DNA from clarified cell lysates with a single histidine–agarose chromatography step." Biotechnology and Applied Biochemistry **45**(3): 131-140.

Sturm, J. and Weill, G. (1989). "Direct observation of DNA chain orientation and relaxation by electric birefringence: Implications for the mechanism of separation during pulsed-field gel electrophoresis." Physical Review Letters **62**(13): 1484-1487.

Sun, B., Yu, X. H., Yin, Y. H., Liu, X. T., Wu, Y. G., Chen, Y., Zhang, X. Z., Jiang, C. L. and Kong, W. (2013). "Large-scale purification of pharmaceutical-grade plasmid DNA using tangential flow filtration and multi-step chromatography." Journal of Bioscience and Bioengineering **116**(3): 281-286.

Sutcliffe, J. G. (1978). "Nucleotide sequence of the ampicillin resistance gene of Escherichia coli plasmid pBR322." Proc Natl Acad Sci U S A. **75**(8): 5.

Tascon, R. E., Colston, M. J., Ragno, S., Stavropoulos, E., Gregory, D. and Lowrie, D. B. (1996). "Vaccination against tuberculosis by DNA injection." Nature Medicine **2**(8): 888-892.

Teja Colluru, V., Johnson, L. E., Olson, B. M. and McNeel, D. G. (2013). "Preclinical and clinical development of DNA vaccines for prostate cancer." Urologic Oncology: Seminars and Original Investigations.

Trahan, D. W. and Doyle, P. S. (2009). "Simulation of electrophoretic stretching of DNA in a microcontraction using an obstacle array for conformational preconditioning." Biomicrofluidics **3**(1): 012803-1 – 012803-14

Urthaler, J., Ascher, C., Wohrer, H. and Necina, R. (2007). "Automated alkaline lysis for industrial scale cGMP production of pharmaceutical grade plasmid DNA." Journal of Biotechnology **128**(1): 132-149.

Urthaler, J., Buchinger, W. and Necina, R. (2005). "Improved downstream process for the production of plasmid DNA for gene therapy." Acta Biochimica Polonica **52**(3): 703-711.

Vologodskii, A. V. and Cozzarelli, N. R. (1994). "Conformational and thermodynamic properties of supercoiled DNA." Annual Review of Biophysics and Biomolecular Structure **23**:609-643.

Voss, C. (2007). Production of plasmid DNA for pharmaceutical use. Biotechnology annual review **13:** 201-222.

Wada, C. and Yura, T. (1984). "Control of F-plasmid replication by a host gene: Evidence for interaction of the mafA gene-product of Escherichia-Coli with the mini-F incC region." Journal of Bacteriology **160**(3): 1130-1136.

Watson, J. D. and Crick, F. H. C. (1953). "Molecular structure of nucleic acids - A structure for deoxyribose nucleic acid." Nature **171**(4356): 737-738.

Watson, M. P., Winters, M. A., Sagar, S. L. and Konz, J. O. (2006). "Sterilizing filtration of plasmid DNA: Effects of plasmid concentration, molecular weight, and conformation." Biotechnology Progress **22**(2): 465-470.

Weintraub, H., Cheng, P. F. and Conrad, K. (1986). "Expression of transfected DNA depends on DNA topology." Cell **46**(1): 115-122.

Wen, E., Cinelli, L. D., Murray, D., Lander, R. J., Sagar, S. L. and Lee, A. L. (2005). "Purification of a polysaccharide conjugate vaccine using microfiltration membranes in backpulsing mode." Journal of Membrane Science **258**(1–2): 23-34.

Wu, H. M. and Crothers, D. M. (1984). "The locus of sequence-directed and protein-induced DNA bending." Nature **308**(5959): 509-513.

Yong Chung, K., Bates, R. and Belfort, G. (1993). "Dean vortices with wall flux in a curved channel membrane system: 4. Effect of vortices on permeation fluxes of suspensions in microporous membrane." Journal of Membrane Science **81**(1–2): 139-150.

Zhao, Y.H., Wee, K. H. and Bai, R. (2010). "Highly hydrophilic and low-protein-fouling polypropylene membrane prepared by surface modification with sulfobetaine-based zwitterionic polymer through a combined surface polymerization method." Journal of Membrane Science **362**(1–2): 326-333.

Zhdanov, R. I., Podobed, O. V. and Vlassov, V. V. (2002). "Cationic lipid-DNA complexes-lipoplexes-for gene transfer and therapy." Bioelectrochemistry **58**(1): 53-64.

Zimm, B. H. (1956). "Dynamics of polymer molecules in dilute solution: Viscoelasticity, flow birefringence and dielectric loss." The Journal of Chemical Physics **24**(2): 269-278.

Zydney, A. L. and Zeman, L. J. (1996) Microfiltration and Ultrafiltration: Principles and Applications, Marcel Dekker.

Appendix

Plasmid DNA vectors maps and sequences

A.1. 2.96 kbp plasmid (p-EMP)

The gene sequence shown below belongs to 2.96 kbp plasmid (p-EMP) used in Chapter 3 and 5. Figure A-1 presents the vector map of this plasmid.

```
   1  CTAAATTGTA AGCGTTAATA TTTTGTTAAA ATTCGCGTTA AATTTTTGTT
  51  AAATCAGCTC ATTTTTTAAC CAATAGGCCG AAATCGGCAA AATCCCTTAT
 101  AAATCAAAAG AATAGACCGA GATAGGGTTG AGTGTTGTTC CAGTTTGGAA
 151  CAAGAGTCCA CTATTAAAGA ACGTGGACTC CAACGTCAAA GGGCGAAAAA
 201  CCGTCTATCA GGGCGATGGC CCACTACGTG AACCATCACC CTAATCAAGT
 251  TTTTTGGGGT CGAGGTGCCG TAAAGCACTA AATCGGAACC CTAAAGGGAG
 301  CCCCCGATTT AGAGCTTGAC GGGGAAAGCC GGCGAACGTG GCGAGAAAGG
 351  AAGGGAAGAA AGCGAAAGGA GCGGGCGCTA GGGCGCTGGC AAGTGTAGCG
 401  GTCACGCTGC GCGTAACCAC CACACCCGCC GCGCTTAATG CGCCGCTACA
 451  GGGCGCGTCC CATTCGCCAT TCAGGCTGCG CAACTGTTGG GAAGGGCGAT
 501  CGGTGCGGGC CTCTTCGCTA TTACGCCAGC TGGCGAAAGG GGGATGTGCT
 551  GCAAGGCGAT TAAGTTGGGT AACGCCAGGG TTTTCCCAGT CACGACGTTG
 601  TAAAACGACG GCCAGTGAGC GCGCGTAATA CGACTCACTA TAGGGCGAAT
 651  TGGAGCTCCA CCGCGGTGGC GGCCGCTCTA GAACTAGTGG ATCCCCCGGG
 701  CTGCAGGAAT TCGATATCAA GCTTATCGAT ACCGTCGACC TCGAGGGGGG
 751  GCCCGGTACC CAGCTTTTGT TCCCTTTAGT GAGGGTTAAT TGCGCGCTTG
 801  GCGTAATCAT GGTCATAGCT GTTTCCTGTG TGAAATTGTT ATCCGCTCAC
 851  AATTCCACAC AACATACGAG CCGGAAGCAT AAAGTGTAAA GCCTGGGGTG
 901  CCTAATGAGT GAGCTAACTC ACATTAATTG CGTTGCGCTC ACTGCCCGCT
 951  TTCCAGTCGG GAAACCTGTC GTGCCAGCTG CATTAATGAA TCGGCCAACG
1001  CGCGGGGAGA GGCGGTTTGC GTATTGGGCG CTCTTCCGCT TCCTCGCTCA
1051  CTGACTCGCT GCGCTCGGTC GTTCGGCTGC GGCGAGCGGT ATCAGCTCAC
1101  TCAAAGGCGG TAATACGGTT ATCCACAGAA TCAGGGGATA ACGCAGGAAA
1151  GAACATGTGA GCAAAAGGCC AGCAAAAGGC CAGGAACCGT AAAAAGGCCG
1201  CGTTGCTGGC GTTTTTCCAT AGGCTCCGCC CCCCTGACGA GCATCACAAA
1251  AATCGACGCT CAAGTCAGAG GTGGCGAAAC CCGACAGGAC TATAAAGATA
1301  CCAGGCGTTT CCCCCTGGAA GCTCCCTCGT GCGCTCTCCT GTTCCGACCC
1351  TGCCGCTTAC CGGATACCTG TCCGCCTTTC TCCCTTCGGG AAGCGTGGCG
1401  CTTTCTCATA GCTCACGCTG TAGGTATCTC AGTTCGGTGT AGGTCGTTCG
1451  CTCCAAGCTG GGCTGTGTGC ACGAACCCCC CGTTCAGCCC GACCGCTGCG
1501  CCTTATCCGG TAACTATCGT CTTGAGTCCA ACCCGGTAAG ACACGACTTA
```

```
1551  TCGCCACTGG CAGCAGCCAC TGGTAACAGG ATTAGCAGAG CGAGGTATGT
1601  AGGCGGTGCT ACAGAGTTCT TGAAGTGGTG GCCTAACTAC GGCTACACTA
1651  GAAGGACAGT ATTTGGTATC TGCGCTCTGC TGAAGCCAGT TACCTTCGGA
1701  AAAAGAGTTG GTAGCTCTTG ATCCGGCAAA CAAACCACCG CTGGTAGCGG
1751  TGGTTTTTTT GTTTGCAAGC AGCAGATTAC GCGCAGAAAA AAAGGATCTC
1801  AAGAAGATCC TTTGATCTTT TCTACGGGGT CTGACGCTCA GTGGAACGAA
1851  AACTCACGTT AAGGGATTTT GGTCATGAGA TTATCAAAAA GGATCTTCAC
1901  CTAGATCCTT TTAAATTAAA AATGAAGTTT TAAATCAATC TAAAGTATAT
1951  ATGAGTAAAC TTGGTCTGAC AGTTACCAAT GCTTAATCAG TGAGGCACCT
2001  ATCTCAGCGA TCTGTCTATT TCGTTCATCC ATAGTTGCCT GACTCCCCGT
2051  CGTGTAGATA ACTACGATAC GGGAGGGCTT ACCATCTGGC CCCAGTGCTG
2101  CAATGATACC GCGAGACCCA CGCTCACCGG CTCCAGATTT ATCAGCAATA
2151  AACCAGCCAG CCGGAAGGGC CGAGCGCAGA AGTGGTCCTG CAACTTTATC
2201  CGCCTCCATC CAGTCTATTA ATTGTTGCCG GGAAGCTAGA GTAAGTAGTT
2251  CGCCAGTTAA TAGTTTGCGC AACGTTGTTG CCATTGCTAC AGGCATCGTG
2301  GTGTCACGCT CGTCGTTTGG TATGGCTTCA TTCAGCTCCG GTTCCCAACG
2351  ATCAAGGCGA GTTACATGAT CCCCCATGTT GTGCAAAAAA GCGGTTAGCT
2401  CCTTCGGTCC TCCGATCGTT GTCAGAAGTA AGTTGGCCGC AGTGTTATCA
2451  CTCATGGTTA TGGCAGCACT GCATAATTCT CTTACTGTCA TGCCATCCGT
2501  AAGATGCTTT TCTGTGACTG GTGAGTACTC AACCAAGTCA TTCTGAGAAT
2551  AGTGTATGCG GCGACCGAGT TGCTCTTGCC CGGCGTCAAT ACGGGATAAT
2601  ACCGCGCCAC ATAGCAGAAC TTTAAAAGTG CTCATCATTG GAAAACGTTC
2651  TTCGGGGCGA AAACTCTCAA GGATCTTACC GCTGTTGAGA TCCAGTTCGA
2701  TGTAACCCAC TCGTGCACCC AACTGATCTT CAGCATCTTT TACTTTCACC
2751  AGCGTTTCTG GGTGAGCAAA AACAGGAAGG CAAAATGCCG CAAAAAAGGG
2801  AATAAGGGCG ACACGGAAAT GTTGAATACT CATACTCTTC CTTTTTCAAT
2851  ATTATTGAAG CATTTATCAG GGTTATTGTC TCATGAGCGG ATACATATTT
2901  GAATGTATTT AGAAAAATAA ACAAATAGGG GTTCCGCGCA CATTTCCCCG
2951  AAAGTGCCA C
```

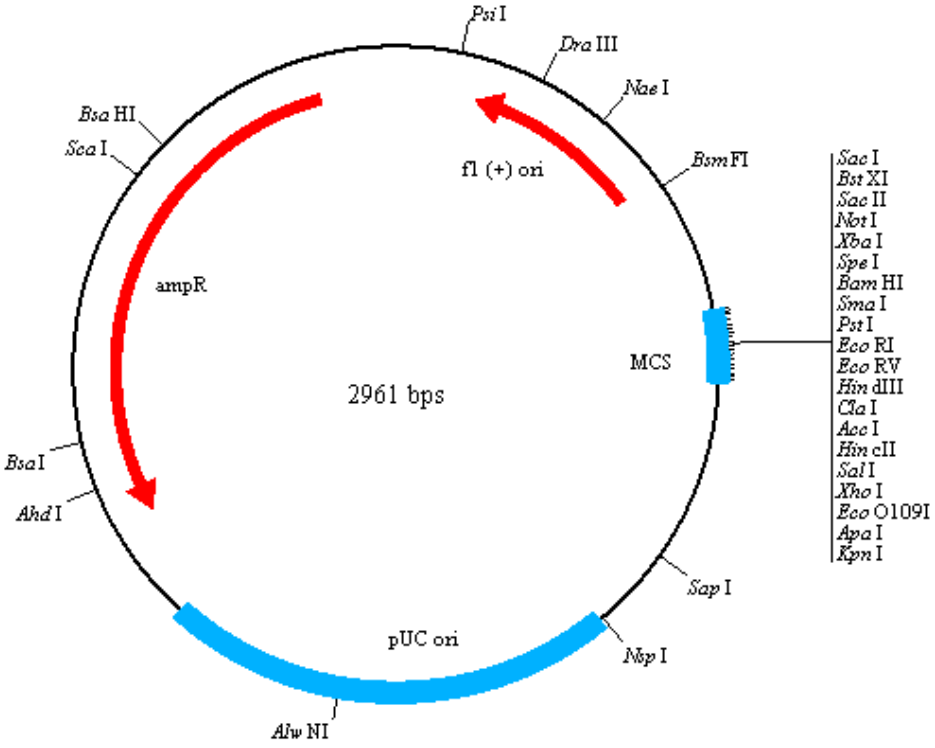

Figure A-1: Vector map of 2.96 kbp plasmid (p-EMP), adopted from (Latulippe, 2010).

A.2. 9.8 kbp plasmid (p-MDY)

Since the gene sequence of 9.8 kbp plasmid (p-MDY) was not available, only its vector map including a human mini-Dystrophin gene segment was shownin Figure A-2. This plasmid was used in Chapters 4 and 6.

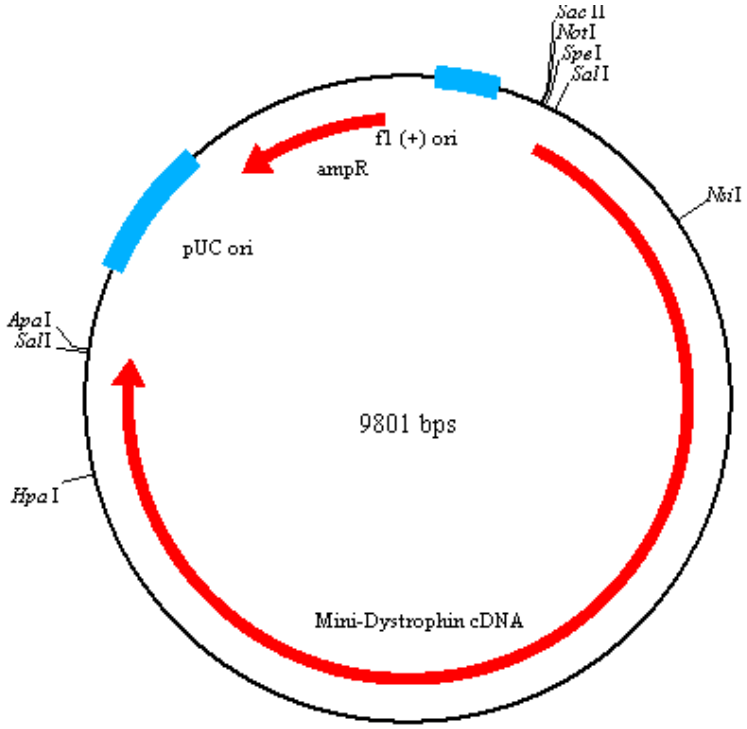

Figure A-2: Vector map of 9.8 kbp plasmid (p-MDY), adopted from (Latulippe, 2010).

A.3. 16.9 kbp plasmid (p-FDY)

Figure A-3 shows the vector map of 16.9 kbp plasmid (p-FDY) used in Chapters 3 and 5 with no gene sequence available to be presented. A murine full-Dystrophin gene segment is included in this plasmid.

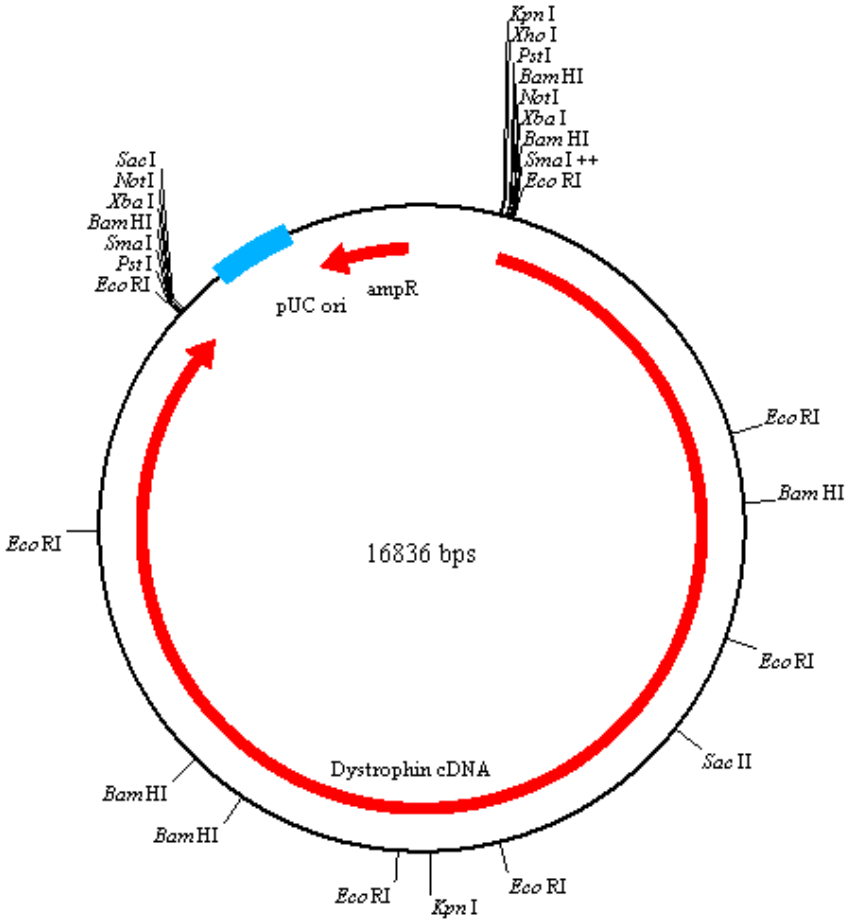

Figure A-3: Vector map of 16.9 kbp plasmid (p-FDY), adopted from (Latulippe, 2010).

VITA

Ehsan Allah Espah Borujeni

EDUCATION

- Doctor of Philosophy, Chemical Engineering (December 2014)
  The Pennsylvania State University, University Park, Pennsylvania
- Master of Science, Chemical Engineering (June 2008)
  Sharif University of Technology, Tehran, Iran
- Bachelor of Science, Chemical Engineering (June 2006)
  Sharif University of Technology, Tehran, Iran

PROFESSIONAL SERVICE

- Judge of the Mid-Atlantic regional AICHE poster competition (2011)
  The Pennsylvania State University, University Park, Pennsylvania

SELECT PEER-REVIEWED PUBLICATIONS

- Borujeni, E.E., Y. Li, A.L. Zydney, J. Membrane Sci. 473 (2014) 102
- Borujeni, E.E., A.L. Zydney, J. Membrane Sci. 450 (2014) 189
- Borujeni, E.E., A.L. Zydney, Biotechniques 53 (2012) 49

SELECT AWARDS AND ACCOMPLISHMENTS

- Travel award of North American Membrane Society conference (NAMS) (2011)
- 1st rank in the National Entrance Examination for M.Sc. in Chemical Engineering, Iran (2006)
- 3rd rank in the National Entrance Examination for M.Sc. in Biotechnology, Iran (2006)

EMPLOYMENT

- September 2008 – present
  Graduate Research Assistant, Department of Chemical Engineering,
  The Pennsylvania State University (University Park, Pennsylvania)
- August 2013 – January 2014
  Graduate Co-Op, Amgen Inc., (Thousand Oaks, California)